ATOMISTIC SIMULATION OF POINT DEFECTS IN IONIC CRYSTALS

A Thesis submitted

in partial fulfillment of the requirement

for the degree of

DOCTOR OF PHILOSOPHY

by

Munima B. Sahariah

Department of Physics

Indian Institute of Technology, Guwahati

Guwahati-781039

INDIA

July, 2005

Acknowledgments

It is a great pleasure and rewarding experience for me to work under the supervision of Dr. Charudatt Y. Kadolkar who has given me constant support and valuable guidance throughout the course of my work. I extend my deep gratitude to Prof. Y.V.G.S. Murti who introduced me to this field of point defects. I feel fortunate to have the opportunity of working under his supervision for two years at the beginning of my research work. I cannot forget the warmth and inspiration given to me by Radha (Dr. Radha D. Banhatti) during the very short interaction I had with her.

I fondly remember my visits to the computational material science group under Prof. Ravindra Pandey in Michigan Technological University, Houghton, Michigan, USA. I am deeply grateful to Prof. Pandey for his care and guidance during my stay in Michigan. My continued interaction with Prof. Pandey and Dr. Miguel has been a constant source of inspiration for me during the later part of my work. I am also thankful to his students Aurora, Huitian, Anil, Gautam, Kah Chun and Mrinalini for their kind cooperation and for making my stay in Houghton very comfortable and homely.

I am grateful to Prof.A. Srinivasan and Dr. S. Ravi for their valuable advice and encouragement all throughout my Ph.D. period. I acknowledge the financial support from DST, INDIA through the project MUDRA (Modeling Utility of Defects by Rapid Analysis). I am also thankful to IIT Guwahati for providing me with all the facilities and a nice aca-

demic environment. I am grateful to all my friends here in IIT Guwahati and specially to Sida, Chandan, Usha, Lokesh, Atul, and Madan for all their help and enjoyable company. A lot of thanks to Amal who has so painstakingly gone through the manuscript.

All these would not have come true without the comfortable support and constant inspiration from my husband Paban who has always been there on my side to cheer me up. I will ever remember the love and support shown to me by my parents, my in-laws and my brothers and sisters all throughout these years.

Abstract

In this thesis, we have presented a comprehensive study of modeling point defects in high and low symmetry crystals with Polarizable Point Ion (PPI) model. We worked out an alternate scheme to estimating energies of point defects through finite size calculations. This new method is tested for cubic *NaCl* crystal and is found to agree well with other existing results. Next, we studied in detail the effect of quadrupoles in the formation energy of vacancies in alkaline earth oxides using the approximate Mott-Littleton (ML) scheme. In agreement with earlier results on *AgCl* and *AgBr*, the quadrupoles are found to have substantial effect on defect energies raising a challenge to the existing dipolar models. We then worked out the PPI formulations for low symmetry crystals, both in perfect and defect environment. A suitable set of short range potential parameters are deduced for monoclinic $\beta-Ga_2O_3$ starting from the rigid ion potentials and it is found that the structural deviation in PPI scheme is very small from that of the rigid one. The polarizabilities of the participating ions are significantly lowered in the crystal environment than their free ion values. We also describe here a method of calculating the defect energies for a single point defect in such low symmetry crystals.

Table of Contents

List of Tables

List of Figures

Chapter 1

Introduction

1.1 Point Defects and Thermodynamics

The basic property of point defects, either intrinsic or extrinsic, that they influence the optical, electrical as well as the transport behaviours of crystalline materials has created a unique position for it's studies in the field of material science and engineering. For theoreticians, it is the modeling of transport processes in ionic materials which has drawn attentions over last several decades. However, to understand the role of point defects in transport processes it is essential to understand the thermodynamics of point defects.

In general, introducing any defect in a crystal has the effect of breaking the regular symmetry of the crystal. Thus the defects are categorized by the dimensionality in which the symmetry breaking extends. The simplest kind of defect is a point defect where the defect is localized to a single point and the local symmetry of the crystal is broken. The two most important kinds of point defects are vacancies and interstitials. As shown in Fig. 1.1 vacancies are the absence of regular ions while interstitials are the presence of extra ions (native or foreign) in a crystal lattice. These defects can occur inside a crystal in three different ways[1]. Firstly, as the crystal grows, impurity atoms incorporate themselves into

the structure. This impurity can exist either as substitutional by replacing a regular ion or as an interstitial on an interstitial site. Secondly, point defects also occur when the crystal contains an element which can exist in more than one charge state within the crystal. In this case, the change in charge of the host ions are balanced by the formation of a compensating defect. This type of defect is termed as non-stoichiometric defect as the stoichiometry of the crystal changes on their formation. Lastly, intrinsic type of defects exist because of the increase in configurational entropy of a crystal on the formation of point defect. Creation of such a defect has two fold effect. It involves an increase in enthalpy of the crystal as well as an increase in entropy due to increasing disorder in the system. At any temperature, for a system without any defect, the decrease in free energy caused by the increase in entropy always tend to dominate the increase in free energy caused by the increase in enthalpy and thus creates a favourable condition for formation of point defects. Thus the existence of these intrinsic point defects is an equilibrium phenomenon unlike the line and surface defects which exist in the metastable configurations of the crystal[2].

An atom in a regular lattice site of a crystal is at energy minimum on a time average over its vibrational motion. To create a vacancy defect, an ion must be extracted from this energy minimum position increasing the crystal energy by u^f. This will destroy the equilibrium of the lattice. To restore the equilibrium state, the ions surrounding the defect site will get relaxed to find new positions of equilibrium. So, a crystal with a point defect has its volume changed by v^f per defect. Moreover, as the relaxed atoms vibrate about their new positions of equilibrium, the frequencies of the normal modes are altered owing to changed force constants. This will associate another thermodynamic parameter ,i.e. s^f, the entropy of formation, to the defect crystal. The free energy of formation of the defect is now defined as

$$g^f = u^f + Pv^f - Ts^f$$

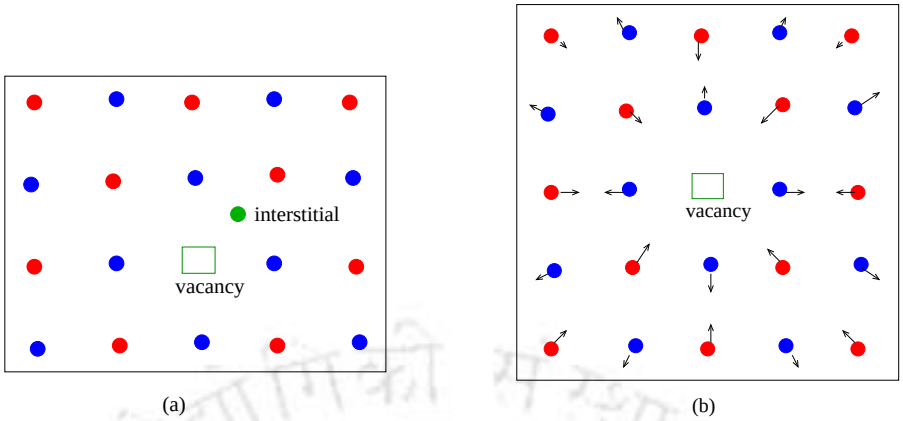

Figure 1.1: (a) Two main types of point defects, vacancy and interstitial. (b) The relaxation of surrounding ions as a point defect (vacancy here) is introduced

Where P is the pressure and T is absolute temperature. At $T = 0K$, $g^f = u^f + Pv^f = h^f$ is the enthalpy of formation of the defect.

In ionic crystal, the sum over the net charge of all point defects must be zero so as to satisfy the charge neutrality condition. There are two ways in which this can be achieved - one is to have a vacancy-interstitial pair of the same species , called the Frenkel defect, and the other is a combination of vacancies of different species with different charges, called Schottky defect as shown in Fig. 1.2. Different materials have different affinities to these defects. For example, in *NaCl*, the Schottky defect formation has a lower formation energy while in *AgCl*, Frenkel defect is more favourable than Schottky.

1.2 Study of Point Defects : Experimental and Theoretical Aspects

There are many experimental and theoretical approaches to study the presence, the type and concentrations of point defects in a crystal and then extract the thermodynamic param-

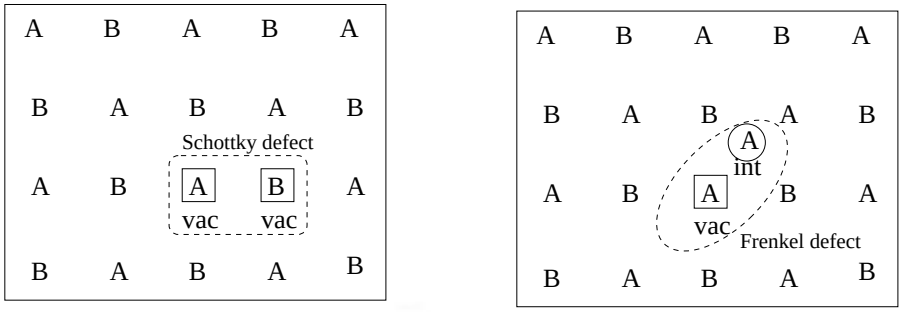

Figure 1.2: A simple diatomic crystal with ions of type A and B having equal and opposite charge states shows (a) Schottky and (b) Frenkel defect

eters like formation energies and formation entropies etc. Experimental methods which are largely applied in semiconductors and metals are the 'differential dilatometry' method[3] and the 'Positron Annihilation' method[4, 5, 6, 7, 8]. On the other hand, methods suitable for ionic crystals are the ionic conductivity[9, 10], relaxation and diffusion measurements . Ionic crystals, which are electronic insulators, have a non vanishing electrical conductivity. It is clear that due to large band gap, the electrons cannot get thermally excited from the valence band to the conduction band. So it is the ions which play the role of charge carriers, not the electrons. The presence of vacancies greatly enhances the ability of the ions to carry electric charge. This is because it takes less effort to carry a vacancy through a crystal than an extra ion in a perfect crystal environment as shown in Fig. 1.3. It has been observed that the conductivity of an ionic crystal increases with temperature exponentially in $\frac{1}{T}$ which also reflects the temperature dependence of the thermal equilibrium vacancy concentration and stands as an evidence that the conduction depends on the movement of the vacancies. In some cases like anion-cation vacancy pairs or impurity vacancy pairs in alkali and silver halides, which are neutral in nature, cannot contribute to the conductivity. But such pairs continually change their orientation as a result of defect jumps under thermal activation, and these jumps may be biased by applied electric or stress fields. This phenomenon

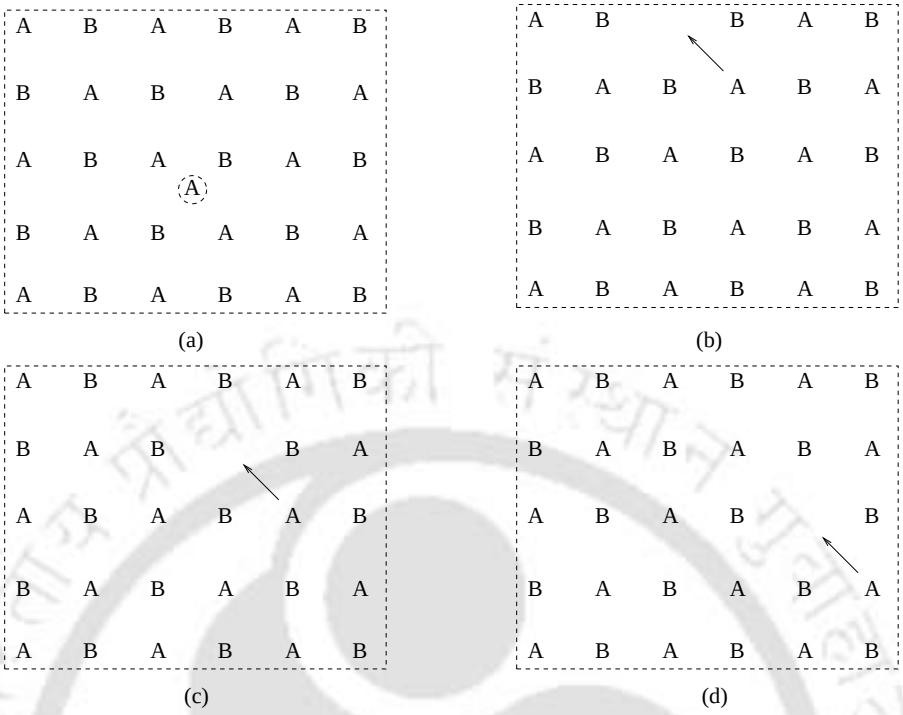

Figure 1.3: Illustrates the relative easiness of movement of ions to neighbouring vacancies in (b)-(d) as compared to the one in a perfect environments in (a)

is used to find the point defect parameters for such neutral defects and is known as the relaxation method. The principle here is the determination of the loss angle between a periodically applied stress and the induced strain. Lastly, the diffusion measurement method is based on the process of self-diffusion or impurity-diffusion. If there are no contributions to the diffusion from neutral defects, the information obtained from diffusion measurements is very similar to that obtained from conductivity. Comparison of the two then gives the correlation factor and hence confirms the mechanism of diffusion.

However, any experimental procedure for finding thermodynamic parameters of point defects involves an extensive amount of care and thoroughness in both measurement and analysis. Designing and implementing a new solid state experiment sometimes becomes much expensive both in cost and time. Some of these efforts also go unrewarded with no

fruitful results. In such cases, theoretical evaluation assumes importance in providing a outstanding background as far as the application and prospect of the outputs are concerned. Presently, the point defects are theoretically simulated in two ways : *ab initio* calculations and atomistic calculations.

In *ab initio* methods, one constructs a numerically solvable model system, and calculates defect properties in that model system from the first principles, i.e. from Schrodinger equation. *ab initio* methods, accompanied by experimental measurements and analytic model systems, can provide good understanding of the microscopic structure of the point defects. However, it is generally impossible to directly solve the many particle Schrodinger equation for the whole macroscopic crystal with roughly 10^{23} cm^{-3} atoms and 10^{24} cm^{-3} interacting electrons numerically. For this, basically two approximations are necessary. First, the many particle interactions are to be somehow simplified. Second, the whole crystal has to be described using a model system with fewer particles. This leads to the density-functional theory (DFT) and the Supercell method. The density-functional theory[11, 12] treats the total energy as a functional of charge density. The major advantage of density functional theory over wavefunction methods such as Hartree-Fock becomes evident when considering energy minimization. If the energy is minimized with respect to wavefunction then the $3n$ spatial co-ordinates of the n contributing electrons must be surveyed. However charge density is only a function of 3 spatial coordinates and so is much easier to treat. The most useful and practical applications of the DFT are based on the Kohn-Sham scheme, the local density approximation (LDA)[13] and the generalized gradient approximation (GGA)[14, 15]. In Supercell method, unit cells with periodic boundary conditions are used to model isolated imperfections like point defects in crystal structures. The size of the Supercell is made large enough to accommodate the defect and enough bulk crystal to separate the defects from their periodic images[16, 17, 18]. An alternative approach to

the Supercell method is the Cluster method[19, 20, 21], in which the crystal is modeled by a large, properly terminated isolated cluster of ions cut from the original crystal structure.

Though first principle methods are fundamental in nature, they are rarely used in simulating defects in ionic crystals. This is because these methods are based on a description of the electronic structure consisting of neutral atoms. Moreover, the long range coulombic interactions necessitate the use of large number of ions in these crystals which in turn asks for enormous computational effort. An alternative to these complexities is to describe the total energy by parametrized functions that depend on the relative atomic positions. Atomistic models based on this concept greatly simplifies the potential energy hypersurface leading to drastic save in computer time.

In the ideal case, the reliability of an atomistic model is checked by the study of four main physical properties. They are (1) Cohesion, (2) Elastic Constants, (3) Dielectric properties and (4) Lattice vibrations. Below we give a short description of these properties.

Cohesion

The main source of cohesion in ionic crystals is the attraction of anions and cations amongst each other. This leads to two main types of interionic interactions: (1) Long range coulomb forces and (2) Short range overlap repulsions which come into play as the electron clouds overlap. While the Coulomb forces are fixed by the charge states of the constituent ions as defined by the model, finding short range potential parameters is somewhat crucial.

Establishing an adequate theory for the non-coulombic part of the interionic forces has been a challenge in solid state science for many years. The majority of current defect calculations are based on two body potentials in which non-coulombic forces are represented by different forms of potentials like Born-Mayer, Lennard-Jones, Morse etc. The Lennard-Jones type of potentials work best in systems like noble gases which are of

non-bonding type having close electronic shells. At large distances, the potential gives a r^{-6} type of attraction, where the coefficient is determined by the atomic polarizability. At short distances, the potentials are strongly repulsive due to Pauli's exclusion principle. However, in case of metals, potentials softer than Lennard Jones' is required. This criterion is fulfilled by the Morse potential. On the other hand, in ionic crystals, the non-coulombic forces are best represented by Born-Mayer type of repulsive interactions[22, 23] which are exponential in nature representing the exponential decrease in electron density at the periphery of an ion. One way to reach the relevant parameters in the Born Mayer form of potential is by an empirical fit to crystal data such as the lattice constant, cohesive energy and compressibility[23] or to the phonon spectra[24, 25, 26]. Later on, there were more efforts to combine empirical and non-empirical approaches to get better set of potentials[27, 28, 29, 30]. However, in spite of the vast application of this semi-empirical approach, there exists a number of drawbacks. Firstly, since the potential coefficients are derived here from equilibrium properties, they are valid only at or near the equilibrium separation and can cause problems when used for configurations which deviate appreciably from equilibrium like in the case of an interstitial defect. Secondly, since the parameters in this approach are determined by empirical fitting to experimental data, pair potential parameters determined from one set of experimental data may give poor results when used to calculate the properties of other systems. This shrinks the range of reliability and applicability of the semi-empirical model. All these were sufficient to initiate the search for non-empirical procedures for interatomic potentials. Besides removing the drawbacks suffered by empirical approach, much care were taken so that these new type of potentials can be adjusted in a systematic way to allow for changes in the potential as a function of the local defect configurations. In practice, however, most quantum mechanical models[31] are too complex in nature and can be applied only to the simplest solid state systems. The first

ever *ab initio* method for potential parameters was based on density functional theory[32] which was followed by several reinvestigations and modifications[33, 34, 35]. The most promising one is however the electron gas theory of Gordon and Kim[36]. Though originally developed for molecular systems, the theory was successfully applied to a number of ionic crystals[37]. The basic idea of the original electron gas (EG) theory[36] and the later modified electron gas theory (MEG)[38] is that the short range pair interaction energy is split into kinetic, exchange, correlation and nonpoint Coulomb electrostatic contributions and each of these is written as a relatively simple functional of the electron densities. The quest for a better and better theory on *ab initio* interionic potential is still going on which includes the many body effects also[39, 40, 41, 42].

Elastic and Dielectric Constants

Elastic constants are a good measure to fit the short range potential parameters either directly or via the compressibility data and offers a good test to the ionic model. The maximum number of independent variables for an arbitrary crystal is 21 which can be further reduced by exploiting the symmetry of the crystal (e.g for a cubic crystal, the number of independent elastic constants is only 3). While, there are good amount of experimental data present for elastic constants of high symmetry crystal, the picture is not encouraging for low symmetry ones where the increasing number of independent parameters demands huge effort from the experimentalists to determine their values. Another important parameter which should be well described by the ionic model particularly for those cases where the point defects polarize the lattice strongly is the dielectric constant of the material. In earlier models, the electronic polarizabilities of the component ions were obtained from the high frequency dielectric constants[43]. However, later on, it was established that it is the Clausius Mossotti equation relating the static dielectric constant and the total polarizability of

the crystal which can properly describe the static response of the defect crystal[44].

Lattice Vibrations

The ions in their regular lattice sites are not fixed but are in constant motion about a mean position which gives rise to the lattice vibrations. The presence of point defects or disorder in a crystal can profoundly alter the character of the normal modes of vibrations of the crystal, and consequently those crystalline properties in which lattice vibrations play the dominant role. The simplest way to model these atomic vibrations within a crystal is with harmonic approximation[45]. There are other more accurate methods of calculating the effect of temperature on thermodynamic properties of solids[46] which are based on Monte Carlo or molecular dynamics simulations and are computationally much more expensive than harmonic calculations. Calculation of lattice vibrational frequencies which are the square roots of the eigenvalues of the dynamical matrix offers a good test to the atomistic model. These vibrational frequencies are a measure of the stability of the crystal both in the perfect and defect environment.

There have been a continuous effort from the theoreticians in the field of condensed matter physics to develop successful and efficient atomistic models for simulating the point defects in solids starting from the early continuum model[47] to the more exact EPPI model[48]. It is the relaxation and polarization around the defect which need to be simulated properly in these models. In the following subsection we give a review of the existing techniques and physical models.

1.2.1 Techniques and Physical Models based on Atomistic Theory

The development of continuum, quasi-lattice and lattice techniques simulating the distortion around a defect is an interesting feature in the field of point defects. The earliest

continuum models are those given by Jost[47] and Eshelby[49]. While Jost's technique is meant for charged defects only, Eshelby dealt with both charged and neutral ones. Jost showed that due to the presence of the charged vacancy, the induced polarization reduces the formation energy drastically, the polarization energy being as large as the defect formation energy. In order to estimate the polarization term, the whole of the crystal was treated as a dielectric continuum subjected to the field of the defect charge.

In the technique presented by Eshelby, the point defects are regarded as singularities in an isotropic elastic continuum. Unlike the previous works, the effect of the free boundary is included here. In fact, the actual displacement of the continuum around the defect is regarded as the sum of the displacement in an infinite medium and an "image" displacement due to the perturbing effect of the boundary. It was found that on neglecting the free boundary effect, any non spherical body uniformly filled with point singularities would suffer a change of shape as well as volume, while there is only a change of volume when the effect is taken care of.

However , representing a lattice as a continuum, dielectric or elastic, was never beyond debates and there were continuous efforts to develop a lattice technique for point defect calculations. The first semi-lattice approach that was successful is the one introduced by Mott and Littleton[50]. The technique has been widely used in different types of crystals with different types of point defects. Here, the whole of the defect crystal is divided into two regions, Region1 and Region2. Region1 consists of the defect and a few neighbourhood ions whose number will vary from structure to structure and model to model. The displacement and dipole moments of Region1 are treated explicitly in an atomistic way by solving a large set of linear equations depending on the no. of Region1 ions. The remainder of the crystal i.e. Region2 is treated as a continuum and is essentially treated as was done by Jost with some modifications. In their original work, Mott and Littleton solved the Re-

gion1 problem by balancing the forces, both coulombic and non-coulombic. The energy of the defect distorted crystal is written as a sum of the rigid lattice energy, coulomb energy, short range energy and the two polarization energies, one due to Region1 and the other due to Region2.

The first ever static lattice technique was developed by Kanzaki[51] who modeled the vacancy distorted crystal in terms of virtual forces known as the Kanzaki forces that reproduce the distortion and energy changes arising from a vacancy. Fig 1.4(a) shows a perfect undistorted crystal with no forces on any atom, Fig 1.4(b) shows the distorted crystal containing the vacancy and Fig 1.4(c) shows the kanzaki lattice which has the same distortion as the defect lattice but without the vacancy. So the work reduces to simulating the force distribution of the distorted lattice shown in Fig 1.4(c). For this, kanzaki used the harmonic approximation and expansion of the atomic displacements in terms of normal (generalized) co-ordinates. However this lattice static method suffers from one serious problem. Near the defect, there is a rapidly varying strain field and one cannot simply assume that the electrostatic field acting on an ion in this region is zero. So, in a real crystal there is every possibility that the ions near the defect will be polarized as well as displaced. This effect doesn't change the form of the long-range displacement but will change their magnitudes. The original work of Kanzaki was therefore extended [52] to allow for electronic polarization and the resultant displacements of certain close neighbours of the defect.

Another method which is formally equivalent to the Kanzaki method but is more powerful and computationally more convenient is the Green-function method[53]. This method, based on the Born-von Karman model where the crystal is represented by an assembly of interacting atoms arranged in a regular geometric pattern, uses the zero frequency limit of the phonon Green function which gives the static response of the lattice to an applied force. Though this model is physically unrealistic, it has the advantage of yielding results

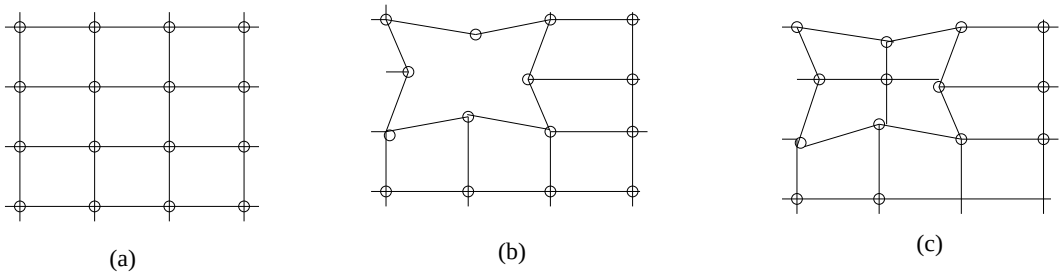

Figure 1.4: Formation of Kanzaki lattice

in closed analytic forms which are very usefull for qualitative discussions.

while all the above techniques implicitely adopted the force balance approach to treat the vacancy problem, it was Kurosawa[54] who first introduced the energy method in treating point defects. This was further generalized by Norgett and Lidiard[55] which is adopted by different models in recent time. The method follows the ML scheme and divides the total energy of the imperfect crystal into three parts: one for Region1, one for Region2 and the last one for the interaction between Region1 and Region2.

Physical Models

Any physical model should first emphasize on how properly it can represent the system it is going to model. The usefulness of a model lies in the transferability of the model amongst similar systems. A model meant for calculation of point defects in a crystal should adequately describe the details of interaction between the atoms and how the energy changes with the change of interaction amongst them. The change in interaction, both coulombic and non-coulombic is caused by the distortion produced by the presence of the defect.

The simplest model definining the constituents of an ionic crystal is the Polarizable Point Ion (PPI) model which is implicit in the Mott-Littleton's work. The model describes each ion to be a point particle with charge and dipole moment. Here the electronic polarizabilities of the ions are related to the refractive indices using the Lorentz-Lorentz equation.

These polarizabilities are widely known as TKS[43] polarizabilities. The local field is evaluated assuming point dipoles located inside Lorentz cavity and cubic symmetry is assumed in the calculations. The relative displacement of the sublattices due to varying charge and polarizabilities makes the low frequency static dielectric constant larger than the high frequency optical one. This displacement polarizability is determined from the force constant of the crystal. To retain the static nature of the defect environment the TKS values for electronic polarizabilities along with the displacement polarizability are used to calculate the static dielectric constant using the Claussius-Mossotti equation. Unfortunately, the static dielectric constant evaluated so, comes out to be much larger than the corresponding experimental value and hence overestimates the polarization energy. This is a failure of the PPI model and was figured out to be the cause of neglecting the finite sizes of the ions. The overlapping of ions reduces the magnitudes of the dipole moments. To take care of this overlap effect, three models were suggested; Shell Model, Deformation Dipole Model and Modified PPI Model.

The Shell model was first introduced by Dick and Overhauser[56]. In this model, the charge of the ion is distributed between a negatively charged massless shell and a positively charged core that interact only via a harmonic potential. The total of shell and core charges should equal to the ionic charge. Interactions between ions include core-core, core-shell and shell-shell coulombic interactions and short range interactions that operate only between shells as shown in Fig. 1.5. Here, the energy surface, either of the bulk or defect crystal, is extensively fitted to the crystal structure, elastic and dielectric properties. It was hardy and Karo[57] who did put another attempt to account for the reduction in polarization due to overlap of ions by adding a deformation dipole in opposition to the induced dipoles via an effective charge e^* to be used instead of e to reproduce the macroscopic properties of the crystal. This deformation dipole model is based on the adiabatic, harmonic, and

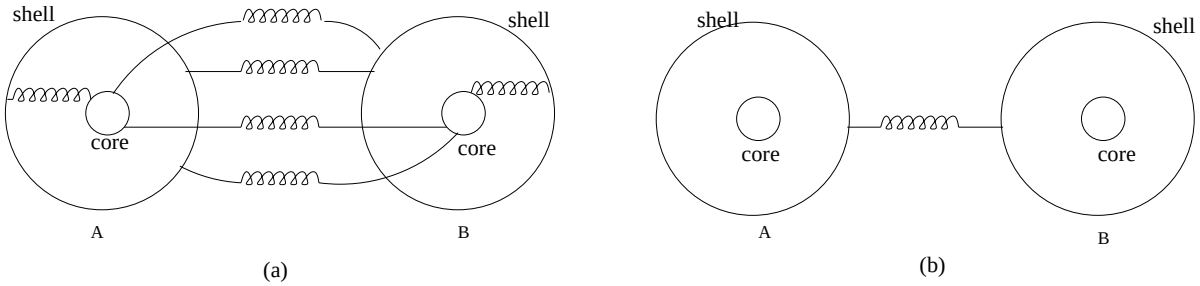

Figure 1.5: Shell model showing (a) coulombic and (b) non-coulombic interactions

linear-dipole approximations, and situates all the dipoles at lattice sites only. In this respect, it can be classified in the same category as the Shell model. The model was later on generalized[58] to introduce interactions called nonlocal electric polarizabilities analogous to the shell-shell interactions in Shell model.

In spite of their sound physical background, both the Shell model and deformation dipole model involve numerous parameters as compared to the PPI model and suffers from complications in formulations even within the dipolar approximation. This was the reason why no attempts were made to take the defect calculations beyond dipoles. It therefore seemed logical to derive a model within the framework of PPI which could also take care of the reduction in polarization. This was done by Murti and Usha[44] who remedied the drawback of PPI model by redefining the electronic polarizabilities as suited to the static lattice environment. This model was named as the MPPI (Modified PPI) model which has the merit of being simple, physical, less parametric and computationally efficient[59]. The success of this MPPI model in a wide variety of defect environments encouraged Murti and Radha[48] to extend the MPPI to include quadrupole polarizabilities of the constituent ions. It was assumed earlier that the electric field of the point defect is spatially homogeneous. This is not true and the extremely high field in the vicinity of the defect results in nonzero field gradient. Thus a new and first ever quadrupolar model was born known as

EPPI (Extended PPI) model. The first application of EPPI[60] was highly successful in demonstrating the reasons for the dominance of the Frenkel disorder on the cationic sublattice of *AgCl* and *AgBr*. The model was also successful in putting insight into the cause of the unusual transport behaviour in these materials[61, 62].

1.3 Atomistic Studies on Thermodynamic Parameters

Before introducing the present work, we briefly go through some studies done on thermodynamic parameters of point defects in ionic crystals with atomistic models. Out of the three basic thermodynamic parameters, namely formation energy, formation volume and formation entropy associated with the formation of a point defect, it is the formation energy which is the largest and the dominant one and hence finds more importance in successive studies of transport properties. Having the simplest rocksalt structure with wide applications in the field of material science, point defects in alkali halides were the first candidate materials which were largely studied with different potential and polarization models. A detailed study of Schottky defects in these ionic crystals were done by Boswarva and Lidiard[63]. The Born model of cohesion was adopted along with the technique of Mott and Littleton. Two kinds of variations were applied - one is the changes in the description of the displacement and polarization field of IInd region and the other is the changes in the form of short range potentials. While the first kind of variation had little effect in the Schottky energy, there were significant change in the energy value with a change in the potential form. The results agreed quite well with the experimental values and was followed by similar studies on *CsCl*-structure alkali halides[64]. There were diffrences in the equilibrium relaxation of nearest neighbours and in inclusion of elastic effects and deformation dipoles. These works were followed by calculation of formation energy of vacancy pairs[65] and interstitial defects[66]. Kanzaki studied monovalent impurities and pairs using lattice statics

method[67]. The calculations were carried out both in the rigid ion model and the polarization ion model. The effect of electronic polarizations came out to be small. A detailed study was made on the formation and migration energies of Schottky and Frenkel defects in all the alkali halide crystals using a set of potentials by Sangster and Atwood. These results were then compared with parallel studies using different potential models.

Thus the overall success of formation energy calculations in alkali halides with different models and techniques pulled the attraction towards a similar system of ionic crystals-i.e. alkaline earth flourides. Catlow and Norgett[68] obtained Shell model potentials for CaF_2, SrF_2 and BaF_2 by fitting models to macroscopic data for these crystals. These potentials were then used to calculate the formation and migration energies in these crystals. This was followed by a comprehensive theoretical survey of mechanisms and energetics of ion transport. This calculation was done with a new set of crystal potential with a more reasonable description of the anion-anion interactions[69]. New computer codes for simulating point defects in rare-earth-doped alkaline-earth fluorides were also developed in FORTRAN [135]. It was found that the calculated reoriention enthalpies were larger than the experimental values. However, the variation of the enthalpy with the size of the rare earth was in reasonable agreement with experiment. With the same high symmetric cubic structure, another important class of ionic crystals are alkaline earth oxides. A detailed study of defect energetics in these crystals was carried out using Shell model[70]. It was found that the defect energies are largely independent of the shell parameterisation, thereby confirming the view that it is important principally to provide for the total dielectric response of the lattice rather than the individual contributions from the constituting ions.

It may be noted that all these studies were carried out for materials with cubic symmetry. The first attempt to deviate from cubic to non-cubic materials was the calculation of Schottky energy and cation migration in Potassium Azide crystals[71]. Potassium azide

which is a member of the family of alkali azide compounds has many similarities with the alkali halides. Here the role of the spherically symmetric halogen ions is taken by the non-spherical azide ion(N_3^-). Owing to the non-spherical shape of the azide ion, the azides crystallize in structures of lower symmetry than the corresponding halides. Potassium azide (KN_3) has a body centered tetragonal structure with the space group $I4/mcm$. The point defect calculations were performed first in a rigid lattice approximation and then with the polarization and relaxation included. The calculations were repeated for three different potentials and it was found that for all three potentials the energy of anion vacancy formation exceeds that for cation vacancy formation. This was a consequence of the additional degrees of relaxational freedom afforded by the rotation of the azide ions neighbouring the cation vacancy. Another attempt of defect calculation in non-cubic materials was done on Zinc Oxide with a hexagonal structure[72] using Shell model. This material having some amount of covalency recieved less attention due mainly to difficulties associated with the derivation of suitable interatomic potentials. The relevant potentials were then obtained from *ab initio* molecular orbital calculations. These calculations were followed by a detailed survey of the defect energetics in $\alpha - Al_2O_3$ and TiO_2[73]. The structure of both the corrundum lattice of alumina and the rutile lattice adopted by TiO_2 are based on hexagonal close packing of the oxide sublattice. This work paid particular attention to the effects on the calculated energetics of the use of Mott-Littleton methods adapted for anisotropic crystals. Another feature considered in detail was the sensitivity of calculated defect energies to the choice of lattice potential and to the size of the atomistically simulated region surrounding the defect. The result supported the dominance of Schottky disorder in both the crystals.

As for the determination of characteristic volumes of point defects in ionic crystals there are a number of works on crystals with rocksalt[74, 75, 76, 77, 78, 79] , caesium

chloride[80], fluorite[81, 82, 79] and other[83] structures. The formation volume of point defects is the quantity which determines the effect of pressure upon the corresponding defect 'reaction'. In general, the free volumes of formation of Schottky defects are greater than or roughly equal to the molecular volume while for Frenkel defects they are a fraction of the molecular volume. The calculation of formation volume is not as straightforward as the formation energy which are most conveniently done at constant volume. The general practice is to use the relationship between the volume of relaxation and the magnitude of the elastic strain field around the defect similar to the static lattice method of Kanzaki[51]. This method yields explicit expressions for the elastic strengths of defects in terms of the forces acting on the atoms of the lattice. In ionic crystals, it is expected that the displacements of the nearest neighbours to the vacancy are outwards. This implies an increase in volume and increase of lattice parameter. The initial theoretical work on volume of formation of Schottkty defects[76] suffered from a serious drawback that it gave negative volume of relaxations and conflicts the experimental values. The outward relaxation was also confirmed by the X-ray diffuse scattering in KBr[84]. A reexamination of the theory[85] also failed to resolve the problem. A probable solution was offered by Bauer and Leutz[86] within the continuum model. However there was a need to go beyond continuum model and solve the problem within the lattice theory. It was Lidiard[78] who observed that there was an anharmonic correction to the usual expression for the defect volume, which in the case of Schottky defects is large and positive. This correction term when added to the previous values[76] partly removed the discrepency in formation volume. Another succesful approach was followed by Gillan[79] who introduced a new method which yielded the correct sign and approximate magnitude for the volume of formation in alkali halides. This work also gives satisfactory agreement with experiment for the formation volume of Frenkel defect pairs in the alkaline earth fluorides having the fluorite structure.

Though the majority of the theoretical studies of defect parameters have concentrated on energy and volume terms, the detailed predictions of the concentration of defects and the rates of defect migration require knowledge of appropiate entropy term. Early works on entropy calculations were based on the ionic displacements produced by the creation of vacancies by Tosi- Fumi model[87]and Einstein model[88]. In the later work[88], both electric and elastic contributions to the ionic displacements were considered. With the same method, anharmonic effects were also included in a later work[89]. Other approaches of calculating defect entopy were based on the Green's function technique, the Supercell technique, and the embedded crystalline method. These techniques have their own merits and demerits[90]. For example, by Green's function method one can obtain the change in the whole spectrum of the crystal, but it is difficult to take a complete account of the perturbation introduced by the defect. In the Supercell technique, on the other hand, it is possible to take account of the perturbation more appropiately than is normally taken in the Green's function method, but it is difficult to calculate the change in the whole phonon spectrum. In the embedded-crystalline method, a region of the crystal containing the defect is allowed to vibrate in a frozen outer region and a convergence in the entropy value is attempted by increasing the size of the inner region. The drawback of this method comes in convergence and in dealing with the vibrations of a large crystallite explicitely. Out of these techniques, however, it is the Green's function technique which have been used widely and successfully. This technique was first introduced by Govindarajan[91] in calculating the non-configurational entropy changes associated with the substitution of Na^+, Rb^+ or Ag^+ in KCl. A rigorous application of this technique was done[92] for calculating the entropy of formation of an interstitial and of an anion vacancy in CaF_2. The calculated values were found to be significantly lower than the experimental values. In these works actually neither the Green's functions nor the perturbation was represented consistently. The method was

improved by Dash et. al.[90] by taking a single set of potentials to calculate both Green's function and perturbation matrices exactly at the temperature where the entropy is to be evaluated. This method was named as 'Determinant method'. In the same work, Green's function was employed to compute the change in the vibrational frequency spectrum due to formation of a Frenkel pair to calculae the entropy through integration and the method was called 'Integration method'. The results obtained through the 'Determinant method' for different alkaline earth fluorides agreed well with the experimental values.

The first computational codes which provided an easy platform to point defect calculations were incorporated in the HADES packages. The earlier HADESII package written by Norgett[93] was confined to cubic systems. An essential feature of HADES methodology is the use of the Mott-Littleton approximation to calculate the displacements around the defect. The polarizabilities of individual ions were taken care of through Shell model. The codes provide maximal use of symmetry to reduce the number of working variables to within reasonable limits. The codes were extended by Catlow, James, Mackrodt and Stewart[73] as HADESIII, which can be used for defect calculations on noncubic systems. With further refinements the same approach as followed in HADES were implemented in GULP (General Utility Lattice Program) codes[94]. This package was designed to perform a variety of tasks relating to three dimensional solids. One important feature in GULP is that it provides fast and efficient optimization programs which is essential for all defect calculations. Here, the structure is optimized with respect to the asymmetric unit fractional co-ordinates and cell strains, using analytical symmetry-adapted first and second derivatives within a Newton-Raphson procedure starting from the exact Hessian matrix.

1.4 The Present Work

The defect calculations based on PPI models were pursued by Murti et al.[44]. The model was also extended to include quadrupole moments[48, 95, 96]. However, the application of these models were limited to highly symmetric cubic structures containing monovalent ions using the standard Mott-Littleton algorithm. The present work was undertaken to remove some of these constraints.

In spite of the enormous progress in computing technology both in speed and memory, most of the atomistic defect calculations, till date, are done with Mott-Littleton approximations as far as simulation of distortion around the defect is concerned. This quasi lattice technique divides the crystal into two regions and treats them on separate footing. However, this raises a question regarding the size of the optimal inner region. There is a need to give a fresh look at computational algorithms to minimize the approximations introduced by quasi lattice technique. In the present work, we proposed a systematic scheme to calculate the defect parameters by studying finite clusters and obtain the thermodynamic limits to calculate defect properties. This scheme is computationally more demanding as far as the computational algorithm is concerned. The usefulness of the scheme is demonstrated in test case of *NaCl* which has been studied thoroughly and the result compares fairly well with the experimental data.

The outstanding success of EPPI model in establishing the quantitative role of induced quadrupoles on the defect formation process in *AgCl* and *AgBr* has indeed opened a new room of studying these parameters afresh in crystals especially with highly polarizable ions. It was found that the results of defect calculations in Alkaline Earth Oxides by Shell model were not satisfactory and therefore these oxides are good candidates to reinvestigate the results. This encouraged us to do some study on Schottky formation energies in these crystals with EPPI formulations. We also give a comparison with the experimental results

for Magnesium Oxide which is the prime member of this family of Oxides.

Above all, a detailed review of the relevant works revealed that even after few decades from the birth of PPI model, no attempt has been made to simulate a low symmetry ionic crystal with PPI formulations. This is probably because it is more complicated to formulate the problem in low symmetry with this model than any other existing ones. The dipole energy terms, though not as notorious as the coulomb terms from convergence point of view, needs a very careful treatment. The problem becomes more severe when the electrostatic force does not vanish even at the perfect ion sites. This electrical imbalance at the lattice sites induces dipole moments to the ions in the perfect lattice. Usually, the short range potential parameters are obtained by fitting bulk properties of the perfect crystal. This ignores the induced atomic dipoles in crystal environment. In case of low symmetry crystals, one can not use the same potential parameters and they are to be derived with a new scheme. In the first part of this study, we propose a method to derive the potential parameters for an optimized crystal. In the second part, we have proposed the possible way to calculate the defect parameters. These calculations were done on the low symmetry monoclinic $\beta - Ga_2O_3$.

1.5 Plan of the Thesis

In this thesis we concentrate to understand the point defect and its thermodynamics based on PPI model and two different techniques. The background of this work has already been outlined in the preceding sections. In Chapter 2, we give the general formulations that will be used to simulate both the perfect and defect crystal. First part of this chapter discusses the short range potential model, the polarization model and the lattice energy of a perfect crystal. In the second part, the most general schemes of defect calculations are given.

In Chapter 3, we describe the first part of our work. This is on the new technique of

finite size simulation of point defects in ionic crystals. A detail of the scheme is given which is followed by energy calculations. Results are presented in a way to reflect the basic idea of the scheme. A comparison of the present result with some earlier results is given at the end of the chapter. In Chapter 4 we describe Schottky defect calculations of Alakaline earth oxides with the quadrupolar EPPI model. Input potential and polarization parameters are listed in the beginning of the chapter along with an outline of the model. Various energy terms are quoted in explicit forms to be used for the final results. Results are presented both in tables and figures to clearly demonstrate the usefulness of the model. We also compare some of the results with the existing experimental data. In Chapter 5, we give an algorithm to simulate low symmetry crystals with MPPI scheme. We choose the low symmetry crystal $\beta - Ga_2O_3$ for our study. The chapter begins wih a description of the structure and symmetry of the crystal. In the second part of the chapter we propose a way of estimating the short range potential parameters in such crystals with MPPI model taking care of the induced dipole moments. This is followed by derivation of defect formulations. The chapter concludes with a fresh proposal to simulate point defects in low symmetry crystals. In Chapter 6, we present a summary of the work and some future prospects.

Chapter 2

Modeling of Perfect Ionic Crystal and Theory of Point Defect Energetics

2.1 Modeling of Perfect Crystal

The accuracy of atomistic calculations for defect formation energy and other defect related studies in a material is largely attributed to the modeling of its constituent ions in the perfect environment. The modeling of a perfect crystal implies the modeling of its interionic potentials. In an ionic crystal, it is the coulomb term which dominates the crystal dynamics and is very long ranged. This results in slow convergence in lattice sums and makes the computation very expensive. The problem is solved by using Ewald's method [Appendix A]. In different PPI models, the Coulomb terms are fixed with fixed charges to the ions. So, it is the polarization and the effect of overlap of the ions which play crucial role in simulating the crystal.

2.1.1 The Short Range Potential Model

van der Waals Interactions

The van der Waal interaction is the principal binding force in solids where the atoms or molecules are electrically neutral. In an ionic material, this interaction comes as a secondary force in addition to the long range electrostatic forces. To understand the origin of this force, we have to look inside an atom. The electrons inside an atom are in constant motion giving rise to a fluctuating charge distribution or temporary dipole moments. The mean value of these dipole moments of individual atoms over any period of time is zero. So, if we imagine a system of uncorrelated atoms, there will be no net force acting on the system. But if the atoms are close enough, like in a crystal, the instantaneous dipole moment of one atom will induce a dipole moment in a nearby atom and so on. The interaction amongst these induced dipole moments give rise to an interaction of the order of r^{-6}, where r is the interatomic distance. Interactions involving fluctuating and induced moments higher than the dipoles will give energies with inverse powers higher than 6.

For our present calculations, we consider van der Waal interactions involving dipole terms only. The general expression for this potential is

$$\Phi(r) = -\frac{C}{r^6} \tag{2.1}$$

where C is the van der Waal coefficient.

Overlap Repulsive Interactions

The modeling of a perfect crystal is incomplete unless we consider the quantum effects between the constituent ions when they come close to each other. As two ions approach each other, their respective electron distributions start to overlap. As soon as this happens,

the electrons in the ions start behaving as independent entities and interact with each other directly thereby increasing the energy of the system. In addition to this, the overlap of electron clouds evoke Pauli's Exclusion Principle and make some of the electrons in the overlapping regions to jump into higher energy states. So there is an overall increase in energy which gives rise to a net repulsion of short range nature. Fig. 2.1 shows the van der Waal attraction and the short range repulsion between a pair of ions.

It is difficult to calculate the repulsive interaction energy between a pair of polyatomic ions by quantum mechanical method. So it is the semi-empirical method which is adopted mostly, in which a functional form with model parameters is used to define the interaction. The most commonly used function for the repulsive interaction is the Born-Mayer function defined as

$$\Phi(r) = A \exp\left(-\frac{r}{\rho}\right) \tag{2.2}$$

The Born-Mayer potential along with the r^{-6} van der Waal dispersive term is known as the Buckingham Potential with the form

$$\Phi(r) = A \exp\left(-\frac{r}{\rho}\right) - \frac{C}{r^6} \tag{2.3}$$

This Buckingham potential is widely used in simulating ionic crystals including a wide range of oxides.The strength parameter A, hardness parameter ρ and van der Waal coefficient C are usually determined empirically by fitting these parameters to the experimental structure as well as mechanical and elastic properties. This needs a reasonable estimate of the starting parameters and an efficient optimization and fitting program. The General Utility Lattice Programme (GULP)[94] provides a tool for estimating these parameters. GULP is based on Shell model.

For a high symmetry crystal, like cubic *NaCl* or *MgO*, where the ions sit at electrically

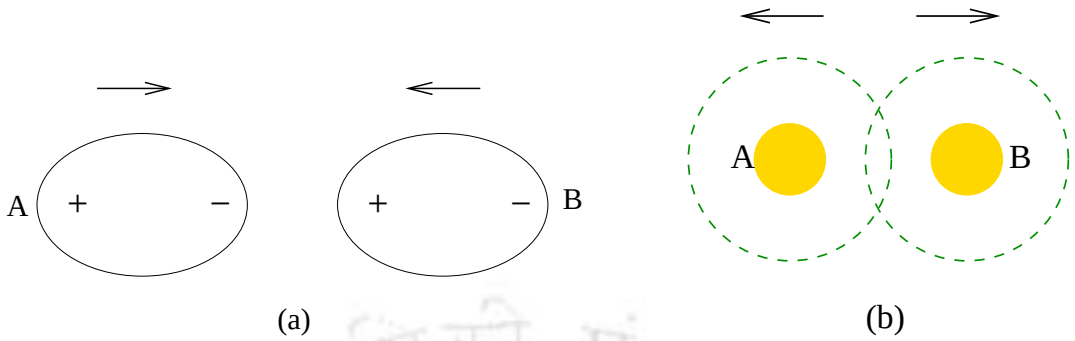

Figure 2.1: (a) The van der Waal attraction and (b) Overlap repulsion between ions A and B

neutral positions, with zero dipole moments, the ionic polarization does not play any role in modeling the short range parameters. There are precalculated reliable sets of potentials for such crystals from semi-empirical as well as first principle approaches which can be used for any atomistic calculations. But the situation is not same in case of a very low symmetry crystal like monoclinic $\beta - Ga_2O_3$ where ions even at their perfect sites experience a net electric field and hence have induced dipole moments. However the crystal has centrosymmetric unit cells and for each ion in the unit cell there is another ion whose dipole moment exactly cancels that of the former one. The polarized ions in Ga_2O_3 in perfect environment makes the simulation rather complicated with PPI formulations. Placed in a uniform electric field, unlike high symmetry crystals where the dynamics of the ions are governed by the change in the short range forces only, the long range electrostatic forces (Coulomb as well as dipole) also come into the picture. The fitting of potential parameters would therefore involve the ionic polarizabilities also as fitted variables, just like spring constants in shell model.

2.1.2 The Polarization Model

The keypoint in any atomistic calculation of an ionic crystal with PPI formulation lies on how we model the polarizabilities of individual ions. There are two manifestations of putting a polarizable point ion in an electric field. Firstly, if the field is strong enough, the ion experiences a bodily displacement giving rise to a displacement polarizability α_d. Secondly, the electronic configuration inside the ion gets distorted imparting electronic polarizability α_i to each of the ions. The total polarizability α of any ion in the crystal is a sum of these two. i.e.

$$\alpha = \alpha_{\mathrm{i}} + \alpha_{\mathrm{d}} \tag{2.4}$$

Displacement Polarizability

With an uniform external electric field $\mathbf{F}_{\mathrm{ext}}$ acting on it, the lattice energy of a crystal can be written as

$$\mathrm{E} = \mathrm{E_o} + \frac{1}{2}\boldsymbol{\xi}^{\mathrm{T}}\mathbf{W}\boldsymbol{\xi} - \mathrm{q}^{\mathrm{T}}(\boldsymbol{\xi}.\mathbf{F}_{\mathrm{ext}}) - \boldsymbol{\mu}.\mathbf{F}_{\mathrm{ext}} \tag{2.5}$$

If there are s ions in one unit cell, $\boldsymbol{\xi}$ is a 3s dimensional vector of displacements, q is an s-dimensional array of charges, $\boldsymbol{\mu}$ is the 3s dimensional vector of ionic dipole moments and $\mathbf{W}$ is the $3\mathrm{s} \times 3\mathrm{s}$ force constant matrix. At equilibrium,

$$\begin{aligned} \frac{\partial(\mathrm{E} - \mathrm{E_o})}{\partial \xi} &= 0 \\ \Rightarrow \mathbf{W}\boldsymbol{\xi} - \mathrm{q}\mathbf{F}_{\mathrm{ext}} - \frac{\partial \boldsymbol{\mu}}{\partial \xi}.\mathbf{F}_{\mathrm{ext}} &= 0 \end{aligned} \tag{2.6}$$

So, the ionic displacement can be expressed in component form as

$$\xi^{\alpha} = \left(\left[\mathbf{W}^{-1}\right]^{\alpha\beta}\left\{\mathrm{q} + \sum_{\gamma}\left(\delta\mu_{\gamma}\right)^{\beta}\right\}\right)\mathrm{F}^{\beta}_{\mathrm{ext}} \tag{2.7}$$

In order to avoid the translational mode in the crystal with the applied electric field, we fix one ion in the unit cell and allow all the other ions to move. Out of the rest $(s-1)$ ions, the displacement dipole moment component of the i^{th} ion can be written as

$$\begin{aligned} p^{\alpha}_{d,i} &= q_i \xi^{\alpha}_i \\ &= q_i \left[\sum_j \sum_{\beta} \left[\mathbf{W}^{-1} \right]^{\alpha\beta}_{ij} \left\{ q + \sum_{\gamma} \left(\delta\mu_{\gamma} \right)^{\beta} \right\} \right] F^{\beta}_{ext} \end{aligned} \tag{2.8}$$

Again,

$$p^{\alpha}_{d,i} = \sum_{\beta} \alpha^{\alpha\beta}_{d} F^{\beta}_{ext} \tag{2.9}$$

So, from 2.8 and 2.9 we get

$$\alpha^{\alpha\beta}_{d,i} = q_i \sum_j \left[\mathbf{W}^{-1} \right]^{\alpha\beta}_{ij} \left\{ q + \sum_{\gamma} \left(\delta\mu_{\gamma} \right)^{\beta} \right\} \tag{2.10}$$

here the indices i and j goes over the $(s-1)$ unit cell ions.

Electronic Polarizability

Ions in a crystal would behave differently when subjected to a high frequency and a low frequency field. With a high frequency optical field the ions as a whole cannot respond to the field. It is only the electronic configuration which undergo distortion giving rise to optical polarizability or the so called TKS polarizability[43]. The TKS polarizabilities are calculated from the Lorentz-Lorentz relation given by

$$\alpha_i = \frac{3v_m}{4\pi} \left(\frac{\epsilon_\infty - 1}{\epsilon_\infty + 2} \right) \tag{2.11}$$

Here v_m is the unit cell volume and ϵ_∞ is the high frequency dielectric constant of the material.

However, in case of a static field, like the one created by a point defect, the ions do respond to the field and the appropriate connection between the macroscopic dielectric constant and microscopic polarizabilities is given by the Claussius-Mossotti relation [Appendix B].

$$\alpha_i + \alpha_d = \frac{3v_m}{4\pi}\left(\frac{\epsilon_s - 1}{\epsilon_s + 2}\right) \tag{2.12}$$

Here, ϵ_s is the static dielectric constant. PPI model in its original form uses the TKS values for electronic polarizabilities which overestimates the static dielectric constant as compared to the experimental value. This is not desirable as the static dielectric constant is a crucial parameter in point defect simulation estimating the static response of the crystal. The Deformation Dipole model and Shell model accounts for the reduction in polarization due to short range forces explicitly.

It is the MPPI (Modified Polarizable Point Ion) model suggested by Murti & Usha[44] where the electronic polarizabilities are redefined as suited to the static lattice environment to reproduce the static dielectric constant within the simple PPI formulation. Once a suitable set of potential parameters are obtained, α_i in eq. 2.12 are fitted to reproduce the experimental value of ϵ_s. We follow this MPPI rule in our present calculations.

2.2 Dipole Moment of Ions in a Perfect Crystal

As discussed in §2.1.1, we cannot neglect the contribution of polarization energy to the perfect lattice energy in case of a low symmetry crystal. With the translational symmetry taken into account, the problem reduces to solving the dipole moments of the unit cell ions.

Neglecting the higher order moments, the exact equation for solving dipole moment of

an ion at site i is

$$\boldsymbol{\mu}_i = \alpha \left(\mathbf{F}_i^m + \mathbf{F}_i^d \right) \tag{2.13}$$

Where α is the electronic polarizability and $\mathbf{F}_i^m$, $\mathbf{F}_i^d$ are the total monopole and dipole fields acting on the ion sitting at i^{th} site.

The problem comes as how to ensure an efficient convergence of the fileds. While convergence in dipole field can be attained by doing direct sum over sufficient number of ion sites, monopole field is not easy to calculate. The only way out is to use Ewald method. This can be done by taking the derivative of the Ewald energy [Appendix A].

The inclusion of perfect dipole moment has the effect of changing the displacement polarizability of the individual ions as shown in §2.1.2 along with changing the lattice energy of the crystal to be discussed in the following section. This in turn affects the equilibrium condition of the crystal.

2.3 Lattice Energy of a Perfect Crystal

The potential energy of a perfect ionic crystal can be straightaway divided into two parts - the long range electrostatic part and the short range overlap repulsion as well as van der Waal part.i.e.

$$\Phi_{ij} = \Phi_{ij}^{LR} + \Phi_{ij}^{SR} \tag{2.14}$$

The short range energy is evaluated using expression 2.3. In the next section we discuss the electrostatic term.

2.3.1 Electrostatic Energy

In the absence of any induced dipole moments, the electrostatic energy of a system of ions can be written as

$$E^{ES} = \sum_{ions} q\Phi - \sum_{ions} \boldsymbol{\mu}.\mathbf{F} \tag{2.15}$$

where Φ and $\mathbf{F}$ are the potential and the field at respective ion sites due to all other ions. We have neglected the higher order terms here.

However if the ions are close enough to influence each other, they will induce polarization in the neighbouring ions. In that case, we need to take care of the dipole self energy term also.

So, the total electrostatic energy of a crystal with polarizable point ions comes out to be

$$E^{ES} = E^{mm} + E^{dm} + E^{md} + E^{dd} + E^{self} \tag{2.16}$$

where, E_{mm} is the monopole-monopole , E^{dm} and E^{md} are the monopole-dipole, and E^{dd} is the diple-dipole interaction energies. The last term E^{self} is the energy of formation of the induced dipole moments.

Writing explicit expressions for the individual terms, E^{ES} becomes

$$\begin{aligned} E^{ES} = & \sum_{i,j\in L, j>i} \frac{q_i q_j}{\left|\mathbf{r}_i - \mathbf{r}_j\right|} + \sum_{i,j\in L, j\neq i} \frac{q_i \left\{\boldsymbol{\mu}_j \cdot \left(\mathbf{r}_i - \mathbf{r}_j\right)\right\}}{\left|\mathbf{r}_i - \mathbf{r}_j\right|^3} \\ & - \sum_{i,j\in L, j>i} \left[3\frac{\left\{\boldsymbol{\mu}_i \cdot \left(\mathbf{r}_i - \mathbf{r}_j\right)\right\}\left\{\boldsymbol{\mu}_j \cdot \left(\mathbf{r}_i - \mathbf{r}_j\right)\right\}}{\left|\mathbf{r}_i - \mathbf{r}_j\right|^5} - \frac{\boldsymbol{\mu}_i \cdot \boldsymbol{\mu}_j}{\left|\mathbf{r}_i - \mathbf{r}_j\right|^3} \right] + \sum_{i\in L} \frac{\mu_i^2}{2\alpha} \end{aligned} \tag{2.17}$$

Here L is the set of entire ion sites. Using

$$\sum_{j\neq i} \frac{q_j \left(\mathbf{r}_i - \mathbf{r}_j\right)}{\left|\mathbf{r}_i - \mathbf{r}_j\right|^3} = \mathbf{F}_i^m \tag{2.18}$$

and

$$\sum_{j\neq i} 3\frac{\left(\mathbf{r}_i-\mathbf{r}_j\right)\left\{\boldsymbol{\mu}_j\cdot\left(\mathbf{r}_i-\mathbf{r}_j\right)\right\}}{\left|\mathbf{r}_i-\mathbf{r}_j\right|^5}-\frac{\boldsymbol{\mu}_j}{\left|\mathbf{r}_i-\mathbf{r}_j\right|^3}=\mathbf{F}_i^d \tag{2.19}$$

we rearrange the terms in E^{ES}

$$E^{ES}=\sum_{i,j\in L,j>i}\frac{q_iq_j}{\left|\mathbf{r}_i-\mathbf{r}_j\right|}-\frac{1}{2}\sum_{i,j\in L}\boldsymbol{\mu}_i\cdot\mathbf{F}_j^m-\sum_i\frac{1}{2}\boldsymbol{\mu}_i\cdot\left[\mathbf{F}_i^m+\mathbf{F}_i^d\right]+\sum_i\frac{\mu_i^2}{2\alpha} \tag{2.20}$$

Now, using eq. 2.13,

$$\sum_i\frac{1}{2}\boldsymbol{\mu}_i\cdot\left[\mathbf{F}_i^m+\mathbf{F}_i^d\right]=\sum_i\frac{\mu_i^2}{2\alpha} \tag{2.21}$$

Thus the last two terms in eq. 2.20 cancels out and we are left with

$$\begin{aligned}E^{ES} &= \sum_{i,j\in L,j>i}\frac{q_iq_j}{\left|\mathbf{r}_i-\mathbf{r}_j\right|}-\frac{1}{2}\sum_{i,j\in L}\boldsymbol{\mu}_i\cdot\mathbf{F}_j^m\\ &= E^{mm}-\frac{1}{2}E^{md}\end{aligned} \tag{2.22}$$

It is essential to evaluate the coulomb term with much care and attention as it is the dominant term for many inorganic materials including oxides. An efficient calculation of this term can be achieved trough the Ewald summation [Appendix A] where the sum over inverse distance is split into two rapidly converging series, one in the real space, and the other in the reciprocal space.

2.4 The Second Derivative or Hessian Matrix of Energy

It is essential to calculate the second derivative or Hessian matrix of the energy to get the static dielectric constant property of the crystal. Moreover, the positive definiteness of the Hessian matrix ensures a true minimum of the multivariative system. We expand the lattice energy U_L with respect to equilibrium state

$$U_L(\mathbf{R}_1 + \mathbf{r}_1, \mathbf{R}_2 + \mathbf{r}_2, ...) = U_L(\mathbf{R}_1, \mathbf{R}_2, ...) + \sum_{i\alpha} \left.\frac{\partial U_L}{\partial r_i^\alpha}\right|_0 r_i^\alpha + \frac{1}{2}\sum_{ij\alpha\beta} r_i^\alpha r_j^\beta \left.\frac{\partial^2 U_L}{\partial r_i^\alpha \partial r_j^\beta}\right|_0 + ... \tag{2.23}$$

where i, j goes over the ions and α, β goes over the three cartesian degrees of freedom. At equilibrium

$$\sum_{i\alpha} \frac{\partial U_L}{\partial r_i^\alpha} = 0$$

So the hessian matrix

$$W^{\alpha\beta} = \left.\frac{\partial^2 U_L}{\partial r_i^\alpha \partial r_j^\beta}\right|_0 \tag{2.24}$$

If Φ_{ij} is the interionic potential energy between any two ions i and j, the lattice energy of one unit cell will be

$$U_L = \frac{1}{2}\sum_l \sum_i \sum_j \Phi_{ij}(|\mathbf{R}_l + \mathbf{R}_i - \mathbf{R}_j + \mathbf{r}_i - \mathbf{r}_j|) \tag{2.25}$$

where l goes over all unit cells.

Φ_{ij} consists of both the long range electrostatic part as well as the short range part. The short range part in turn consists of the Born-Mayer overlap repulsion potential and the attractive van der Waal potential arising from the dipole-dipole interaction. Similarly, the

long range electrostatic part has both the Coulomb as well as dipole interactions.

$$\Phi_{ij}(|\mathbf{r}|) = \frac{q_i q_j}{r_{ij}} + q_i \frac{\boldsymbol{\mu}_j \cdot \mathbf{r}_{ij}}{r_{ij}^3} + q_j \frac{\boldsymbol{\mu}_i \cdot \mathbf{r}_{ji}}{r_{ij}^3} - A_{ij} \exp\left(-\frac{r_{ij}}{\rho_{ij}}\right) + \frac{C_{ij}}{r_{ij}^6} \tag{2.26}$$

Here, q's and μ's are the electrostatic charges and dipole moments. r_{ij} is the distance between the pair of ions. We take the second derivative of U_L which gives

$$W^{\alpha\beta} = \delta_{km} \sum_{l} \sum_{j \neq k} \frac{\partial^2 \Phi_{kj}(r)}{\partial r^\alpha \partial r^\beta} - \sum_{l} \frac{\partial^2 \Phi_{kj}(r)}{\partial r^\alpha \partial r^\beta} \tag{2.27}$$

The second derivative of energy is easy and straightforward to calculate only when the ions in the perfect environment are at electrostatically neutral positions. That means there are only monopole and short range terms. As soon as the dipole term comes into the picture, it involves a calculation of second derivative of dipole moment which is rather complicated and expensive. In that case, it is more viable to go for numerical calculation of the Hessian matrix than an analytical derivation.

Let $f(x_1, .., x_i, .., x_j, ..x_n)$ be the energy function, where $x_1, x_2 ... x_n$ are the relaxations of the unit cell ions. Then using Stirling's formula[97], the first derivative of function $f(x_1, .., x_i, .., x_j, ..x_n)$ w.r.t. x_i can be written as

$$\frac{\partial f}{\partial x_i} = \frac{f(x_1, .., x_i + h, .., x_n) - f(x_1, .., x_i - h, .., x_n)}{2h} \tag{2.28}$$

h is a small number to be fixed by convergence test.

This formula can be extended to get the second derivative of energy as

$$\frac{\partial^2 f}{\partial x_i \partial x_j} = \frac{1}{4h^2} (f1 - f2 - f3 - f4) \tag{2.29}$$

Here,

$$f1 = f(x_1, .., x_i + h, .., x_j + h, ..x_n)$$

$$f2 = f(x_1, .., x_i + h, .., x_j - h, ..x_n)$$

$$f3 = f(x_1, .., x_i - h, .., x_j + h, ..x_n)$$

$$f4 = f(x_1, .., x_i - h, .., x_j - h, ..x_n)$$

2.5 Energetics of Point Defects

Putting a point defect in an ionic crystal has a long range electrostatic effect. It has been a challenge to simulate the point defects in the ionic crystals efficiently so as to get a reliable set of thermodynamic parameters which are crucial for subsequent study of defect oriented transport properties in those crystals. The quest is still far from its goal in case of a low symmetry crystal where the simulation of the perfect crystal itself is not really an easy task.

From computational point of view it is impossible to treat all the ions in an infinite crystal at atomistic level. There must be some approximations so as to treat the ions far away from the defects in a less expensive way. Mott and Littleton (ML)[50] therefore devised a scheme for such defect calculation which has been used widely over last several decades of time.

2.5.1 ML Scheme

In Mott-Littleton scheme, the whole of the crystal with the defects in it are divided into two regions, Region1 and Region2, as shown in fig. 2.2. Region1 consists of the defects and a few number of ions around them. Region2 covers the rest of the crystal. Region1 is treated atomistically with the displacements and the dipole moments of individual ions under MPPI

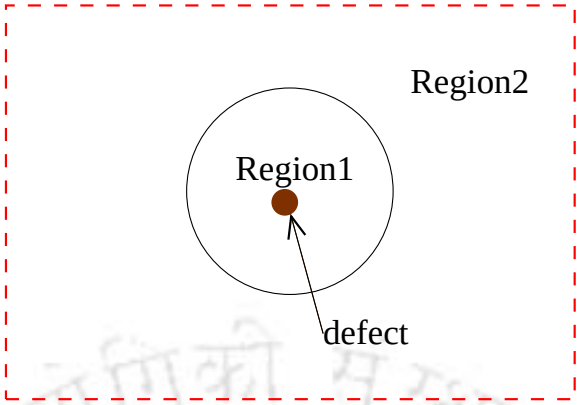

Figure 2.2: ML scheme

model evaluated exactly. Region2 is treated harmonically with the assumption that most of the effects of the defect are already consumed by Region1. In spite of the debate[60, 98] regarding the compatibility of splitting the crystal into two regions at different footing and using macroscopic polarization in the theory of defect calculations, the ML scheme, with some limitations, has come out to be a well established scheme at quasi-continuum level.

The most relevant and important question at this stage is regarding the size of Region1. The smaller we can keep Region1, faster will be the calculations. However, MPPI model plays a very optimistic role here by saying that if we simulate the interionic forces in the crystal in such a way that it shows the electric response to the static field as suited to the experimental observables, Region1 is sure to be small enough comprising of only a few shells around the defect. This makes the computation less expensive.

2.5.2 Splitting the Energy Terms with ML Scheme

As the ML scheme dictates, the defect energy of the crystal can be splitted as[99]

$$E = E_I(\mathbf{s}, \boldsymbol{\mu}) + E_{I,II}(\mathbf{s}, \boldsymbol{\mu}, \boldsymbol{\xi}) + E_{II}(\boldsymbol{\xi}) \tag{2.30}$$

Here, $E_I(\mathbf{s}, \boldsymbol{\mu})$ is the energy of Region1, $E_{I,II}(\mathbf{s}, \boldsymbol{\mu}, \boldsymbol{\xi})$ is the Region1 and Region2 interaction energy while $E_{II}(\boldsymbol{\xi})$ is the energy of Region2. $\mathbf{s}$ and $\boldsymbol{\mu}$ are the displacement and diple moment of Region1 describing the configuration of Region1 and $\boldsymbol{\xi}$ is the displacement of Region2 ions.

It has been a well established practice to make harmonic approximations for Region2 to avoid the infinite sum associated with it. In this approximation, $E_{II}(\boldsymbol{\xi})$ is defined to be a quadratic function of $\boldsymbol{\xi}$.

$$E_{II}(\boldsymbol{\xi}) = \frac{1}{2}\boldsymbol{\xi}^T \mathbf{A} \boldsymbol{\xi} \tag{2.31}$$

$\mathbf{A}$ is the hessian matrix. Eq. 2.31 together with the condition of equilibrium $\frac{\partial E}{\partial \xi} = 0$ leads us to

$$E_{II}(\boldsymbol{\xi}) = -\frac{1}{2} \left. \frac{\partial E_{I,II}(\mathbf{s}, \boldsymbol{\mu}, \boldsymbol{\xi})}{\partial \xi} \right|_{\xi=\xi_o} \cdot \boldsymbol{\xi}_o \tag{2.32}$$

where $\boldsymbol{\xi}_o$ are the equilibrium values of $\boldsymbol{\xi}$ corresponding to arbitrary values of $\mathbf{s}$. So, we can now write the total energy as

$$E = E_I(\mathbf{s}, \boldsymbol{\mu}) + E_{I,II}(\mathbf{s}, \boldsymbol{\mu}, \boldsymbol{\xi}) - \frac{1}{2} \left. \frac{\partial E_{I,II}(\mathbf{s}, \boldsymbol{\mu}, \boldsymbol{\xi})}{\partial \xi} \right|_{\xi=\xi_o} \cdot \boldsymbol{\xi}_o \tag{2.33}$$

Let us now find an explicit representation of the energy by considering the two body interaction potential. The energy of the perfect lattice E_L is written as

$$E_L = \sum_{i>j} \Phi_{ij} \left(|\mathbf{R}_i - \mathbf{R}_j| \right) \tag{2.34}$$

and the energy of the defective lattice E_D can be written as

$$E_D = \sum_{i>j}{}' \Phi_{ij} \left(|\mathbf{r}_i - \mathbf{r}_j| \right) \tag{2.35}$$

here $\mathbf{r}_i = \mathbf{R}_i + \boldsymbol{\xi}_i$ and $\mathbf{r}_j = \mathbf{R}_j + \boldsymbol{\xi}_j$, $\mathbf{R}_i$, $\mathbf{R}_j$ being the undisplaced positions of the respective ions. Φ_{ij} is the interaction potential between ions i and j.

With certain summation conventions[100], both the sums $\sum$ and $\sum'$ can be treated as equivalent. Thus the energy of the defect can be written as

$$\mathrm{E} = \sum_{\mathrm{i>j}} \left\{ \Phi_{\mathrm{ij}} \left(\left| \mathbf{r}_{\mathrm{i}} - \mathbf{r}_{\mathrm{j}} \right| \right) - \Phi_{\mathrm{ij}} \left(\left| \mathbf{R}_{\mathrm{i}} - \mathbf{R}_{\mathrm{j}} \right| \right) \right\} \tag{2.36}$$

The summation extends over all the ions in the lattice.

Comparing eq. 2.36 with eq. 2.30, we see that while $\mathrm{E_I}$ and $\mathrm{E_{I,II}}$ terms have simple summations, corresponding $\mathrm{E_{II}}$ term is no longer a quadratic function of displacement $\boldsymbol{\xi}$ of the second region. This means that to make harmonic approximation work, $\mathrm{E_{II}}$ is to be rearranged so as to make it quadratic in $\boldsymbol{\xi}$.

For this, we expand $\mathrm{E_{II}}$ to second order terms in $\boldsymbol{\xi}_i$ and $\boldsymbol{\xi}_j$.

$$\begin{aligned}
\mathrm{E_{II}} &= \sum_{\mathrm{i,j\in II,i>j}} \left\{ \Phi_{\mathrm{ij}} \left(\left| \mathbf{r}_{\mathrm{i}} - \mathbf{r}_{\mathrm{j}} \right| \right) - \Phi_{\mathrm{ij}} \left(\left| \mathbf{R}_{\mathrm{i}} - \mathbf{R}_{\mathrm{j}} \right| \right) \right\} \\
&= \sum_{i,j\in II,i>j} \left\{ \frac{\partial \Phi_{ij} \left(\left| \mathbf{R}_i - \mathbf{r}_j \right| \right)}{\partial \mathbf{r}_j} \cdot \boldsymbol{\xi}_j + \frac{\partial \Phi_{ij} \left(\left| \mathbf{r}_i - \mathbf{R}_j \right| \right)}{\partial \mathbf{r}_i} \cdot \boldsymbol{\xi}_i + \frac{1}{2} \left[\boldsymbol{\xi}_j \cdot \frac{\partial^2 \Phi_{ij} \left(\left| \mathbf{R}_i - \mathbf{r}_j \right| \right)}{\partial \mathbf{r}_j \partial \mathbf{r}_j} \cdot \boldsymbol{\xi}_j \right] \right. \\
&\qquad \left. + \frac{1}{2} \left[\boldsymbol{\xi}_{\mathrm{i}} \cdot \frac{\partial^2 \Phi_{\mathrm{ij}} \left(\left| \mathbf{r}_{\mathrm{i}} - \mathbf{R}_{\mathrm{j}} \right| \right)}{\partial \mathbf{r}_{\mathrm{i}} \partial \mathbf{r}_{\mathrm{i}}} \cdot \boldsymbol{\xi}_{\mathrm{i}} \right] + \text{cross terms} \right\}
\end{aligned} \tag{2.37}$$

which shows that $\mathrm{E_{II}}$ has linear dependance. To eliminate the linear terms we define a new function $\mathrm{E^{new}}$ as

$$\begin{aligned}
\mathrm{E^{new}} &= \sum_{\mathrm{i\in I,j\in II}} \left\{ \Phi_{\mathrm{ij}} \left(\left| \mathbf{R}_{\mathrm{i}} - \mathbf{r}_{\mathrm{j}} \right| \right) - \Phi_{\mathrm{ij}} \left(\left| \mathbf{R}_{\mathrm{i}} - \mathbf{R}_{\mathrm{j}} \right| \right) \right\} \\
&= \sum_{\mathrm{i\in I,j\in II}} \left\{ \frac{\partial \Phi_{\mathrm{ij}} \left(\left| \mathbf{R}_{\mathrm{i}} - \mathbf{r}_{\mathrm{j}} \right| \right)}{\partial \mathbf{r}_{\mathrm{j}}} \cdot \boldsymbol{\xi}_{\mathrm{j}} + \frac{1}{2} \left[\boldsymbol{\xi}_{\mathrm{j}} \cdot \frac{\partial^2 \Phi_{\mathrm{ij}} \left(\left| \mathbf{R}_{\mathrm{i}} - \mathbf{r}_{\mathrm{j}} \right| \right)}{\partial \mathbf{r}_{\mathrm{j}} \partial \mathbf{r}_{\mathrm{j}}} \cdot \boldsymbol{\xi}_{\mathrm{j}} \right] \right\}
\end{aligned} \tag{2.38}$$

Adding linear terms from E_{II} and E^{new} as L

$$\begin{aligned}
L &= \sum_{i,j\in II, i>j} \left\{ \frac{\partial \Phi_{ij}\left(\left|\mathbf{R}_i - \mathbf{r}_j\right|\right)}{\partial \mathbf{r}_j} \cdot \boldsymbol{\xi}_j + \frac{\partial \Phi_{ij}\left(\left|\mathbf{r}_i - \mathbf{R}_j\right|\right)}{\partial \mathbf{r}_i} \cdot \boldsymbol{\xi}_i \right\} + \sum_{i\in I, j\in II} \frac{\partial \Phi_{ij}\left(\left|\mathbf{R}_i - \mathbf{r}_j\right|\right)}{\partial \mathbf{r}_j} \cdot \boldsymbol{\xi}_j \\
&= \sum_{i,j\in II, i\neq j} \frac{\partial \Phi_{ij}\left(\left|\mathbf{R}_i - \mathbf{r}_j\right|\right)}{\partial \mathbf{r}_j} \cdot \boldsymbol{\xi}_j + \sum_{i\in I, j\in II} \frac{\partial \Phi_{ij}\left(\left|\mathbf{R}_i - \mathbf{r}_j\right|\right)}{\partial \mathbf{r}_j} \cdot \boldsymbol{\xi}_j \\
&= \sum_{i\in I\&II, j\in II, i\neq j} \frac{\partial \Phi_{ij}\left(\left|\mathbf{R}_i - \mathbf{r}_j\right|\right)}{\partial \mathbf{r}_j} \cdot \boldsymbol{\xi}_j \\
&= \sum_{j\in II} \boldsymbol{\xi}_j \cdot \sum_{i\in \text{entire lattice}, i\neq j} \frac{\partial \Phi_{ij}\left(\left|\mathbf{R}_i - \mathbf{r}_j\right|\right)}{\partial \mathbf{r}_j} \\
&= 0 \qquad \text{(for lattice at equilibrium)}
\end{aligned} \tag{2.39}$$

So, $E_{II} + E^{new}$ is now a quadratic function of ξ. However to keep the original expression of E intact, we subtract E^{new} from it and redefine E_I, $E_{I,II}$, and E_{II} as

$$\begin{aligned}
E_I &= \sum_{i\in I, j\in I} \left[\Phi_{ij}\left(\left|\mathbf{r}_i - \mathbf{r}_j\right|\right) - \Phi_{ij}\left(\left|\mathbf{R}_i - \mathbf{R}_j\right|\right)\right] \\
E_{I,II} &= \sum_{i\in I, j\in II} \left[\Phi_{ij}\left(\left|\mathbf{r}_i - \mathbf{r}_j\right|\right) - \Phi_{ij}\left(\left|\mathbf{R}_i - \mathbf{r}_j\right|\right)\right] \\
E_{II} &= -\frac{1}{2} \sum_{i\in I, j\in II} \left[\frac{\partial}{\partial \mathbf{r}_j}\Phi_{ij}\left(\left|\mathbf{r}_i - \mathbf{r}_j\right|\right) - \frac{\partial}{\partial \mathbf{r}_j}\Phi_{ij}\left(\left|\mathbf{R}_i - \mathbf{r}_j\right|\right)\right] \cdot \left(\mathbf{r}_j - \mathbf{R}_j\right)
\end{aligned} \tag{2.40}$$

This brings us to the following expression for the defect energy

$$\begin{aligned}
E &= \sum_{i\in I, j\in I} \left[\Phi_{ij}\left(\left|\mathbf{r}_i - \mathbf{r}_j\right|\right) - \Phi_{ij}\left(\left|\mathbf{R}_i - \mathbf{R}_j\right|\right)\right] + \sum_{i\in I, j\in II} \left[\Phi_{ij}\left(\left|\mathbf{r}_i - \mathbf{r}_j\right|\right) - \Phi_{ij}\left(\left|\mathbf{R}_i - \mathbf{r}_j\right|\right)\right] \\
&\quad -\frac{1}{2} \sum_{i\in I, j\in II} \left[\frac{\partial}{\partial \mathbf{r}_j}\Phi_{ij}\left(\left|\mathbf{r}_i - \mathbf{r}_j\right|\right) - \frac{\partial}{\partial \mathbf{r}_j}\Phi_{ij}\left(\left|\mathbf{R}_i - \mathbf{r}_j\right|\right)\right] \cdot \left(\mathbf{r}_j - \mathbf{R}_j\right)
\end{aligned} \tag{2.41}$$

2.6 Energy Minimization

For any kind of perfect or imperfect crystal calculations, we are interested only in the equilibrium state of the system. This requires the minimization of energy as a prerequisite condition for subsequent calculations. The cost of minimization is directly proportional to the number of variables involved. So it is essential to minimize the number of variables for a faster minimization process. Another point worth discussing here is the use of first derivative of the function in minimization. In most of the systems, the inclusion of first derivative speeds up the process of minimization considerably in spite of the extra computational time required for its calculation.

2.6.1 Stationary Points: Maxima, Minima and Saddle Points

In a 3-dimensional lattice system, a stationary point means zero gradients for all host atoms (or ions) in all three directions.

To start with, let us consider a single variable function f(x)[101]. Now the points which satisfy the condition $\frac{df(x)}{dx} = 0$ are either extrema (maxima or minima) or saddle points. The question is, how to differentiate one from the other? This requires the calculation of the second derivative of the function f(x) at $x = x_a$ which corresponds to a stationary point. Now, there are three distinct situations : if $f^{(2)}(x_a) < 0$, x_a is a minimum; if $f^{(2)}(x_a) > 0$, x_a is a maximum and if $f^{(2)}(x_a) = 0$, x_a is a saddle point.

The definition can be extended to a real-valued function of several variables. For a real-valued function $f(x_1, x_2, ...x_n) = f(x)$, a point $\mathbf{x} = \mathbf{x_a}$ is a stationary point if

$$\frac{\partial f(\mathbf{x})}{\partial \mathbf{x}_i} = 0 \qquad \text{for} \quad i = 1, 2, ..., n \tag{2.42}$$

To determine the nature of the stationary point, a matrix $\mathbf{A}_k$ known as the hessian matrix is

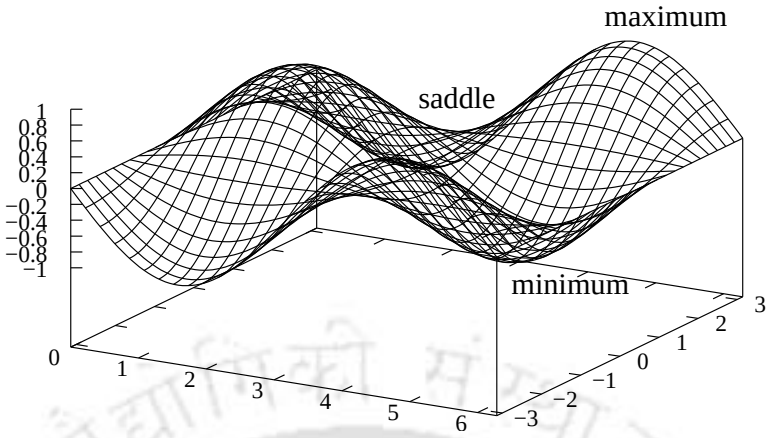

Figure 2.3: Maximum, minimum and saddle point on a two dimensional surface

defined as

$$\mathbf{A}_k = \begin{pmatrix} f_{x_1x_1} & f_{x_1x_2} & \cdots & f_{x_1x_k} \\ f_{x_2x_1} & & & \vdots \\ \vdots & & \ddots & \\ f_{x_kx_1} & \cdots & & f_{x_kx_k} \end{pmatrix}$$

where $f_{x_ix_j} = \dfrac{\partial^2 f}{\partial \mathbf{x}_i \partial \mathbf{x}_j}$. The stationary point $\mathbf{x} = \mathbf{x_a}$ is a point of minimum if

$$|\mathbf{A}_k|_{\mathbf{x}=\mathbf{x}_a} > 0 \qquad k = 1, 2, ..., n$$

All the three types of stationary points i.e. maxima, minima and saddle points are shown in fig. 2.3 for a sample function $f(x, y) = \sin(x) * \cos(y)$.

One important property of the lattice i.e. the vibrational frequencies can be calculated from this hessian matrix[102]. These frequencies are obtained by diagonalising the dynamic matrix **D** which consists of the mass weighted hessian for an isolated cluster or for a solid at the Γ-point.

$$\mathbf{D} = m^{-\frac{1}{2}} \mathbf{A} m^{-\frac{1}{2}} \tag{2.43}$$

The square roots of the eigenvalues of this dynamical matrix are the vibrational frequencies. So, any negative eigenvalue will correspond to an imaginary frequency and will identify the system to be an unstable one with respect to the distortion given by the eigenvector of the imaginary mode. Due to the translational symmetry of the lattice, the first three vibrational frequencies should be equal to zero.

2.6.2 Search Techniques

Our interest is to find the local minima of the potential energy surface for a given system. There are many search techniques, the most common of which are the method of steepest descent (ascent) and the Newton-Raphson method [1, 101]. These are gradient search methods.

In the method of steepest descent, the key idea is to seek the minimum by always proceeding in the direction which yields the greatest rate of decrease of energy $E(\mathbf{r})$. The first step is to find the direction in the n-dimensional Euclidean space along which $E(\mathbf{r})$ tends to have maximum decrease starting from a point $\mathbf{r}^o = \begin{bmatrix} r_1^o & r_2^o & .... & r_n^o \end{bmatrix}$. It can be shown that the greatest incremental change of $E(\mathbf{r})$ for a fixed incremental distance moved from $\mathbf{r} = \mathbf{r}_o$ is yielded along the gradient direction $\mathbf{g}(\mathbf{r}_o)$.

The Newton-Raphson method ensures quadratic convergence, but requires evaluation of second partial derivatives and inverse matrices. In the vicinity of the current search point $\mathbf{r} = \mathbf{r}_k$, the energy $E(\mathbf{r})$ can be adequately represented by truncating the Taylor's series expansion to second order.

$$E(\mathbf{r}) = E(\mathbf{r}_k) + (\mathbf{r} - \mathbf{r}_k) \cdot \nabla E(\mathbf{r}_k) + \frac{1}{2}(\mathbf{r} - \mathbf{r}_k)\,\mathbf{A}\,(\mathbf{r} - \mathbf{r}_k) \tag{2.44}$$

so the gradient at $\mathbf{r}$ is given by

$$\nabla E(\mathbf{r}) = \nabla E\left(\mathbf{r}_k\right) + \mathbf{A} \cdot (\mathbf{r} - \mathbf{r}_k) \tag{2.45}$$

At minimum,

$$\nabla E(\mathbf{r}) = 0 \tag{2.46}$$

so the step required for reaching minimum is

$$\mathbf{r} - \mathbf{r}_k = -\mathbf{A}^{-1} \cdot \nabla E(\mathbf{r}_k) \tag{2.47}$$

Prior to the inversion of $\mathbf{A}$, $\mathbf{A}$ should be tested for positive definiteness. Otherwise, Newton search may diverge. However, the effort involved in a single iteration of Newton search is huge. First, with n number of atoms in the system, n components of the gradient are to be computed at $\mathbf{r} = \mathbf{r}_k$. Secondly, the number of distinct components of the matrix $\mathbf{A}$ is $\frac{n(n+1)}{2}$ and these correspond to the second partial derivatives of $E(\mathbf{r})$ evaluated at $\mathbf{r} = \mathbf{r}_k$. Thirdly, the inverse of the $\mathbf{A}$ matrix must be obtained. This is the reason why quasi-Newtonian algorithms became more popular than the simple Newton-Raphson method. In this approach, instead of explicitely calculating the second derivative matrix, the inverse of it is constructed and updated in each iteration through Newton-Raphson algorithm so that it becomes the exact inverse second derivative matrix when the function is close to the minimum. The most widely used approaches for hessian update are Broyden-Fletcher-Goldfarb-Shanno (BFGS)[103] method and Davidson-Fletcher-Powell (DFP)[104] method.

For large systems, storing the Hessian matrix may cause problem as the storage requirement increases with the square of the number of atoms. Moreover, for complex systems, like defects in a low symmetry crystal, the gradient calculation itself is a complicated task.

In such cases, conjugate direction methods are useful. Here, a series of line searches are performed over the energy surface in order to find the minimum. The first step is down the steepest gradient from the starting point and the subsequent steps are downhill but perpendicular to the pevious step. The extended form of Powell's method[105] is a conjugate direction method which does not require evaluation of derivatives.

Chapter 3

Finite Size Calculations in NaCl: A New Approach to Point Defect Simulation

In conventional atomistic calculations of point defects, typically there are two levels of approximations. The first approximation lies in the model itself in simulating the microscopics of the problem. The second level of approximation comes in facilitating the actual computations. In this work, we propose a new method of exactly calculating the defect parameters by finite size calculations. In usual defect computations that are based on PPI model, to facilitate actual computing, the crystal is divided into two regions. The region around the defect is treated exactly (in PPI sense), whereas the outer region is treated as continuum. Typically the inner region is restricted to nearest neighbours. There have been some studies on the size of inner region, though in practice, the size is chosen in an ad-hoc manner. Such ad-hoc choice of Region1 gives an approximate result. The approximation can be reduced by choosing an appropriate computational scheme.

3.1 Scheme of Calculation

The conventional PPI model has been used which describes each ion in the crystal as point particles with fixed charges and induced moments (dipoles and quadrupoles). The electrostatics of the problem can therefore be solved completely. Calculations with this scheme, however has been restricted to only dipoles.

In the proposed scheme, we consider the defect energy of finite crystals as a function of the crystal size L and then take a careful limit as L tends to infinity to calculate the defect energy. The finite size crystal even without the defect, has surface effects. Since there is mechanical force imbalance at the surface, the surface is deformed, that is the ions on the surface will displace so as to minimize the surface energy. At the same time the electrical force imbalance will also induce dipole moments to the ions at the surface. However, these surface effects do vanish in the infinite size limit.

The dipole moments of individual ions are found by solving a large set of linear equations. This is followed by an exact calculation of the various energy terms contributing to the lattice energy. The surface effects are implicitly calculated as a part of the total energy of the crystal. The only variables are the displacements of the ions. The stable configuration of the crystal is then obtained by running an optimization code which finds the minimum of the total energy by varying the positions of the ions.

In principle, energy minimum must be found by allowing all ions to relax. However, this will introduce large displacements at the surface, which in turn will affect the defect energy. This means that, though in the limiting case, the defect energy will yield its correct value, the process will be demanding from computational point of view. In order to avoid this, the crystal is divided into two regions, Region1 with few shells around the centre of the crystal and Region2 with the rest of the shells. This sounds similar to the conventional ML scheme. But unlike the ML scheme, where Region2 is treated as a continuum, here

both the regions are treated on the same footing to the extent that the dipole moments are calculated exactly for the entire crystal. However, the relaxations of the ions are restricted to Region1 ions only. Then two limits are taken, first letting crystal size to infinity, and then taking a limit for size of Region1. This way we will avoid the complications arising due to the interaction between Region1 and surface of the crystal. The whole of the procedure is then carried out for a crystal with and without a vacancy.

If R is the radius of the Region1, the defect energy of the crystal of size L is given by

$$W_d^R(L) = W_{Def}^R(L) - W_{Full}^R(L) \tag{3.1}$$

where $W_{Def}^R(L)$ and $W_{Full}^R(L)$ are the total energies with and without the defect. The defect energy is then found by taking the following limits

$$W_d = \lim_{R\to\infty} \lim_{L\to\infty} W_d^R(L). \tag{3.2}$$

The order in which limits are taken is important. It is necessary to keep R, radius of Region1 small on comparison to L, the size of the crystal.

We have applied this scheme to the familiar case of *NaCl* crystal. First reason for this is that there is an extensive literature for defects in *NaCl* and it would be easy to compare our results with those of other schemes. Secondly, *NaCl* has O_h point group symmetry. Introduction of vacancy or an interstitial at special site breaks the translational symmetry but preserves the cubic symmetry. This enables computations of large crystals.

3.2 Dipole Moment and Energy Terms

The actual computations start in finding the dipole moments of the ions and then calculating the different energy terms. We consider a cubic crystal of size L. L gives the number of ions enclosed in one dimension. Here, the points which lie on the surface of a sphere with center at the center of the crystal, are symmetry related. A collection of such ions are referred here as shells. In energy calculations , only one point is used to represent a shell.

In general, the dipole moments of ions in regular lattice sites are not radial. So all three components of dipole moments are considered here. We denote the charge of an ion at position x by q_x and the dipole moment by $\boldsymbol{\mu}_x$. If α_x is the electronic polarizability of the ion at site x, the dipole moment of this ion is given by

$$\boldsymbol{\mu}_{\mathrm{x}} = \alpha_{\mathrm{x}} \left\{ \mathbf{E}_{\mathrm{x}}^{\mathrm{mono}} + \mathbf{E}_{\mathrm{x}}^{\mathrm{dip}} \right\} \tag{3.3}$$

where $\mathbf{E}_x^{mono}$ is the electric field due monopole charges and $\mathbf{E}_x^{dip}$ is the electric field due to the dipoles at site x. These equations are linear in $\boldsymbol{\mu}$ and can be written in matrix form as

$$\mathbf{D}\mu = \mathbf{M} \tag{3.4}$$

Here $\mathbf{D}$ is a square matrix of order $3s$, where s is the no of shells. $\boldsymbol{\mu}$ and $\mathbf{M}$ are column matrices. Matrix $\mathbf{D}$ can be considered as $s \times s$ matrix with each element given by 3×3 matrix

$$\mathbf{D}_{\mathrm{y,x}} = \delta_{\mathrm{x,y}} \mathbf{I}_3 - \sum_{\sigma,\mathrm{x}} \frac{\alpha_{\mathrm{y}}}{\mathrm{O_y}} \left\{ \frac{\sigma \cdot \mathbf{r} \otimes \mathbf{r}}{\mathrm{r}^5} - \frac{3\sigma}{\mathrm{r}^3} \right\} \tag{3.5}$$

Similarly the matrix $\mathbf{M}$ can be written as

$$\mathbf{M}_y = \alpha_y \left\{ \frac{Q\mathbf{Y}}{Y^3} + \sum_{x,\sigma} \frac{q_x \mathbf{r}}{O_x r^3} \right\} \tag{3.6}$$

where $\mathbf{r} = \mathbf{Y} - \sigma\mathbf{X}$, σ are symmetry operators and O_x is order of the coset group of symmetry group of x. x goes over the shells. Q is the central charge and $\mathbf{X}$ and $\mathbf{Y}$ are the position vectors of the representative ions of the shells. σ is summed over all elements of cubic symmetry group O_h.

Now the total energy of the crystal can be written as

$$W_{tot} = W_{Cen} + W_{coul} + W_P + W_{SR} \tag{3.7}$$

Here W_{Cen} is the contribution from the central charge to the energy term and will be absent for a defect (vacancy) crystal where the central charge is removed. The other terms W_{coul}, W_P and W_{SR} represent the Coulomb, Polarization and Short Range terms respectively. The explicit expressions for all these components are

$$W_{Cen} = \sum_y \frac{Qq_y}{|\mathbf{Y}|} - \sum_y \frac{Q\boldsymbol{\mu}_y \cdot \mathbf{Y}}{|\mathbf{Y}|^3} + 6\phi(r_0) \tag{3.8}$$

$$W_{coul} = \frac{1}{2}\sum_y \sum_{x\neq y} \frac{q_x q_y}{|\mathbf{Y}-\mathbf{X}|} \tag{3.9}$$

$$W_P = -\frac{1}{2}\sum_y \sum_{x\neq y} \frac{q_x \boldsymbol{\mu}_y \cdot (\mathbf{Y}-\mathbf{X})}{|\mathbf{Y}-\mathbf{X}|^3} \tag{3.10}$$

$$W_{SR} = \sum_y \sum_{x\neq y} \phi(r) \tag{3.11}$$

r_o is the nearest neighbour distance. The short range potential is taken to be of the form

$$\phi(r) = A\exp\left(-\frac{r}{\rho}\right) - \frac{C}{r^6} \tag{3.12}$$

where the first term is Born-Mayer repulsive potential and second term is van der Waals dipole-dipole interaction. We restrict the short range interactions to first neighbours only. In all the equations 3.8, 3.9, 3.10 and 3.11 the summations are over all lattice points. The

Table 3.1: Input parameters for *NaCl*

r_o(Å)	A(eV)	ρ(Å)	C(eVÅ^6)	α_c(Å^3)	α_a(Å^3)	W_{RLE}(eV)
2.834795	1736.3	0.3049	3.693	0.149	1.032	7.9222

Schottky defect energy is given by

$$W_S = W_{av} + W_{cv} - W_{RLE} \tag{3.13}$$

where W_{av} and W_{cv} are the formation energies of anion and cation vacancies respectively, and W_{RLE} is the rigid lattice energy of the crystal

3.3 Results and Discussions

This new technique of finite size calculation is demonstrated using the well studied crystal of *NaCl*. The short range parameters A, ρ, C and polarizabilities α_c (for cation), α_a (for anion) are taken from Banhatti and Murti[96] and are listed in table 3.1. The value of r_o and W_{RLE} were calculated by using only Coulomb and Born-Mayer potentials in an infinite crystal. As we have discussed in the previous section, it is essential that the surface of the crystal is sufficiently away from the defect site so that the distortions at the surface do not interact with that of the defect. The crystal size was varied from $L = 7$ to $L = 21$. The crystal size with corresponding number of shells and ions are listed in table 3.2. Fig. 3.1 shows how the two regions are getting separated with the increasing size of the crystal. For the largest crystal size i.e. 21, the size of the D matrix is of the order 852. This matrix is inverted several times in each optimization, making the computations time consuming. The size of Region1 $R1$ is in terms of number of shells.

Even for a cluster without defect, surface effects will cause a displacement of Region1

Table 3.2: The increasing crystal size with associated shells and number of ions

L	No. of shells	No. of ions
7	18	342
9	33	728
11	54	1330
13	82	2196
15	118	3374
17	163	4912
19	218	6858
21	284	9260

ions. This induces dipole moments. Fig. 3.2(a) shows induced dipole moments as a function of distance from the centre with $L = 21$, $R1 = 9$ and Cl sitting at the centre. Fig 3.2(b) shows the same in the presence of a vacancy at the centre of the cluster. It can be seen that the induced dipole moments in the neighbourhood of the defect and those on the surface are clearly separated. The induced dipole moments in presence of the defect are a order of magnitude larger than the one without defect. Fig. 3.2(c) shows the net induced dipole moment due to the defect. The average magnitude falls of approximately as $\frac{1}{r^2}$ as expected. A vector plot of the dipole moments lying on XY-plane is shown in fig. 3.3.

Typical plots for defect energy $W_d^R(L)$ for anion and cation vacancies are plotted as a function of crystal size for fixed Region1 sizes in fig 3.4. From the plots it is easy to see that the defect energies follow two separate series, one with $L = 7, 11, 15, 19$ and the other with $L = 9, 13, 17, 21$. This is due to the fact that the outermost ions in each of the series are different and hence the coulomb energy oscillates. The infinite size defect energy is found by linearly extrapolating each series and then taking the average of the two limiting values. A detail of the various energy terms along with maximum displacement s and anion defect energy W_{av} and cation defect energy W_{cv} are listed in table 3.3 for fixed $R1$ and L.

The Schottky energy W_S is calculated for increasing Region1 sizes and are plotted in

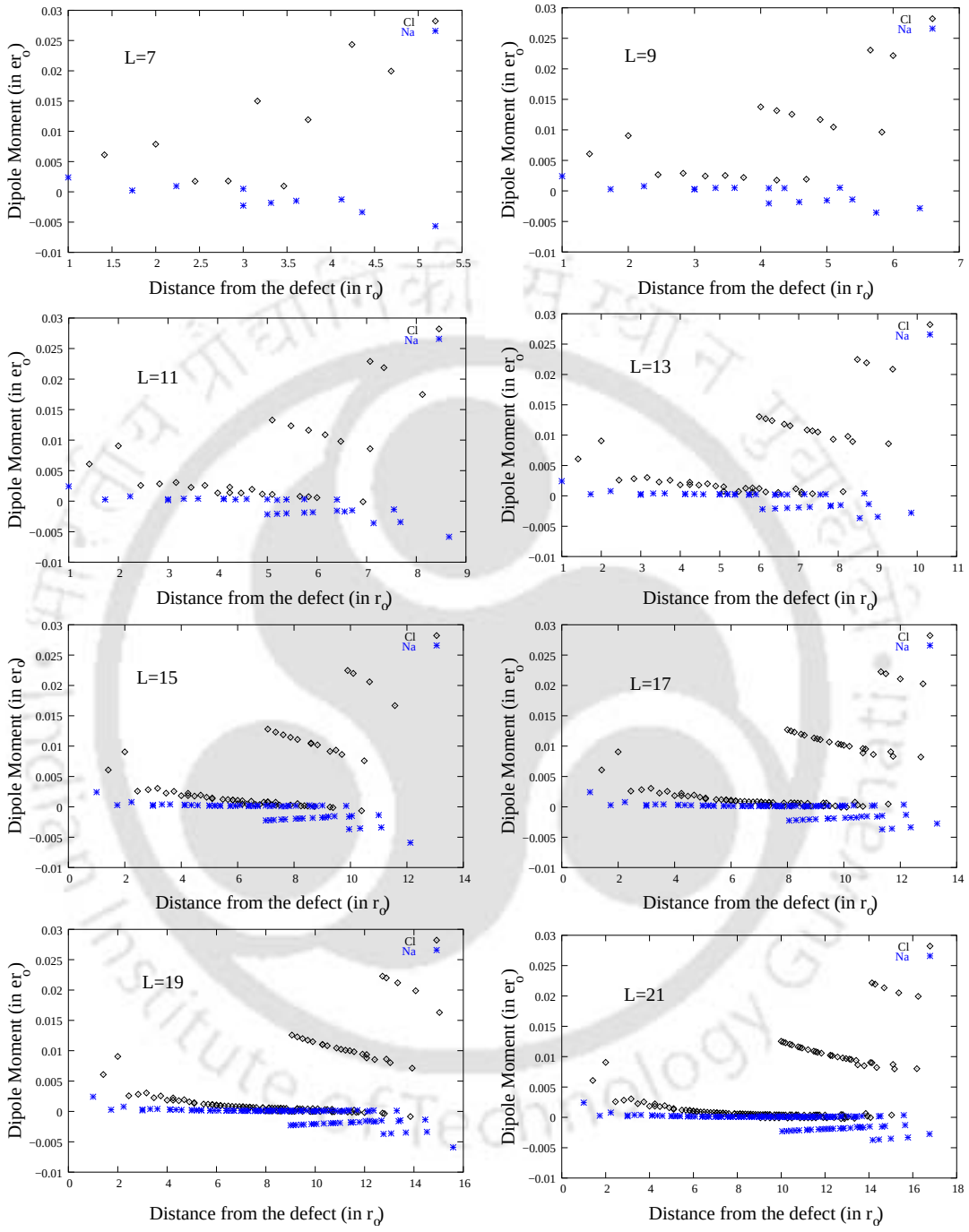

Figure 3.1: Shows how the surface effect and the effect due to defect separates out as the crystal size increases with Region1 size fixed at R1 = 9

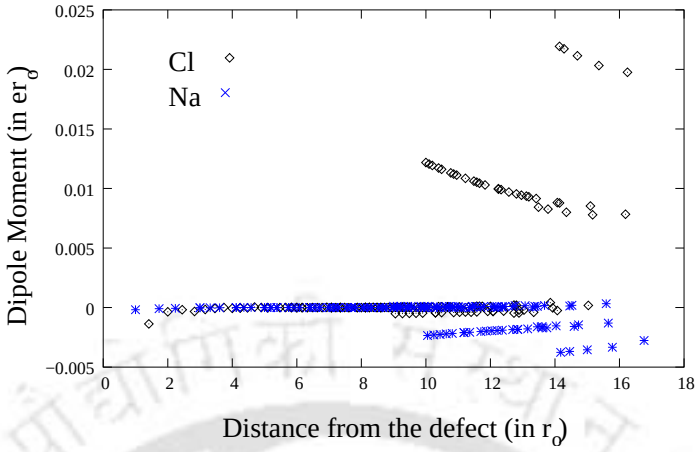

(a) without defect

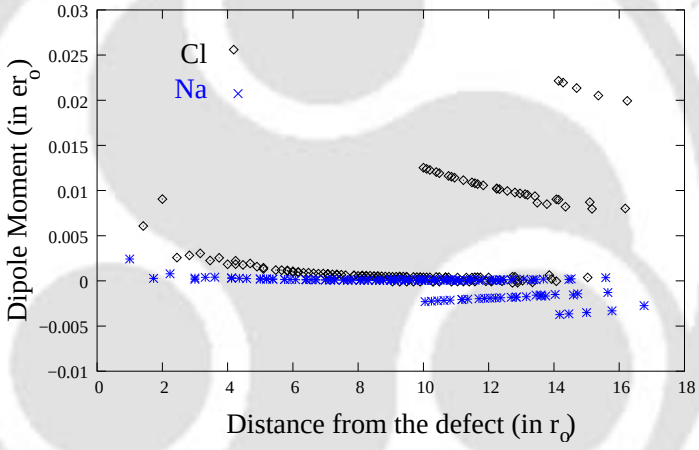

(b) with vacancy defect

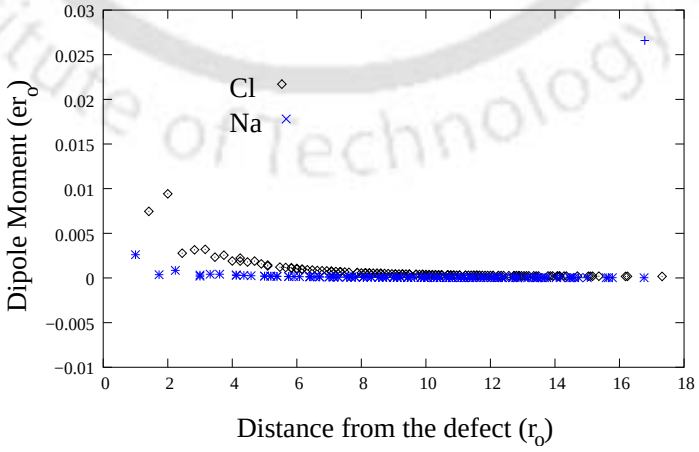

(c) with only defect

Figure 3.2: Induced dipole moments for L = 21 and R1 = 9

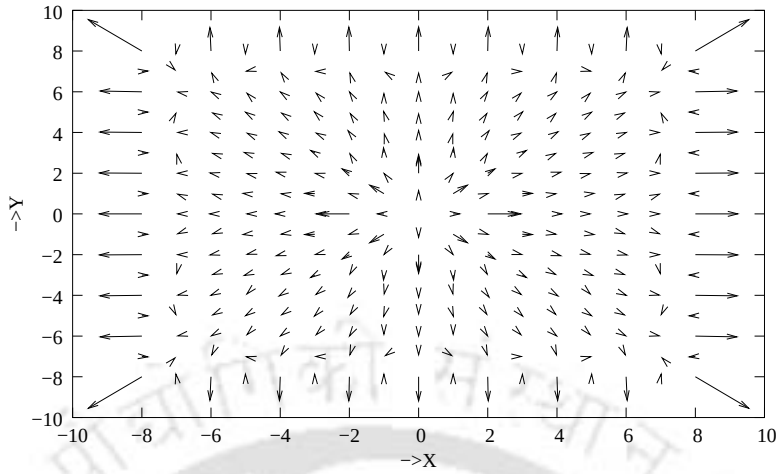

Figure 3.3: Vector plot of the dipoles for (001) plane with $R1 = 7$ and $L = 17$

Table 3.3: Various full and defect energy terms for $R1 = 9$ and $L = 21$ with (a) Anion central charge and (b) Cation central charge

(a) Anion at centre

	s (in r_o)	W_{Cen} (in eV)	W_{Coul} (in eV)	W_P (in eV)	W_{Sre} (in eV)	W_{tot} (in eV)	W_{av} (in eV)
Full	-0.0046	-7.063985	-40643.39	-16.12	4016.29	-36650.29	
Defect	-0.0888	0.0	-40646.36	-16.59	4017.47	-36645.48	4.81

(a) Cation at centre

	s (in r_o)	W_{Cen} (in eV)	W_{Coul} (in eV)	W_P (in eV)	W_{Sre} (in eV)	W_{tot} (in eV)	W_{cv} (in eV)
Full	-0.0055	-7.664072	-40643.52	-15.43	4016.32	-36650.29	
Defect	-0.0817	0.0	-40646.27	-15.68	4017.39	-36644.55	5.74

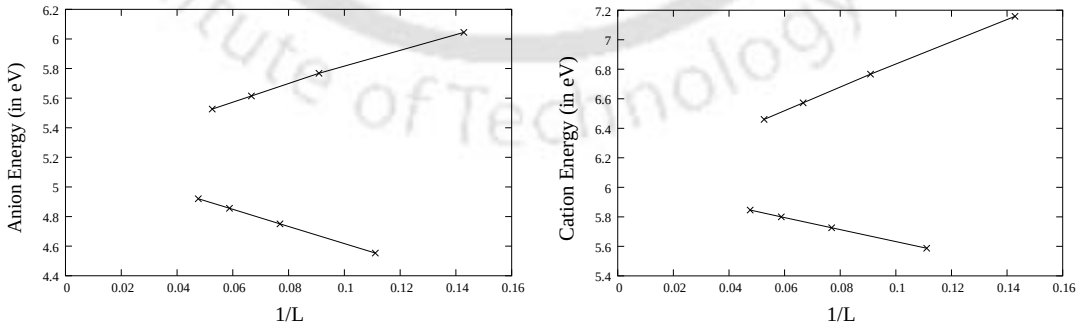

Figure 3.4: Anion and cation defect energies as functions of crystal size for $R1 = 5$

Table 3.4: Calculated Schottky energies as a function of Region1 size

$R1$	No.of ions	W_{av}(in eV)	W_{cv} (in eV)	W_S (in eV)
1	6	5.747	6.519	4.344
2	18	5.366	6.204	3.648
3	26	5.339	6.172	3.589
4	32	5.338	6.173	3.588
5	56	5.215	6.048	3.341
6	80	5.144	5.991	3.213
7	92	5.115	5.962	3.156
8	116	5.104	5.946	3.128
9	124	5.092	5.932	3.102

Table 3.5: Schottky energies from the present and previous works

	Experimental	MPPI (ML)	Shell	Present
Schottky Energy (in eV)	2.5[106]	2.55[107]	2.23[76]	2.51

fig. 3.5(a) as a function of $R1$. The fluctuation in energy is expected to be because of fluctuation in the total charge encompassed by Region1. The energy values are also listed in table. 3.4 along with the corresponding anion and cation vacancy energies.

The schottky energy is calculated from anion and cation defect energies which in turn consist of several energy terms. There are contributions from second region also which is sufficiently large as compared to Region1. In such case, it becomes difficult to estimate the leading order term in defect energy. We tried various polynomial fits to decide the extrapolation and found that W_S vs $\frac{1}{\sqrt{R1}}$ gives the best fit as $R1 \rightarrow \infty$. Fig. 3.5(b) shows the W_S vs $\frac{1}{\sqrt{R1}}$ plot. This plot is extrapolated to estimate the value of the energy at infinite limit. The calculated result is then compared with the experimental as well as other theoretical models (MPPI and shell model) in table 3.5. It shows that while shell model estimates a much lower value than that of the experimental, both ML (Mott Littleton) and Finite size calculations based on MPPI model give better results.

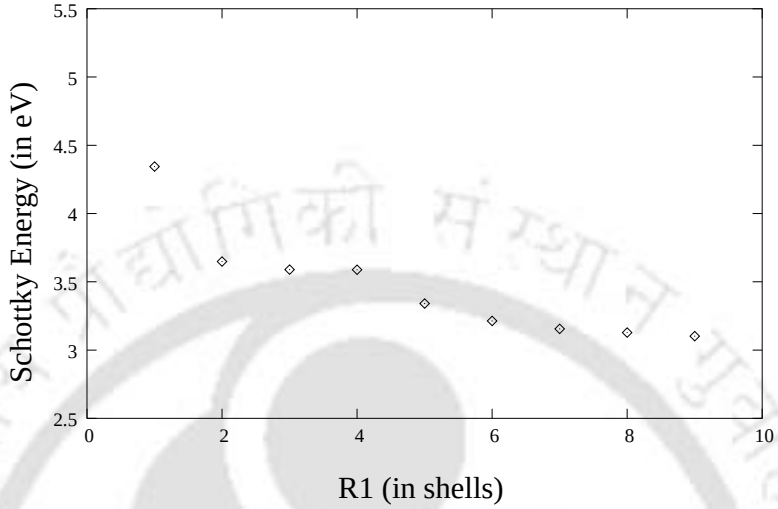

(a) Energy vs. Region1 size

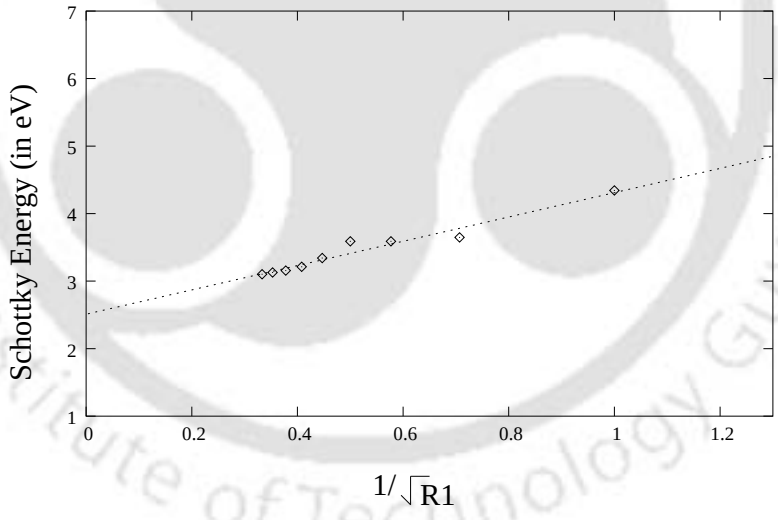

(b) Energy fi t plot

Figure 3.5: Schottky energy plots

For optimization, we used the va04 hsl (Harwell Subroutine Library) package. This package is meant to find minimum of a general function $F(x)$ of n variables $x = x_1, x_2, x_3, ...x_n$ where values of the derivatives are not required. The method is iterative and requires the use of an initial estimate of the minimum position. All our calculations were done in an Intel Pentium-IV processor of 2.4 GHZ speed. The typical time of calculation for one optimization run with the maximum crystal sixe of L = 21 with 9 shells in Region1 is 8.53 minutes.

Chapter 4

Schottky Defect Enthalpies in Alkaline Earth Oxides using EPPI Model

In recent years, point defects in ceramic oxide materials have attracted attention, firstly because the family of ceramic oxides *MgO*, *CaO*, *SrO*, *BaO* have the rocksalt structure, are essentially ionic and have very high melting points. Secondly, the transport properties in these oxides exhibit some puzzling features in respect of anion diffusion[108]. Thirdly, oxygen atomic ordering and oxygen vacancies are believed to play a significant role in the superconducting transition of high T_c oxide materials[109] .

The existing picture on the point defect energetics in oxides is quite unsatisfactory. It is argued that owing to the bivalency, Coulomb forces tend to prevail over other interactions resulting in rather large Schottky formation energies (7-8 eV)[109]. On the other hand, a much smaller Schottky defect formation energy is reported by Harding and Price[110] on the basis of their cation self-diffusion measurements. The shell model calculations that use a HADES software package led to values of Schottky defect energy h_S^f which are much larger (7.5 eV e.g. in *MgO*)[111]. These authors have ignored the conclusions drawn from self-diffusion experiments. Recent studies[48, 95, 96] have indicated clearly that

it is important to take into account of the inhomogeneous electric fields and the induced quadrupoles in the defect environment, if one is to satisfactorily model the point defects especially for systems whose ions are highly polarizable. This is certainly the case for oxygen ions. It is thus important to explore the nature of the Schottky disorder in these systems afresh.

Furthermore, the EPPI model was shown to be successful and in fact essential to resolve the many anomalies of the transport behaviour relating to Schottky and Frenkel defects in the case of the silver halides. In this chapter, we plan to apply this model for the case of alkaline earth oxides with a view to observe the effect of the induced quadrupoles on the Schottky defect formation.

4.1 Potential and Polarization Parameters for Defect Calculations

The short range potential for a pair of ions of type i and j at separation r_{ij} is taken to be of the form

$$\varphi = \mathrm{A_{ij}} \exp \frac{-\mathrm{r_{ij}}}{\rho_{\mathrm{ij}}} - \frac{\mathrm{C_{ij}}}{\mathrm{r_{ij}^6}} \tag{4.1}$$

where A_{ij}'s are the strength coefficients for the overlap repulsion potential and ρ_{ij}'s are the hardness parameters. The values of these constants for all the pairs (*Mg-O*, *Ca-O*, *Sr-O*, *Ba-O*, *Mg-Mg*, *Ca-Ca*, *Sr-Sr*, *Ba-Ba* and *O-O*) taken from Stoneham's compilation [112] for separations appropriate for these crystals, are listed in Table 4.1. The subscripts c and a stand for cation and anion respectively. The C_{ij}'s are the constants for the dipole-dipole van der Waals(vdW) interactions.These coefficients are notoriously hard to estimate either from its *ab initio* calculations or by semiempirical methods. Here we adopt an approach similar to the one in [48] successfully followed for AgCl and AgBr. The constants C_{cc} and

Table 4.1: Short range overlap repulsion parameters

Salts	A_{ca}(eV)	A_{cc}(eV)	A_{aa}(eV)	ρ_{ca}(nm)	ρ_{cc}(nm)	ρ_{aa}(nm)
MgO	2214.39	18147.9	871.489	0.02756	0.01452	0.03679
CaO	1996.35	54898.1	583.532	0.0318	0.01896	0.04026
SrO	2187.61	91113.2	538.788	0.0338	0.02068	0.04103
BaO	1994.97	588445.0	444.76	0.0362	0.0207	0.0426

C_{aa} are related to the cation-anion coefficient C_{ca} through the relations based on London's one-level approximation for the van der Waals dipole-dipole potential:

$$C_{cc} = (\alpha_c/\alpha_a)\left(\frac{E_c + E_a}{2E_a}\right)C_{ca} \tag{4.2}$$

$$C_{aa} = (\alpha_a/\alpha_c)\left(\frac{E_c + E_a}{2E_c}\right)C_{ca} \tag{4.3}$$

E_c and E_a are the second excitation energies of the cation and that of anion respectively. The coefficient C_{ca} is obtained by using the equilibrium condition of the lattice at 0^oK.

$$\frac{dW_L}{dr_0} = 0 \tag{4.4}$$

where r_0 is the anion-cation shortest separation and W_L is the lattice energy given by

$$\begin{aligned} W_L = & -\frac{\alpha_M(Ze^2)}{4\pi\varepsilon_0 r_0} + 6A_{ca}e^{\frac{-r_0}{\rho_{ca}}} + 6A_{cc}e^{\frac{-\sqrt{2}r_0}{\rho_{cc}}} + 6A_{aa}e^{\frac{-\sqrt{2}r_0}{\rho_{aa}}} - \frac{6.5952}{r_0^6}C_{ca} \\ & -\frac{1.8067}{r_0^6}(C_{cc} + C_{aa}) \end{aligned} \tag{4.5}$$

where α_M is the Madelung constant. Only nearest neighbour interactions are considered for the short range energy.The short range potentials as a function of the interionic distances

are shown in fig 4.1 for $Mg - Mg$, $Mg - O$ and $O - O$. As for the dipolar polarizabilities,

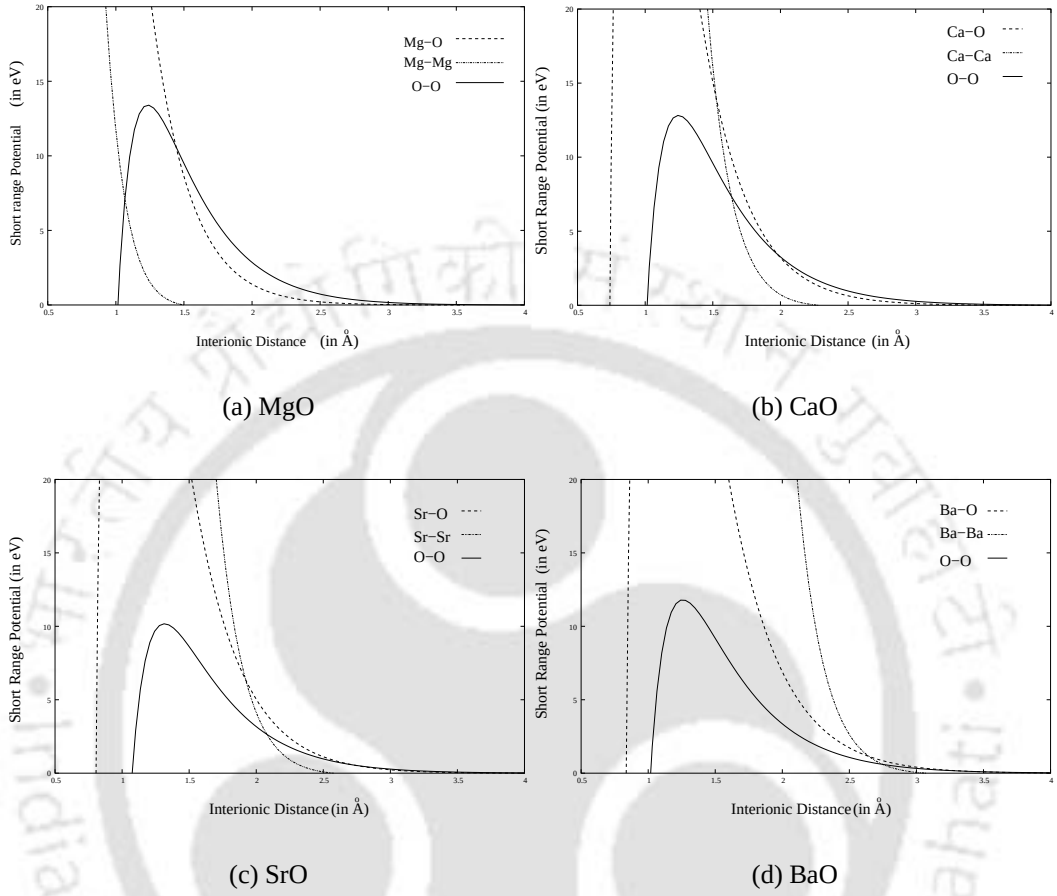

(a) MgO (b) CaO

(c) SrO (d) BaO

Figure 4.1: Short range potential plots

we are using the displacement polarizability α_d as fixed by the short-range potential and the static dielectric constant ε_s to find α_c and α_a .

$$\alpha_d = K/e^2 \tag{4.6}$$

$$\alpha_c + \alpha_a + 2\alpha_d = (3r_0^3/2\pi)\left(\frac{\varepsilon_s - 1}{\varepsilon_s + 2}\right) \tag{4.7}$$

$$(\alpha_c/\alpha_a) = (r_c/r_a)^3 \tag{4.8}$$

Table 4.2: van der Waals paramaters and polarizabilities

Salts	C_{ca} (eVÅ^6)	C_{cc} (eVÅ^6)	C_{aa} (eVÅ^6)	α_c (Å^3)	α_a (Å^3)	α_d (Å^3)	r_c (Å)	r_a (Å)	r_o (Å)	ε_s
MgO	11.076	6.822	60.182	0.024	0.244	1.541	0.65	1.4	2.11	9.86
CaO	31.642	46.164	50.911	0.222	0.628	2.151	0.99	1.4	2.41	11.1
SrO	54.71	103.72	60.398	0.603	1.146	2.411	1.13	1.4	2.58	13.1
BaO	67.188	176.01	45.203	1.582	1.764	2.928	1.35	1.4	2.76	34.0

Table 4.3: Quadrupole polarizabilities

	Mg^{2+}	Ca^{2+}	Sr^{2+}	Ba^{2+}	O^{2-}
α^q (in Å^5)	0.0266	0.450	1.176	7.198	3.943

where K is the force constant of the total short range potential (vdW and overlap repulsion) and r_c, r_a are the radii of the cation and anion respectively and e is the electronic charge. ε_s is the static dielectric constant. This procedure ensures a correct simulation of the static dielectric response of the material so important for the defect modeling[44]. Table 4.2 gives the van der Waals parameters along with the electronic and displacement polarizabilities. The values of quadrupole polarizabilities are taken from Schmidt et.al. [113]. They calculated the quadrupolar polarizabilities for several closed-shell ions including the influence of crystal environment. The effect of crystal adaptance was positive in case of cations and negative for anions as compared to the free ion values. The values of these quadrupole polarizabilities for various ions of materials studied here are listed in table 4.3.

4.2 The Physical Model

The calculations are based on ML scheme as described in Chapter 2. The relaxations and dipole moments of all the ions of the Region2 are solved by a semicontinuum approach in

which the defect charge and the crystal dielectric constant essentially simulate the response. In the continuum limit, the polarization **P** of an ion located at a position **r** from the defect is given by

$$\mathbf{P}(\mathbf{r}) = \frac{(\varepsilon_s - 1)q_d\mathbf{r}}{4\pi\varepsilon_s(|\mathbf{r}|)^3} \tag{4.9}$$

where q_d is the charge of the defect. The dipole moments of the cations and anions of Region2 are then apportioned to the electronic and displacement polarizabilities of the ions as

$$\boldsymbol{\gamma}_{c,a}(\mathbf{r}) = \left[\frac{\alpha_{c,a} + \alpha_d}{\alpha_c + \alpha_a + 2\alpha_d}\right] v_m \mathbf{P}(\mathbf{r}). \tag{4.10}$$

where v_m is the volume of the primitive cell.

Similarly, the displacement of an ion i in Region2, having a charge q_i is given by

$$\boldsymbol{\xi}_i(\mathbf{r}) = \left[\frac{\alpha_d}{\alpha_c + \alpha_a + 2\alpha_d}\right] \frac{v_m}{q_i} \mathbf{P}(\mathbf{r}) \tag{4.11}$$

As for Region1, we take only the defect and its six nearest neighbours to construct Region1. Once the defect is inserted, the full cubic symmetry breaks down to give a residual site symmetry of C_{4v}. The Region1 without and with the defect are shown in fig 4.2. The solutions for these ions are derived by a fully atomistic method. In addition, in the EPPI model, the distortions of the ions in Region1 are taken to the quadrupolar approximation. An outline of the model along with actual formulations are given below.

4.2.1 Outline of the EPPI Model

Quadrupole Moment and Electric Field Gradient

The quadrupole moment is a second rank, symmetric, traceless tensor and has six independent components. It is a measure of the departure from the spherical symmetry of the

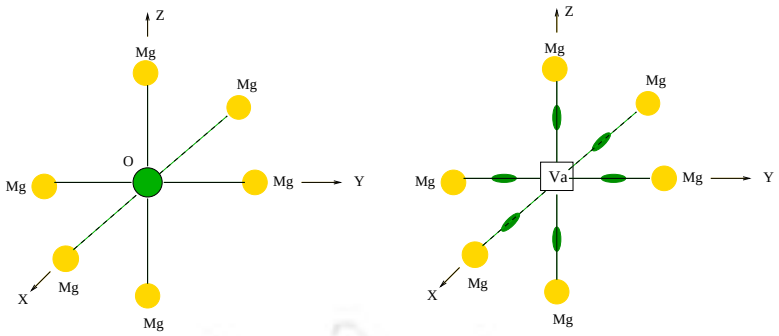

Figure 4.2: Region1 construction

charge distribution. The ij component of the tensor is defined as

$$Q_{ij} = \alpha^{q}_{ijkl} F_{kl} \tag{4.12}$$

where α_{ijkl} is the quadrupole polarizability and F_{kl} is the kl component of the electric field gradient tensor.

In all first principle calculations, α^{q}_{ijkl} is treated as spherically symmetric in free ion environment. It is then represented as a scalar quantity. But, in the crystal environment, the quadrupole polarizability tensor satisfying the isotropy condition have the following relations[60].

$$\alpha^{q}_{xxxx} = \alpha^{q}_{yyyy} = \alpha^{q}_{zzzz} = (2/3)\alpha^{q}$$

$$\alpha^{q}_{xyxy} = \alpha^{q}_{yzyz} = \alpha^{q}_{zxzx} = (1/2)\alpha^{q}$$

$$\alpha^{q}_{xxyy} = \alpha^{q}_{yyzz} = \alpha^{q}_{zzxx} = -(1/3)\alpha^{q}$$

all the other components being zero.

With the residual C_{4v} symmetry in the presence of the vacancy defect, we have

$$\sum F_{kl} = 0, \qquad k \neq l \tag{4.13}$$

The principal axes x', y' and z' of the electric field gradient tensor are oriented along [1 0 0], [0 1 0] and [0 0 1]. We consider the displacement of the ions to be radial to the defect. In such cases, the diagonal elements of the F_{kl} tensor follow the following relation

$$\sum F_{x'x'} = \sum F_{y'y'} = -\left(\frac{1}{2}\right)\sum F_{z'z'}$$

here z' is taken along the symmetry axis in the radial direction of the field point.

Now as we put these symmetry relations for the quadrupolar polarizability and electric field gradient tensor in eq. 4.12, the quadrupole moment tensor also turn out to be cylindrically symmetric, i.e.

$$Q_{x'x'} = Q_{y'y'} = -\left(\frac{1}{2}\right)Q_{z'z'}$$

$$Q_{x'y'} = Q_{x'z'} = Q_{y'z'} = 0$$

So there is only one independent component of the quadrupole moment, i.e. $Q_{z'z'}$ which is to be detremined here.

Solving Dipole and Quadrupole Moments

In EPPI model, the contribution from the quadrupoles to the defect enthalpy is to be taken into account. We take quadrupoles for Region1 ions only and ignore them in Region2 ions. For an anion vacancy, the equations for dipole and quadrupole moments of one of the nearest neighbours of the defect with the symmetric axis along z' are

$$p^c_{z'} = \alpha^d_c \left\{F^1_m + F^1_d + F^2_d + F^1_q\right\}_{z'} \tag{4.14}$$

$$Q^c_{z'z'} = \alpha^q_c \frac{\partial}{\partial z'} \left\{F^1_m + F^1_d + F^2_d + F^1_q\right\}_{z'} \tag{4.15}$$

where $\mathbf{F}_m^1$ is the field due to monopoles of Region1, $\mathbf{F}_d^1 + \mathbf{F}_d^2$ is the total dipole field due to Region1 and Region2 and $\mathbf{F}_q^1$ is the quadrupole field of Region1 only.

The explicit expressions for the field terms are

$$F^1_{m,z} = \frac{e}{(1+s_c)^2 r_0^2} - \left[\frac{1.6642}{(1+s_c)^2} - \frac{1}{(2+s_c)^2} - \frac{4(1+s_c)}{\{(1+s_c)^2+1)\}^{1.5}}\right]\frac{e}{r_o^2} \quad (4.16)$$

$$F^1_{d,z} = \frac{2.3713 p_c}{r_0^3(1+s_c)^3} \quad (4.17)$$

$$F^2_{d,z} = \frac{e}{r_0^2}\{odds(s_c)M_c + evens(s_c)M_a\} \quad (4.18)$$

$$F^1_{q,z} = \frac{0.8893}{r_0^4(1+s_c)^4}Q_c \quad (4.19)$$

and those for field gradients are

$$F^1_{m,zz} = \frac{2e}{(1+s_c)r_o^3} + \frac{4e\{2(1+s_c)^2-1\}}{\{(1+s_c)^2+1\}^{2.5}r_o^3} - \frac{2.9571e}{(1+s_c)^3 r_o^3} \quad (4.20)$$

$$F^1_{d,zz} = \frac{3.5570 p_c}{(1+s_c)^4 r_o^4} \quad (4.21)$$

$$F^2_{d,zz} = \frac{e}{r_o^3}\{odds'(s_c)M_c + evens'(s_c)M_a\} \quad (4.22)$$

$$F^1_{q,z} = -\frac{2.7066}{(1+s_c)^5 r_o^5}Q_c \quad (4.23)$$

where

$$M_{c,a} = \frac{(\alpha_{c,a} + \alpha_d)(\varepsilon_s - 1)}{8\pi\varepsilon_s(\alpha_c + \alpha_a + 2\alpha_d)} \quad (4.24)$$

and s_c is the fractional displacement of Region1 cations.

Here *odds*(s_c) and *evens*(s_c) represent the magnitudes of appropriate lattice sums for the field at the site $(1 + s_c, 0, 0)r_0$ due to the dipole moments induced in ions of Region2 corresponding to cation and anion shells surrounding the defect, respectively. First the field at the desired $(0, 0, 1 + s_c)r_o$ site is evaluated for a mesh of the relaxations(s_c) and then fitted to a fourth degree polynomial in s_c. The derivative of this field term is obtained

Table 4.4: Dipole and quadrupole moments

Salts	MPPI				EPPI			
	Cation Vacancy		Anion Vacancy		Cation Vacancy		Anion Vacancy	
	$p_c(e\text{Å})$	$Q_c(e\text{Å}^2)$	$p_a(e\text{Å})$	$Q_a(e\text{Å}^2)$	$p_c(e\text{Å})$	$Q_c(e\text{Å}^2)$	$p_a(e\text{Å})$	$Q_a(e\text{Å}^2)$
MgO	-0.4458	0.0	0.0231	0.0	-0.4432	4.5028	0.0231	-0.0334
CaO	-0.8043	0.0	0.1528	0.0	-0.8053	3.1281	0.1524	-0.3957
SrO	-1.4242	0.0	0.4139	0.0	-1.4262	2.6043	0.4169	-0.9068
BaO	-1.84	0.0	0.9266	0.0	-1.8464	2.1096	0.9671	-4.8180

just by taking the derivatives of these polynomials written as $odds'(s_c)$ and $evens'(s_c)$. The polynomials are only structure dependant and we take them from the work on *AgCl* and *AgBr*[60].

$$evens(s_c) = -4.7166s_c^4 + 14.8716s_c^3 + 9.2984s_c^2 - 2.1459s_c - 1.9659 \quad (4.25)$$

$$odds(s_c) = -1.056s_c^4 + 0.2219s_c^3 + 0.1847s_c^2 - 0.6753s_c - 0.3888 \quad (4.26)$$

Similar relations can be obtained for cation vacancy also. Solving eqns. 4.14, 4.15 and those for cation vacancy, we obtain the set of values for dipole moments p_c, p_a and quadrupole moments Q_c, Q_a of the Region1 cations and anions respectively surrounding a defect of opposite species for all four crystals (*MgO*, *CaO*, *SrO*, *BaO*). These values are listed in table 4.4

4.3 Energy Terms

For a vacancy defect, where we extract either a cation or an anion from the regular site, the defect energy terms can be written as

$$W_{defect} = W_{rl} + W_{co} + W_{sr} + W_p + W_q \quad (4.27)$$

where W_{rl} is the rigid lattice energy needed to create the defect when all the other ions are fixed at their perfect sites, W_{co} is the coulomb monopole interaction energy, W_{sr} is the short range energy due to the relaxation of the 1st region, W_p is the total dipole polarization energy and W_q is the quadrupolar contribution. Below, we give explicit expressions for the defect terms in case of an anion vacancy[60]. The relaxations of the ions have been taken to be radial to the defect.

Rigid Lattice Energy

The creation of a vacancy can be imagined as the breaking of bonds between the ions at the site of vacancy and its neighbours. In case of a rigid lattice, where the ions do not get polarized and remain fixed at their regular sites, the energy required to snatch out an ion is given by the rigid lattice energy W_{rl}. For a fcc lattice with the short range interaction accounted for only first and second neighbours, W_{rl} can be written as

$$\begin{aligned} W_{rl} &= \frac{\alpha_M e^2}{r_o} - 6A_{ca}\exp\left(-\frac{r_o}{\rho_{ca}}\right) - 12A_{aa}\exp\left(-\frac{\sqrt{2}r_o}{\rho_{aa}}\right) \\ &\quad + \frac{6.5952C_{ca}}{r_o^6} + \frac{1.8067C_{aa}}{r_o^6} \end{aligned} \tag{4.28}$$

Here the first term is the Madelung term which involves an infinite sum over the lattice represented by the Madelung constant α_M. Rest of the terms are the short range repulsive and van der Waal terms.

Monopole Energy

For a defect lattice, with a vacancy in it, the ions surrounding the defect (in this case, the 1st shell ions) get displaced. Eventually, we can imagine virtual charges at the defect site as well as the vacated lattice sites and real charges at the displaced sites as far as coulomb

interaction is concerned. So the total contribution to the monopole monopole energy from Region1 ions is

$$\begin{aligned} W_{co} &= 6\left(-\frac{e^2}{(2+s_c)r_o}+\frac{e^2}{(1+s_c)r_o}-\frac{4e^2}{\{(1+s_c)^2+1\}^{\frac{1}{2}}\,r_o}\right) \\ &\quad +6\left(\frac{1.6642e^2}{(1+s_c)r_o}\right)+6\left(\frac{0.6642e^2}{r_o}\right) \end{aligned} \tag{4.29}$$

here, s_c as defined earlier is the displacement of the first shell cations.

Short Range Energy

The total short range energy can be splitted into three terms

$$W_{sr} = W_{sr}^{1} + W_{sr}^{12} + W_{sr}^{2} \tag{4.30}$$

The first term is the change in short range energy between cations of Region1. The second term is the interaction between the 1st region cations with their first and second neighbours coming from Region2 and the third term is the harmonic approximation term. Here

$$W_{sr}^{1} = \sum_{i,j\in 1}\left\{\phi_{ij}\left(\left|\mathbf{r}_i-\mathbf{r}_j\right|\right)-\phi_{ij}\left(\left|\mathbf{R}_i-\mathbf{R}_j\right|\right)\right\} \tag{4.31}$$

$$W_{sr}^{12} = \sum_{i\in 1,j\in 2}\left\{\phi_{ij}\left(\left|\mathbf{r}_i-\mathbf{r}_j\right|\right)-\phi_{ij}\left(\left|\mathbf{R}_i-\mathbf{r}_j\right|\right)\right\} \tag{4.32}$$

$$W_{sr}^{2} = -\frac{1}{2}\sum_{i\in 1,j\in 2}\left\{\frac{\partial\phi_{ij}\left(\left|\mathbf{r}_i-\mathbf{r}_j\right|\right)}{\partial\boldsymbol{\xi}_j}-\frac{\partial\phi_{ij}\left(\left|\mathbf{R}_i-\mathbf{r}_j\right|\right)}{\partial\boldsymbol{\xi}_j}\right\}\Bigg|_{\boldsymbol{\xi}_{j,o}}.\boldsymbol{\xi}_{j,o} \tag{4.33}$$

with

$$\phi_{ij}\left(\left|\mathbf{r}_{ij}\right|\right) = A_{ij}\exp\left(-\frac{r_{ij}}{\rho_{ij}}\right)-\frac{C_{ij}}{r_{ij}^{6}} \tag{4.34}$$

and $\boldsymbol{\xi}_{j,o}$ is the ML displacement of the Region2 ions as given in section 4.2

Polarization Energy

The various contributions to the polarization energy both from Region1 and Region2 are

$$W_p = W^1_{p,m} + W^1_{p,d} + W^2_{p,d} \tag{4.35}$$

Where the first term is the monopole-dipole term, second term is the interaction of displacement dipoles of Region1 with the field of Region2 dipoles and the last term is the contribution from Region2 dipoles.

$$W^1_{p,m} = -3p_c \cdot \mathbf{F}^1_m \tag{4.36}$$

$$W^1_{p,d} = -3(es_c r_o)\mathbf{F}^2_{d,z} \tag{4.37}$$

$$W^2_p = \frac{1}{2} V^2_p q_d \tag{4.38}$$

Here V^2_p is the potential of a dipole $\boldsymbol{\gamma}_{c,a}$ of an ion i in Region2 at the position $\mathbf{r}_i$ from the origin, q_d is the charge of the defect,F^1_m and $F^2_{d,z}$ are the monopole and dipole fields as given in section 4.2.1. p_c is the induced dipole moment of the Region1 cations.

$$\begin{aligned} V^2_p &= -\sum_i \frac{\boldsymbol{\gamma}_{c,a} \cdot \mathbf{r}_i}{|\mathbf{r}_i|^3} \\ &= -\frac{q_d}{r_o}\left(M_c \sum_{i\in odd} \frac{1}{|\mathbf{r}'_i|^4} + M_a \sum_{i\in even} \frac{1}{|\mathbf{r}'_i|^4} \right) \end{aligned} \tag{4.39}$$

$|\mathbf{r}'_i|$ has been defined as $|\mathbf{r}'_i|\, r_o$. The infinite odd and even sums can be obtained by using Ewald sum[Appendix A].

Quadrupole Energy

The quadrupolar polarization energy for Region1 is given by

$$W_q^1 = 6\left(\left(\frac{1}{2}\right).\left(-\frac{1}{6}\right).\sum_{ij} F_{m,ij}^1\right) \tag{4.40}$$

Here the factor $\frac{1}{2}$ comes from the induced nature of the quadrupoles. Using the symmetry properties of the electric field gradient tensor along with the cylindrical symmetry of the quadrupole moments eq. 4.40 reduces to the following form

$$W_q^1 = -\frac{3}{4}Q_c F_{m,zz}^1 \tag{4.41}$$

4.4 Results and Discussions

A complete split-up of the various energy terms for defect formation energy in different crystals are listed in table 4.5. In fig 4.3, anion and cation vacancy energies (AVE and CVE respectively) are plotted as a function of relaxation for both MPPI and EPPI models. For *MgO*, the quadrupolar polarizability of *Mg* being very small, AVE plots for MPPI and EPPI nearly coincide. For other compounds, the separation between AVE plots for MPPI and EPPI increases with increasing Quadrupolar polarizability of the cations. As expected, the EPPI energies lie lower than MPPI in all the plots. The resulting Schottky defect enthalpies are shown in table 4.6. From table 4.6, we see that the h_s^f values decreases with increasing r_o. This is obvious because ions get more and more loosely bound as their distances with the nearest neighbours increases. The most important feature of this study is that the contribution from quadrupolar distortion is pretty significant, as high as $2.9eV$ in case of *MgO*.

Table 4.5: Various energy terms for anion and cation vacancy with MPPI and EPPI Models

I. Anion Vacancy ::

a) MPPI

	Relaxation	W_c (eV)	W_{sre} (eV)	W_p (eV)	W_q (eV)	W_L (eV)	E_{av} (eV)
MgO	0.1025	-13.4695	6.4309	-8.8939	0.0	40.3316	24.3991
CaO	0.0955	-11.1516	5.4454	-8.2431	0.0	35.7024	21.7532
SrO	0.0815	-9.1580	4.5829	-8.5011	0.0	36.3355	20.2892
BaO	0.0705	-7.5810	3.5542	9.2549	0.0	31.2518	17.9701

a) EPPI

	Relaxation	W_c (eV)	W_{sre} (eV)	W_p (eV)	W_q (eV)	W_L (eV)	E_{av} (eV)
MgO	0.1025	-13.4695	6.4309	-8.8938	-0.0194	40.3316	24.3799
CaO	0.0935	-10.9644	5.294	-8.4359	-0.1607	35.7024	21.5961
SrO	0.0775	-8.783	4.3012	-8.575	-0.3254	33.3655	19.9832
BaO	0.0495	-5.5678	2.3457	-9.7569	-1.6223	31.2518	16.6506

II. Cation Vacancy ::

a) MPPI

	Relaxation	W_c (eV)	W_{sre} (eV)	W_p (eV)	W_q (eV)	W_L (eV)	E_{av} (eV)
MgO	0.0805	-11.0841	5.2464	-10.1623	0.0	42.3878	26.3877
CaO	0.0765	-9.3011	4.3831	-9.7029	0.0	37.1248	22.5041
SrO	0.0605	-7.1100	3.3109	-10.6519	0.0	34.4965	20.0454
BaO	0.0575	-6.3575	2.8579	-11.1193	0.0	32.3013	17.6824

a) EPPI

	Relaxation	W_c (eV)	W_{sre} (eV)	W_p (eV)	W_q (eV)	W_L (eV)	E_{av} (eV)
MgO	0.0585	-8.4425	3.4610	-10.6350	-3.2465	42.3878	23.5248
CaO	0.0635	-7.9378	3.4615	-9.9969	-1.4767	37.1248	21.1749
SrO	0.0505	-6.0635	2.6704	-10.9261	-1.0683	34.4965	19.1091
BaO	0.0495	-5.5678	2.3972	-11.3561	-0.7103	32.3013	17.0643

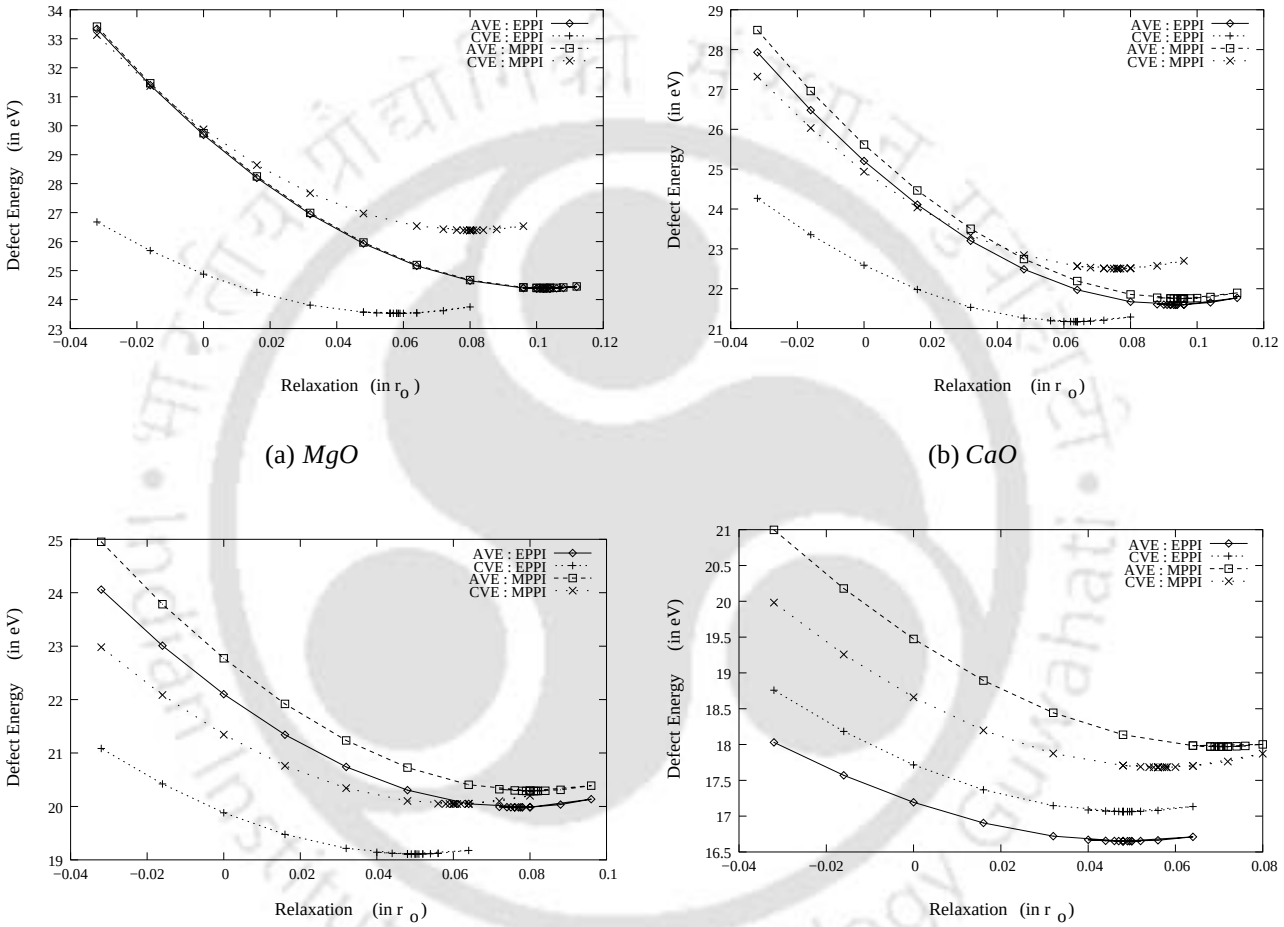

(a) *MgO* (b) *CaO*

(c) *SrO* (d) *BaO*

Figure 4.3: Effect of quadrupoles on the cation and anion vacancy energies. AVE and CVE stand for anion and cation vacancy energy.

Table 4.6: Theoretical Schottky defect enthalpies

Salts	r_o(Å)	$h_S^f(eV)$ (SHELL)	$h_S^f(eV)$ (MPPI)	$h_S^f(eV)$ (EPPI)	diff.
MgO	2.11	7.5	8.76	5.88	2.9
CaO	2.41	6.7	7.41	5.93	1.5
SrO	2.58	6.0	5.92	4.68	1.2
BaO	2.76	3.4	3.44	1.50	1.9

4.5 Comparison with Experimental Results

We present here some analysis on the experimental work done by Harding & Price[110] on cation self diffusion in single crystal *MgO* with an attempt to compare our theoretical values with their experimental one.

4.5.1 Self Diffusion in Ionic Crystals

Self dffusion in a crystal means the diffusion of regular atoms in the crystal. The most common and easiest mechanism of self diffusion in an ionic crystal is the vacancy mechanism. The cation self diffusion by vacancies in a cubic crystal is given by

$$\mathrm{D} = \mathrm{KTf}\mu_c\mathrm{x_c}/\mathrm{e} \tag{4.42}$$

Where f is the correlation factor, K the Boltzmann's constant, T the absolute temperature, x_c is the cation vacancy concentration and e is the charge of the species. Mobility μ_c of the vacancy defect is given by

$$\mu_c = \frac{4\mathrm{a}^2\mathrm{e}\nu_c}{\mathrm{KT}} \exp\left(-\frac{\Delta \mathrm{g^m}}{\mathrm{KT}}\right) \tag{4.43}$$

Here a is the nearest neighbour distance, ν_c is the cation jump frequency and g^m is the free energy of migration.

For intrinsic diffusion,

$$x_c = x_o = \exp\left(-\frac{g_s^f}{2K_BT}\right) \tag{4.44}$$

where g_s^f is the free energy of formation. Eq. 4.42 becomes

$$D = KTf \exp\left(-\frac{g_s^f}{2K_BT}\right)\frac{4a^2e\nu_c}{KT}\exp\left(-\frac{\Delta g^m}{KT}\right) \tag{4.45}$$

x_o is the equilibrium defect concentration.

For extrinsic diffusion, $x_c = c$, where c is the impurity concentration. So eq. 4.42 becomes

$$D = KTfc\frac{4a^2e\nu_c}{KT}\exp\left(-\frac{\Delta g^m}{KT}\right) \tag{4.46}$$

Splitting the free energies into entropy and formation energies, the self diffusion coefficient D for intrinsic and extrinsic regions come out to be

$$D_{int} = D_o \exp\left(\frac{s_s^f}{2K_B}\right)\exp\left(\frac{s_c^m}{K_B}\right)\exp\left\{-\frac{\left(\frac{1}{2}h_s^f + h_c^m\right)}{K_BT}\right\} \tag{4.47}$$

$$D_{ext} = D_o c \exp\left(\frac{s_c^m}{K_B}\right)\exp\left(-\frac{h_c^m}{K_BT}\right) \tag{4.48}$$

where $D_o = KTf$. h_s^f, h_c^m are the Schottky formation and migration enthalpies and s_s^f, s_c^m are the corresponding entropy values.

An Arrhenius plot of $\ln(D)$ vs. $(KT)^{-1}$ will give straight lines with slopes $\frac{1}{2}h_s^f + h_c^m$ for the intrinsic region and h_c^m for the extrinsic one.

4.5.2 Impurity-Vacancy Association Effect

In the above discussion, as for the intrinsic region, it is assumed that the concentration of vacancies introduced by the impurities is constant. This is not always true. Because of the

effective charges on the impurity and the vacancy, there exists a strong coulombic attraction between them , which generates stable impurity-vacancy pairs. These pairs behave just like electric dipoles and donot contribute to the charge transport process.

For tetravalent impurity in a divalent crystal (like *MgO*), we have an impurity-vacancy diad as

$$g_b + X \rightleftharpoons V + C$$

where X is the imp-vacancy complex, g_b is the free energy of association, V and C are the vacancy and interstitials. The equation for the concentration of associated pairs x_k is

$$\begin{aligned} \frac{x_k}{x_c(c - x_k)} &= z \exp\left(\frac{g_b}{K_B T}\right) \\ &= K_1 \end{aligned} \tag{4.49}$$

Here x_c is the concentration of the vacancies and c is the total impurity concentration. $c_i = (c - x_k)$ is the concentration of the dissolved impurity. z gives the number of distinct orientations of the pair in the lattice.

Now the charge neutrality condition is

$$x_c = x_a + (c - x_k) \tag{4.50}$$

If the intrinsic defect concentration $x_o << c$, $x_c \approx c - x_k$. Putting $x_k = \beta c$, eq. 4.49 becomes

$$\beta^2 - \beta\left(2 + \frac{1}{z \exp\left(\frac{1}{\eta}\right) c}\right) + 1 = 0 \tag{4.51}$$

where $\eta = \dfrac{KT}{g_b}$.

For trivalent and monovalent impurities, we have an impurity-vacancy triad instead of

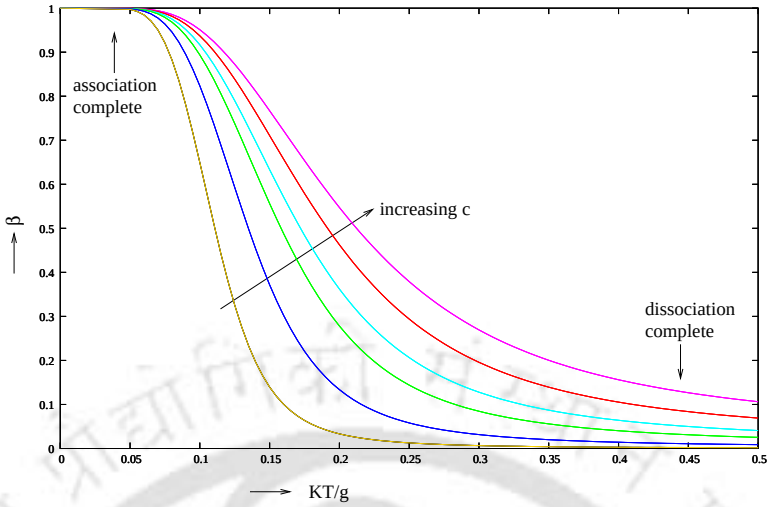

Figure 4.4: β vs. $\frac{KT}{g_b}$ plots for impurity-vacancy diad

a diad. The corresponding charge balance equation is

$$\beta^3 - 3\beta^2 - \left(3 + \frac{2}{z\exp\left(\frac{1}{\eta}\right)c^2}\right)\beta + 1 = 0 \tag{4.52}$$

The β vs. $\dfrac{KT}{g_b}$ plots at different total impurity concentrations for impurity-vacancy diad are shown in Fig. 4.4. Under the condition of complete association, $\beta \approx 1$ and so

$$\begin{aligned} x_c \approx c_i &= c^{\frac{1}{2}}\exp\left(-\frac{g_b}{2KT}\right) && \text{,for impurity-vacancy diad} \\ &= 2^{-\frac{2}{3}}c^{\frac{1}{3}}\exp\left(-\frac{g_b}{3KT}\right) && \text{,for impurity-vacancy triad} \end{aligned}$$

Similarly, for complete dissociation, $\beta \approx 0$ and so

$$x_c = c$$

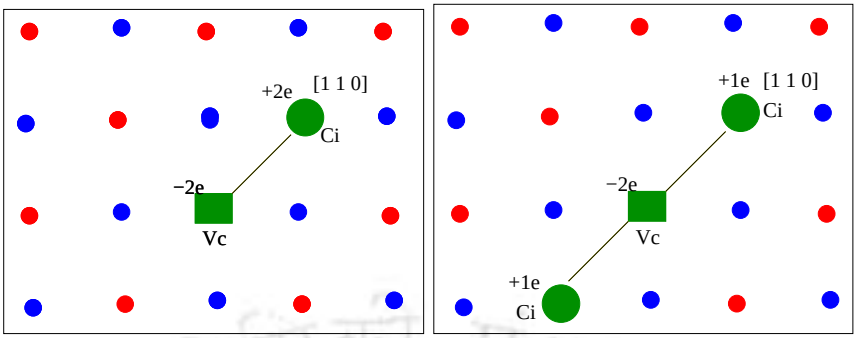

(a) Si^{4+} (b) Al^{3+} and Fe^{3+}

Figure 4.5: Impurity - vacancy clusters for different impurities

4.5.3 Re-interpretation of Experimental Data

As discussed above, we see that considering the impurity-vacancy association effect, the slope of the Arrhenius plot in the extrinsic region is not simply h^m but $h^m + \frac{1}{2}g_b$ in case of a impurity- vacancy diad and $h^m + \frac{1}{3}g_b$ in case of a triad. Without considering these effects harding and Price[110] interpreted their experiental result to give Schottky defect enthalpy of MgO as 3.8 ± 0.3 eV.

An analysis of the MgO crystal from the same source[114] showed that the impurities present in the MgO crystal are Si^{4+} , Al^{3+} and Fe^{3+}. The possible clusters formed by these impurities with the native vacancies are shown in Fig 4.5. Fig 4.5(a) is for Si^{4+} and Fig 4.5(b) is for Al^{3+} and Fe^{3+}. To estimate the binding energy g_b of the impurity-defect clusters in the three cases we use the simple electrostatic approximation

$$g_b = \sum_{i,j} \frac{q_i q_j}{r_{ij}} \tag{4.53}$$

where q_i 's are the effective charges of the defect impurity in the cluster, r_{ij} is the interionic distance and the summation is over all the pairs of point charges in the cluster. Table 4.7

shows the binding energy (g_b) and the values of Schottky formation enthalpy for the different impurity types taking care of the impurity-vacancy association.

Table 4.7: Experimental Schottky defect enthalpies

Impurity	g_b (eV)	c (ppm)	β	degree of association	$h^m(eV)$	$h_S^f(eV)$
Si^{4+}	2.0	400	0.96	high	0.56	5.8
Al^{3+}, Fe^{3+}	1.7	200	0.003	low	0.99	3.8

Thus we see that the dominant impurity in the crystal sample of Harding and Price which is Si^{4+} (400 ppm) suggests the most probable value of h_S^f to be 5.8 eV for MgO in excellent agreement with the theoretical value of the present work with EPPI model (5.88 eV).

Chapter 5

Atomistic Simulation of Low Symmetry $\beta - Ga_2O_3$ in MPPI Framework

The atomistic simulations of low symmetry materials are usually difficult for variety of reasons. First, such structures are complex and have large number of ions per unit cell. Secondly, the number of independent variables becomes very large. More importantly, even in perfect crystals, the electric fields at ionic sites do not vanish. If the ions are highly polarizable, the electric fields polarize the ions. Even though, the net polarization is absent, individual ions have dipole moments. In simulations based on Shell model, ionic polarizations are treated by means of springs connecting the cores and shells. Hence, the Shell model only deals with rigid monopole charges, though the number of monopoles may be double to that of ions. The low symmetry adds to complexity only by increasing the number of ions, but the formulation is exactly same and straight-forward.

In contrast to Shell model, the point polarization ion (PPI) models[50], become very complex. For this reason, the atomistic simulations in various PPI models were restricted only to high symmetry structures, mostly the simple cubic structures. Usually, in high symmetry materials, ions in the perfect crystals do not have dipole moments. Hence the short

range potentials can be obtained by optimizing the crystals with rigid ion approximation. The defect calculations, then use the same short range potentials. With the low symmetry crystals, we must evolve a method to obtain the short range potentials in presence of ionic dipoles.

Another difficulty arises due to lack of knowledge of electronic polarizabilities. Free ion values of electronic polarizabilities overestimate the polarizations in defect calculations. The polarizabilities in crystal environment are usually suppressed. The MPPI model[44] has clearly demonstrated this point. In MPPI, since the short range potentials are already known, displacement polarizabilitities are calculated using the force constants and are used in turn to calculate the electronic polarizabilities. The generalization of this procedure to low symmetry crystals is not straight forward, since the perfect crystal simulations itself must use electronic polarizabilities. Thus the electronic polarizabilities and short range parameters must be simultaneously deduced by perfect crystal optimizations.

The motivation behind this study is two-fold. First, the formalism of MPPI (and later, EPPI) needs be generalized to include low symmetry materials. These models have been very successful in defect simulation of high symmetry materials, mostly cubic. Secondly, to make these calculations accessible to material scientists, we need to develop packages like GULP or HADES. These packages were built on Shell model and are very popular. There is a lack of such packages for MPPI models. In this work, first we have formulated and built algorithms for modeling of perfect crystals, based on MPPI models. Then we have suggested formulations for the defect calculations. All through this work, we have applied these formulations to monoclinic $\beta - Ga_2O_3$ as an example.

$\beta - Ga_2O_3$ is the most stable phase at room temperature out of the five existing phases (α, β, γ, δ and ϵ)[115]. It is intrinsically an insulator with a band gap of $4.8eV$. However when synthesized under reduced conditions, the material becomes an n-type semiconductor[116].

In Gallium Oxide, the gallium and oxygen atoms are bonded ionically . Like any other metallic oxides, this material has wide applications in the field of material science and optoelectronics. It is used as a component in preparing the anodic oxide on $GaAs$ which has drawn subsequent attention in the semiconductor industry[117] and also acts as an important MASER material when doped with Cr^{3+}[118]. Very recently, it has found its application as an ultraviolet transparent conducting oxide in excimer LASER[119] and has created sensations in the environmental technology by being used as a gas sensor. The new gas sensors based on Ga_2O_3 films have very stable operating characteristics and are largely insensitive to humidity[120].

β–Ga_2O_3 which exhibits some features like blue luminescence and ultra violet emission [121, 122] implying the presence of grown oxygen vacancies as well as some impurities, stands as a very interesting candidate for studying the point defects and defect induced transport properties. Owing to the low symmetry structure of the material, there is lack of enough theoretical work to describe the complete picture of energetics in the perfect and imperfect crystals of $\beta - Ga_2O_3$. One common approach for this is the semi-empirical atomistic simulation. In the present work, we present the atomistic simulations using MPPI models.

5.1 Structure and Symmetry of $\beta - Ga_2O_3$

Single crystals of $\beta - Ga_2O_3$ can be grown by several techniques like Verneuil technique, chemical transport method, vapour phase reaction method etc.[123, 124, 125, 126]. In spite of some debate[127], several investigations[128, 129, 130] on these crystals have shown that the crystal is monoclinic in structure with a space group of $C2/m$. There are four Ga_2O_3 molecules per unit cell out of which two galliums (Ga_I and Ga_{II}) and three oxygens (O_I, O_{II} and O_{III}) are crystallographically inequivalent to each other. An interesting feature

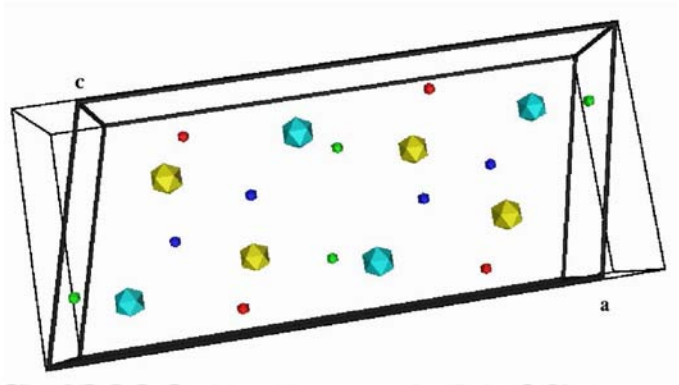

(a) along the symmetry axis

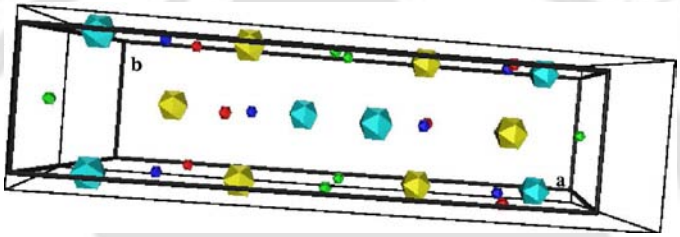

(b) perpendicular to the symmetry axis

Figure 5.1: Cross sections of the Ga_2O_3 unit cell. Big spheres are galliums, small ones are oxygens.

of this structure is that the Ga^{3+} ions show two different co-ordinations in the unit cell. Ga_I ions are surrounded by tetrahedra each of four oxygens while Ga_{II} are surrounded by octahedra each of six oxygens. The oxygens on the other hand do not show any definite co-ordination. The cross sections of the unit cell along and perpendicular to the unique axis *b* are shown in fig 5.1. The reported experimental values of the cell dimensions, fractional co-ordiantes and average interionic distances[128] are listed in table 5.1. With the space group symmetry of $C - 2/m$, the multiplicity of each atom in the unit cell of $\beta - Ga_2O_3$ is 8. The cross-sectional view of the symmetry elements perpendicular to and along the symmetry axis are shown in fig 5.2. These figures are reproduced from the International

Table 5.1: Experimental structural parameters for $\beta - Ga_2O_3$

a) Cell Parameters

a(in Å)	b(in Å)	c(in Å)	β (in degree)
12.23 ± 0.02	3.04 ± 0.01	5.80 ± 0.01	103.7 ± 0.3

b) Average Interionic Distances

$Ga-O$ (in Å) tetrahedral	$Ga-O$ (in Å) octahedral	$O-O$ (in Å) tetrahedron edge	$O-O$ (in Å) octahedron edge
1.83	2.00	3.02	2.84

c)Fractional Co-ordinates

Atom	x	y	z
Ga_I	0.0904	0.0	-0.2052
Ga_{II}	0.3414	0.0	-0.3143
O_I	0.1674	0.0	0.1011
O_{II}	0.4957	0.0	0.2553
O_{III}	0.8279	0.0	0.4365

Tables for Crystallography edited by Theo Hahn.

5.2 Perfect Crystal Calculations

Typically, for high symmetry ionic crystals, the pair-wise potentials are Coulomb potentials and short range potentials. The short range potential parameters are taken to be independent variables. The structural paramters (cell parameters and ionic coordinates) are then found by minimizing lattice energy. Symmetry of the crystals is preserved while optimizing the lattice energy. Bulk properties like dielectric constant, elastic constants etc are then calculated. The independent variables are varied until the computed bulk properties fit the experimental data.

In case of low symmetry perfect crystals, as discussed earlier, induced ionic dipole moments are also present along with the monopoles. Since the electronic polarizabilities are not known a priori, we need to find these along with the potential parameters. In MPPI model, the electronic polarizabilities are fitted to the static dielectric constant rather than

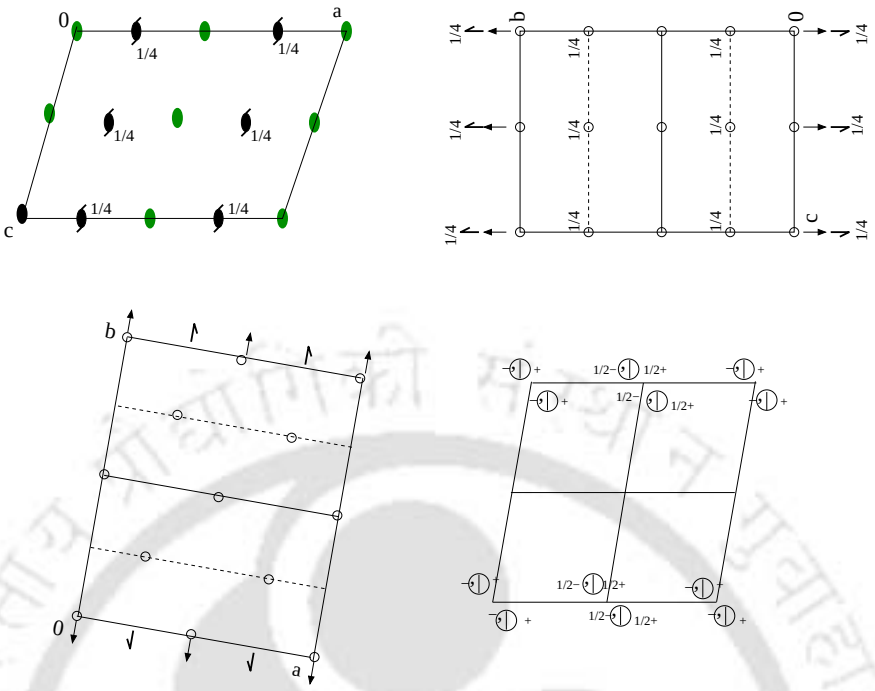

Figure 5.2: Symmetry elements of the unit cell of $\beta - Ga_2O_3$

high-frequency dielectric constant. Thus we treat electronic polarizabililities as independent variables along with the potential parameters. Designing a full fledged code to fit the short range potential parameters under MPPI model is beyond the scope of this work. We have split the problem into two steps.

It has been shown, in MPPI model calculations, that the electronic polarizabilities are suppressed in the crystal environment and their contribution to the total lattice energy is small[60]. It also has been shown that even with the TKS polarizabilities, the difference in the structural paramenters with and without dipole moments is not very large[131]. With this approximation, we suggest that the starting guess for potential parameters can be obtained by using a rigid ion calculation.

Hence, in the first step, we find the short range potential paramenters using rigid ion model using package GULP. In the second step, we perform a full MPPI model in presence

of dipole moments and obtain electronic polarizabilities such that the computed properties fit with the empirical data, like static dielectric constant and structural parameters. An algorithm of these calculations is presented in fig. 5.3.

5.2.1 Rigid Ion Calculations

GULP is primarily based on Shell model and is designed for both perfect and defect crystal calculations. However, it can be used for calculations based on rigid model by eliminating the shells and putting whole of the ionic charge to the core. Thus we get a system of non-polarizable ions which interact with each other via coulomb and short range terms only.

In GULP, the relation between dielectric constant and the polarizability is given by

$$\varepsilon_s = 1 + \frac{4\pi}{v_m}\alpha_d. \tag{5.1}$$

Where ε_s is the static dielectric constant and α_d is the displacement polarizability. v_m is the unit cell volume.

This relationship is based on Maxwell's field and neglects the local field correction [AppendixB]. This is plausible, however, only for systems with low molecular concentration like in a gaseous medium where the polarization **P** is also small and the local field becomes more or less the same as the average field[132]. On the other hand, for liquids and solids, appropriate equation is Claussius-Mossotti (CM)equation which has been derived taking into account of the local field contributions.

$$\varepsilon_s = \frac{1 + \frac{8\pi}{3v_m}\alpha}{1 - \frac{4\pi}{3v_m}\alpha} \tag{5.2}$$

Here α is the total polarizability, both electronic and displacement.

This requires us to fit the rigid ion calculations to a lower value of dielectric constant. In

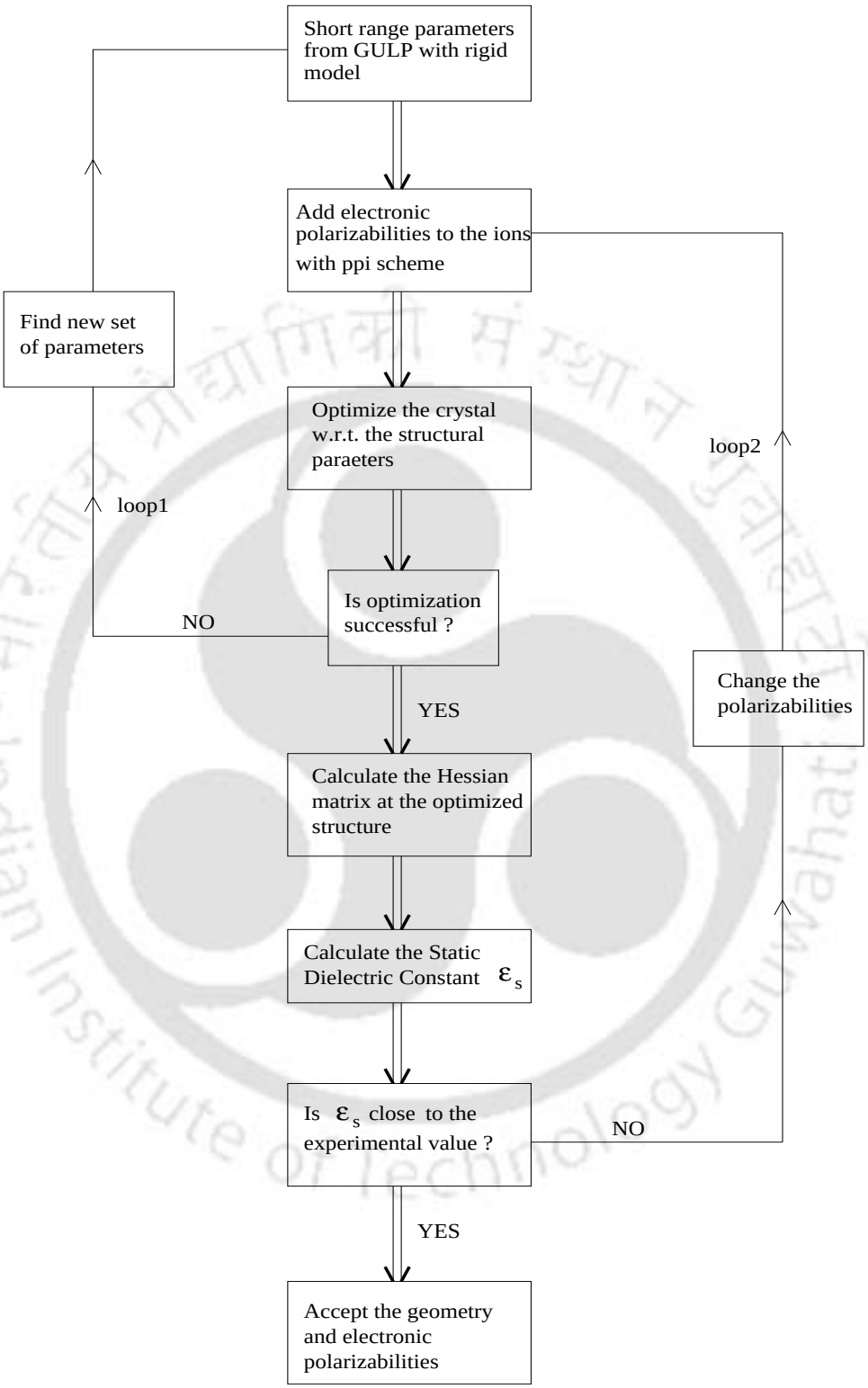

Figure 5.3: Algorithm for perfect crystal simulations

addition, we can see from the CM relation, the dielectric constant is directly proportional to the polarizability. Our aim is to use the rigid model potential parameters in a MPPI model where the polarizability will be enhanced by contributions from the electronic part. Our initial guess is that the lower value of dielectric constant will be compensated by the addition of electronic polarizability. This is however not so staightforward as the displacement polarizability will assume new value in the MPPI scheme but still is expected to help in getting a good starting parameters for the MPPI calculations.

In GULP, The parameters were fitted at constant volume. Relax fitting was used, where at each point during the fit, the structure is optimized and the displacement of the structural parameters are calculated instead of the gradients

5.2.2 MPPI Calculations

The next step in the algorithm is to find optimal values of electronic polarizabilities by doing a full MPPI calculation. In the MPPI calculations, a stable structure is found by minimizing the lattice energy. Only now, the dipole moments make the calculations more involved. The details of lattice energy terms, its gradients and dipole moments are given in subsequent sections.

Once we have found the potential parameters, full MPPI calculation is done over and again by varying the electronic polarizabilities until the experimental values are reproduced. However it may happen that the optimization fail to converge to a stable structure. In this case, we go back to the rigid ion calculations to find a new set of potential parameters.

The optimization was done using the hsl(Harwell Subroutine Library) package va06. va06 calculates the least value of a multivariative function F ($x_1, x_2, ..., x_n$) of n variables, where $n \geq 2$. The user has to provide an initial estimate of the required values of the vari-

Table 5.2: Electric field at experimental sites of symmetry unique ions in $\beta - Ga_2O_3$

	E_x ($eV/Å^2$)	E_y ($eV/Å^2$)	E_z ($eV/Å^2$)
Ga_I	-0.306689	0.0	-0.217690
Ga_{II}	-0.648151	0.0	0.6555744
O_I	4.781664	0.0	0.136894
O_{II}	3.481877	0.0	1.760299
O_{III}	1.637611	0.0	1.700481

ables ($x_1, x_2, ..., x_n$) and a subroutine that calculates F ($x_1, x_2, ..., x_n$) and the first derivatives $\frac{\partial F}{\partial x_i}$, i = 1, 2, .., n, for any ($x_1, x_2, ..., x_n$). The energy gradient input makes the code work faster than va04 described in Chapter 3. The optimization technique used in this package is a combination of the steepest descent algorithm and the generalized Newton iteration. The Newton characteristics provide a fast final rate of convergence to the least value of the function and the steepest descent characteristics ensure a satisfactory accuracy criterion. The true minima are tested by finding the vibrational frequencies of the system. All of them come positive with first three null values for translational mode of the system.

5.2.3 Induced Dipole Moments

As discussed in §2.1.1, the nonzero electric field at the ions in the perfect lattice sites of low symmetry crystals give rise to dipole moment of the ions. This is the case of constituent ions in the Ga_2O_3 crystal. Table 5.2 gives the net electric field at the experimental symmetry unique sites of the $\beta - Ga_2O_3$ unit cell. Putting the explicit expressions for F_i^m and F_i^d in eq. 2.13 we get the expression for the dipole moment of the i^{th} ion in the unit cell as

$$\mu_i^\alpha = \alpha_i \sum_l \sum_j \left(\frac{q_j}{r^3} r^\alpha + 3\frac{\sum_\beta \mu_j^\beta r^\beta}{r^5} r^\alpha - \frac{\mu_j^\alpha}{r^3} \right)\Bigg|_{r\neq 0} \tag{5.3}$$

where l is the lattice vector. i and j goes over the ions per unit cell, α, β, γ are for the three cartesian co-ordinates and $\mathbf{r} = \mathbf{l} + \mathbf{r}_i - \mathbf{r}_j$, $\mathbf{r}_i$ and $\mathbf{r}_j$ being the position vectors of i^{th} and j^{th} ions. α_i, as defined all throughout is the electronic polarizability.

Eq. 5.3 can be written in the matrix form as

$$\sum_j \sum_\beta D_{ij}^{\alpha\beta} \mu_j^\beta = M_i^\alpha \tag{5.4}$$

where

$$D_{ij}^{\alpha\beta} = \begin{cases} \delta_{\alpha\beta} + \sum_l \left(-3\alpha_i \frac{r^\alpha r^\beta}{r^5} + \alpha_i \frac{\delta_{\alpha\beta}}{r^3} \right) & i = j \\ \sum_l \left(-3\alpha_i \frac{r^\alpha r^\beta}{r^5} + \alpha_i \frac{\delta_{\alpha\beta}}{r^3} \right) & i \neq j \end{cases}$$

and using Ewald's method, the monopole field component M_i^α, as derived in Appendix A, becomes

$$M_i^\alpha = -\alpha_i \left(\sum_l \sum_j q_j f1(r) \frac{r^\alpha}{r} \Big|_{r \neq 0} + \sum_j \frac{4\pi q_j}{V_c} \sum_{G \neq 0} f2(G) G_\alpha \sin(\mathbf{G}.\mathbf{r}) \right) \tag{5.5}$$

with

$$f1(r) = -\frac{2}{\sqrt{\pi}} \frac{g}{r} e^{-g^2 r^2} - \frac{1}{r^2} erfc(gr) \quad \text{and} \quad f2(G) = \frac{\exp\left(-\frac{G^2}{4g^2}\right)}{G^2}$$

Here $erfc$ is the complementary error function, g is a free parameter and G is the reciprocal lattice vector. It is not only the monopoles and short range forces which will define the stability of the crystal. We have dipolar forces at individual ion sites owing to the dipoles of all other ions.

5.2.4 Lattice Energy

Due to the translational symmetry, the energy of one unit cell in the perfect environment is exactly same as another unit cell in the crystal. As discussed in §2.3, the self energy term of induced dipoles reduces the electrostatic part of the energy only to monopole-monopole and monopole-dipole contributions. The short range term, on the other hand, has straightforward contribution to the total energy of the crystal. Thus we can write the lattice energy of a unit cell of the crystal as

$$E_L = E^{mm} - \frac{1}{2}E^{md} + E^{SR} \tag{5.6}$$

with

$$E^{mm} = \sum_{ij} \frac{q_i q_j}{r}$$

$$\begin{aligned} E^{md} &= \frac{1}{2}\sum_i \mu_i \cdot \sum_j \frac{q_j\left(\mathbf{r}_i - \mathbf{r}_j\right)}{r^3} \\ &= \frac{1}{2}\sum_i \mu_i \cdot M_i \end{aligned}$$

and

$$E^{SR} = \sum_{i,j}\left[-A_{ij}\exp\left(-\frac{r}{\rho_{ij}}\right) + \frac{C_{ij}}{r^6}\right]$$

where i goes over the ions in the unit cell and j eventually goes over the rest of the ions in the crystal. For short range term, the sum is terminated at some reasonable cut-off limit. Ewald's sum is used for M_i and E^{mm}. M_i is already given by eq. 5.5 and E^{mm} as derived in

Appendix A comes out to be

$$\begin{aligned} E^{mm} &= \frac{1}{2}\sum_{l=0}^{\infty}\sum_{i,j}\frac{Q_i Q_j}{4\pi\varepsilon_o}\frac{\mathrm{erfc}\,(gr(l))}{r(l)} \\ &\quad + \frac{1}{2}\sum_{i,j}\frac{Q_i Q_j}{4\pi\varepsilon_o}\frac{4\pi}{V_c}\sum_{G}\frac{\exp\left(-\frac{G^2}{4g^2}\right)}{G^2}\exp\left(i\mathbf{G}\cdot\left(\mathbf{r}_j-\mathbf{r}_i\right)\right) + W_{self} \end{aligned} \tag{5.7}$$

Here *i* and *j* both go over the unit cell ions while l goes over different unit cells.

5.2.5 Gradient of the Lattice Energy

As mentioned in §2.6, the availability of the first derivative of energy is useful in the minimization of energy. The effort in this case lies entirely in finding the gradient of dipole moment associated with the monopole-dipole energy. This is because the dipole moments are in turn associated to the different field terms of the system through a set of linear equations.

The simple derivative terms of the monopole and short range energies are

$$\delta E^{mm} = \sum_i q_i M_i \tag{5.8}$$

and

$$\delta E^{SR} = \sum_i \sum_j \left\{ -\frac{1}{\rho_{ij}} A_{ij} \exp\left(-\frac{r}{\rho_{ij}}\right) + \frac{6C_{ij}}{r^7} \right\} \tag{5.9}$$

For E^{md} term we start with the derivative of E^{md} w.r.t. r_k^γ

$$\begin{aligned} \delta_k^\gamma E^{md} &= -\frac{1}{2}\sum_i \left\{ \left(\delta_k^\gamma \mu_{i,\alpha}\right) M_{i,\alpha} + \mu_{i,\alpha}\left(\delta_k^\gamma M_{i,\alpha}\right) + \left(\delta_k^\gamma \mu_{i,\alpha}\right) M_{i,\alpha} + \mu_{i,\alpha}\left(\delta_k^\gamma M_{i,\alpha}\right) \right. \\ &\qquad \left. + \left(\delta_k^\gamma \mu_{i,\alpha}\right) M_{i,\alpha} + \mu_{i,\alpha}\left(\delta_k^\gamma M_{i,\alpha}\right) \right\} \\ &= -\frac{1}{2}\sum_{i,\alpha} \left\{ \left(\delta_k^\gamma \mu_{i,\alpha}\right) M_{i,\alpha} + \mu_{i,\alpha}\left(\delta_k^\gamma M_{i,\alpha}\right) \right\} \end{aligned} \tag{5.10}$$

The derivative of μ_i^α can be written as

$$\delta_k^\gamma \mu_i^\alpha = \sum_{j,\beta} \left(D^{-1}\right)_{ij}^{\alpha\beta} \left(\delta_k^\gamma M\right)_j^\beta - \sum_{l,\delta} \sum_{j,\beta} \left(D^{-1}\right)_{il}^{\alpha\delta} \left(\delta_k^\gamma D\right)_{lj}^{\delta\beta} \mu_j^\beta \tag{5.11}$$

The derivative of D is

$$\delta_k^\gamma D_{ij}^{\alpha\beta} = \begin{cases} 0 & \text{if} \quad i = j \\ 0 & \text{if} \quad k \neq i, k \neq j \\ \sum_l \frac{\alpha_i}{r^7} \left(15 r^\alpha r^\beta r^\gamma - 3r^2 \left(r^\alpha \delta_{\beta\gamma} + r^\beta \delta_{\alpha\gamma} + r^\gamma \delta_{\alpha\beta}\right)\right) & \text{if} \quad k = i, k \neq j \\ \sum_l -\frac{\alpha_i}{r^7} \left(15 r^\alpha r^\beta r^\gamma - 3r^2 \left(r^\alpha \delta_{\beta\gamma} + r^\beta \delta_{\alpha\gamma} + r^\gamma \delta_{\alpha\beta}\right)\right) & \text{if} \quad k = j, k \neq i \end{cases}$$

We define a function $U_{ij}^{\alpha\beta\gamma}$ such that

$$\delta_k^\gamma D_{ij}^{\alpha\beta} = U_{ij}^{\alpha\beta\gamma} \delta_{kj} - U_{ij}^{\alpha\beta\gamma} \delta_{ki} \tag{5.12}$$

So

$$U_{ij}^{\alpha\beta\gamma} = \begin{cases} 0 & \text{if} \quad i = j \\ \sum_l \frac{\alpha_i}{r^7} \left(15 r^\alpha r^\beta r^\gamma - 3r^2 \left(r^\alpha \delta_{\beta\gamma} + r^\beta \delta_{\alpha\gamma} + r^\gamma \delta_{\alpha\beta}\right)\right) & \text{if} \quad i \neq j \end{cases}$$

$U_{ij}^{\alpha\beta\gamma}$ is symmetric under permutations of α, β, γ and that of i and j

The derivative of M,

$$\delta_k^\gamma M_i^\alpha = \begin{cases} -\alpha_i \left[\sum_l q_j \left(\frac{\partial f1(r)}{\partial r} \frac{r^\alpha r^\gamma}{r^2} + f1(r) \left(\delta_{\alpha\beta} \frac{1}{r} - \frac{r^\alpha r^\gamma}{r} \right) \right) \Big|_{r \neq 0} \right. \\ \left. + \frac{4\pi q_j}{V_c} \sum_{\mathbf{G} \neq 0} f2(G) G_\alpha G_\gamma \cos(\mathbf{G} \cdot \mathbf{r}) \right] & \text{if} \quad k \neq i \\ \alpha_i \left[\sum_l \sum_j q_j \left(\frac{\partial f1(r)}{\partial r} \frac{r^\alpha r^\gamma}{r^2} + f1(r) \left(\delta_{\alpha\beta} \frac{1}{r} - \frac{r^\alpha r^\gamma}{r} \right) \right) \Big|_{r \neq 0} \right. \\ \left. + \sum_j \frac{4\pi q_j}{V_c} \sum_{\mathbf{G} \neq 0} f2(G) G_\alpha G_\gamma \cos(\mathbf{G} \cdot \mathbf{r}) \right] & \text{if} \quad k = i \end{cases}$$

here

$$\frac{\partial f1(r)}{\partial r} = \frac{4}{\sqrt{\pi}} g \left(g^2 + \frac{1}{r^2} \right) e^{-g^2 r^2} + \frac{2}{r^3} \mathrm{erfc}(gr)$$

Putting $\delta_k^\gamma \mu$ and $\delta_k^\gamma M$ in eq. 5.10, we get $\delta_k^\gamma E^{md}$ and so the total derivative term is

$$\delta E^{md} = \sum_{k,\gamma} \delta_k^\gamma E^{md} \tag{5.13}$$

5.3 Results of Perfect Crystal Calculations

After going through several iteration through *loop1* in the algorithm of fig. 5.3, the final set of potential parameters from rigid ion calculations is given in table 5.3. The structural parameters are given in table 5.4. The short range potential as a function of the interionic separation are plotted in fig. 5.4.

Table 5.3: Short range potential parameters from rigid ion model

	A(in eV)	ρ(in Å)	C (in Å^6)
$Ga - O$	246171.374421	0.166441	145.768417
$O - O$	664.800374	0.542162	57.096413
$Ga - Ga$	45240.235760	0.266733	0.513166

In table 5.4 (CM) means, the dielectric constants listed are from Claussius Mossotti re-

Table 5.4: Fitted parameters from GULP

a) Structural :

Lattice Energy		-500.99 *eV*	
		x	*z*
Position	Ga_I	0.0896	0.7909
	Ga_{II}	0.3397	0.6853
	O_I	0.1651	0.1030
	O_{II}	0.4972	0.2515
	O_{III}	0.8285	0.4364

a) Dielectric :

	Input	Calculated
Dielectric Constant	5.32(CM)	5.36(CM)

Table 5.5: Fitted values of dielectric constant and polarizabilities with MPPI scheme

	Dielectric Constant		Polarizability		
	Experimental	Calculated	Anion ($Å^3$)	Cation ($Å^3$)	Displacement per unit cell($Å^3$)
SET-I	10.2	10.29	0.25	0.458	33.84
SET-II	10.2	10.16	0.35	0.25	33.99

lation. Electronic polarizabilities, both of gallium and oxygen are varied independently to reproduce the experimental dielectric constant. Each time the polarizabilities are changed, the crystal is re-optimized through *loop2* of the algorithm. We produce here two sets of polarizabilities with which the calculated values of dielectric constants agree well with the experimental value. These electronic polarizabilities along with the calculated displacement polarizabilities and dielectric constants are listed in table 5.5. The displacement polarizability is actually a 3×3 matrix. We neglect the anisotropic effect as it is very small and take the average of the diagonal elements. The final values of structural parameters for both the set of polarizabilities are listed in table 5.6.

Table 5.7 gives the net electric field and dipole moments of the symmetry unique ions in the crystal for the optimized structure. It is observed that the electric field at individual ion

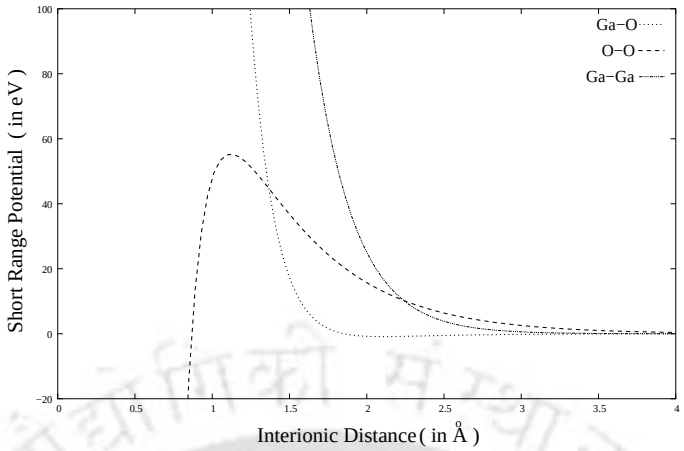

Figure 5.4: Short range potential with fitted parameters for $Ga-O$, $O-O$ and $Ga-Ga$ plotted as a function of interionic distance

Table 5.6: Structural parameters after MPPI simulation

		SET-I		SET-II	
Lattice Energy		-501.642 *eV*		-501.806 *eV*	
		x	*z*	*x*	*z*
Position	Ga_I	0.0895747	0.791027	0.089536	0.791143
	Ga_{II}	0.339707	0.685384	0.339725	0.685523
	O_I	0.165167	0.103006	0.165284	0.103009
	O_{II}	0.49714	0.251485	0.497088	0.251548
	O_{III}	0.828538	0.436339	0.828523	0.436299

sites are considerably suppressed in the MPPI scheme as compared to those from table 5.2 for experimental structure. Vector plots of the dipole moments for both SET-I and SET-II are presented for a single unit cell in fig 5.5. With increasing polarizabilities, the dipole moments of the oxygens increase in SET-II as compared to SET-I. Reverse is the case for galliums. Figs. 5.6(a) and 5.6(b) show the minima of *Ga* and *O* energy surfaces in two dimensions picked up from SET-I.

The phonon frequencies for both the cases have been listed in table 5.8. We observe that the first three values in both the cases are sufficiently small in comparison to the other

Table 5.7: Electric field and dipole moment at symmetry unique ions

SET-I ::

	Electric Field (in $e^2/Å^2$)		Dipole Moment(in $eÅ$)	
	x-component	z-component	x-component	z-component
Ga_I	-0.017666	0.021214	-0.013494	0.012161
Ga_{II}	0.009381	0.056758	0.003771	0.029015
O_I	0.278301	0.052550	0.070729	0.011887
O_{II}	0.176177	0.058606	0.044325	0.014959
O_{III}	-0.024107	0.087750	-0.003674	0.022822

SET-II ::

	Electric Field (in $e^2/Å^2$)		Dipole Moment(in $eÅ$)	
	x-component	z-component	x-component	z-component
Ga_I	-0.016434	0.020033	-0.008699	0.007892
Ga_{II}	0.007663	0.055515	0.002061	0.017069
O_I	0.281236	0.0526475	0.098620	0.015277
O_{II}	0.175750	0.061230	0.063283	0.018862
O_{III}	-0.024143	0.087040	-0.003172	0.0319074

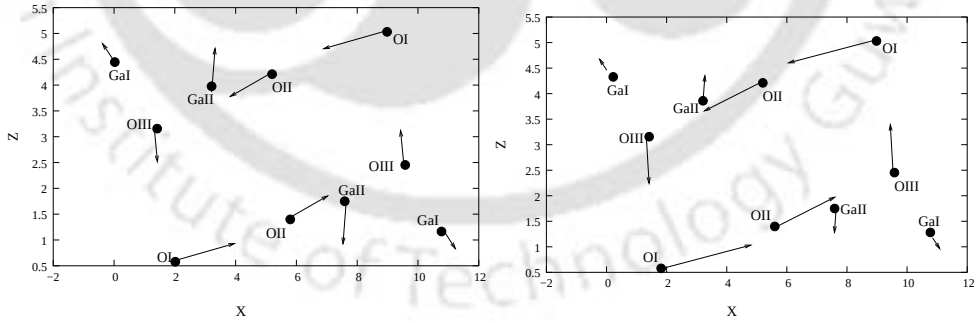

(a) SETI (b) SETII

Figure 5.5: Vector plot of dipole moments for (010) plane of the unit cell

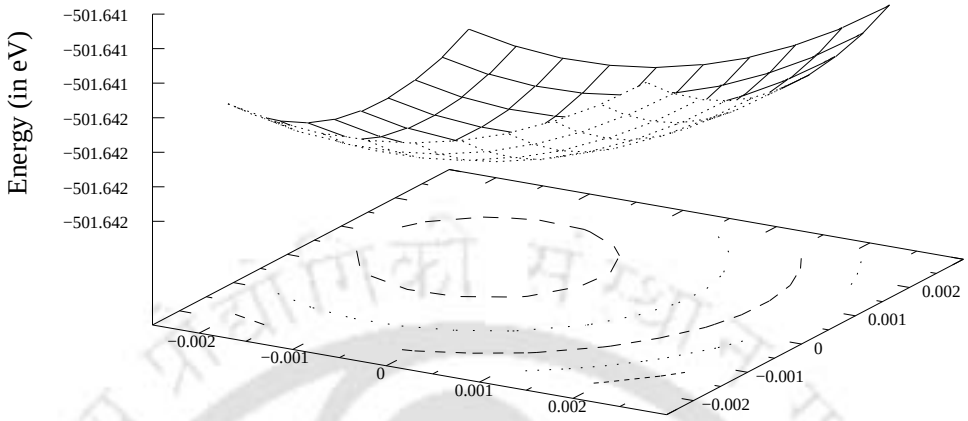

(a) Ga surface

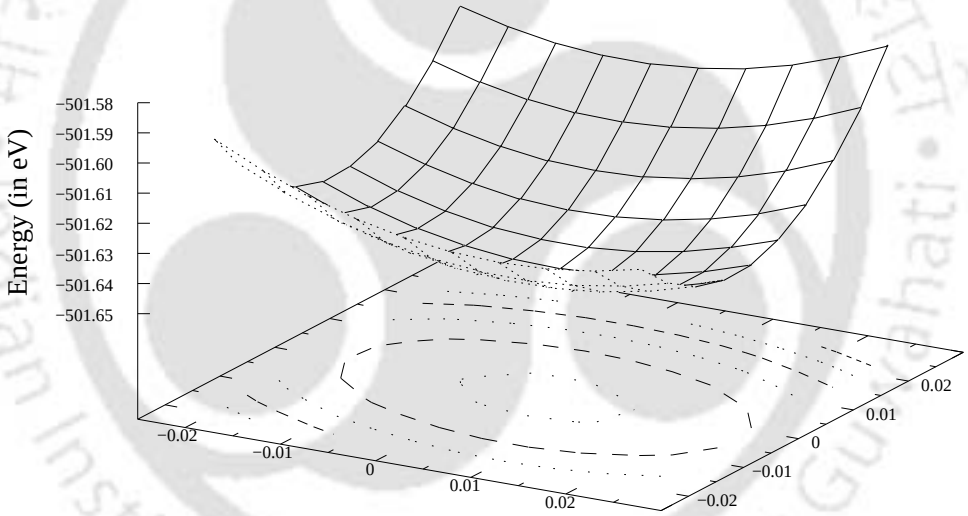

(b) O surface

Figure 5.6: Optimized energy surfaces showing minima for arbitrarily chosen *Ga* and *O* ion co-ordinates from SET-I. The *Ga* surface here is obtained by varying x-coordinate of *Ga* at (0.089 0.0 0.79) with respect to x-coordinate of *Ga* at (0.91 0.0 0.21), whereas the *O* surface is obtained by varying x-coordinate of *O* at (0.16 0.0 0.10) with respect to the z-coordinate of the same ion. The actual minima lies in a 60-dimensional space defined by 20 ions in the unit cell of the crystal.

Table 5.8: Phonon frequencies

SET-I				SET-II			
mode	freq.(cm^{-1})	mode	freq.(cm^{-1})	mode	freq.(cm^{-1})	mode	freq.(cm^{-1})
1	9.51	31	685.98	1	9.54	31	685.16
2	2.44	32	700.30	2	1.06	32	700.17
3	7.15	33	715.34	3	8.19	33	714.03
4	156.31	34	760.84	4	155.93	34	760.86
5	175.64	35	767.19	5	176.11	35	773.52
6	175.84	36	768.25	6	177.26	36	773.99
7	195.44	37	847.60	7	195.38	37	856.75
8	229.06	38	849.40	8	227.88	38	859.66
9	237.25	39	901.44	9	235.08	39	900.71
10	252.07	40	1095.46	10	251.37	40	1093.50
11	292.07	41	1114.50	11	289.01	41	1114.57
12	313.18	42	1205.60	12	309.60	42	1192.81
13	329.92	43	1208.69	13	325.54	43	1213.71
14	359.65	44	1223.77	14	359.35	44	1213.77
15	363.12	45	1326.47	15	361.94	45	1323.57
16	374.66	46	1364.24	16	372.94	46	1367.90
17	472.07	47	1414.24	17	470.39	47	1421.66
18	475.37	48	1422.42	18	471.34	48	1424.10
19	476.32	49	1429.25	19	474.90	49	1433.33
20	484.83	50	1429.37	20	477.45	50	1433.42
21	485.51	51	1433.78	21	484.49	51	1435.50
22	497.33	52	1461.28	22	500.91	52	1467.19
23	506.02	53	1461.71	23	509.29	53	1467.25
24	520.74	54	1473.33	24	518.56	54	1478.81
25	524.23	55	1550.95	25	519.89	55	1554.20
26	584.09	56	1590.08	26	583.91	56	1595.04
27	628.91	57	1710.46	27	626.52	57	1711.34
28	630.90	58	1764.77	28	627.85	58	1765.21
29	668.42	59	1766.21	29	668.92	59	1766.59
30	670.59	60	1792.18	30	670.82	60	1792.70

values. Actually, these small values are due to computer round of error propagating from the Hessian matrix and eigenvalue calculations. They can be approximated to zero representing the three translational modes of the system. The positive definite values of all the other modes confirms the stability of the crystal at the particular structure.

5.4 Defect Crystal Calculations

Given a scheme of finding the short range potential parameters in the low symmetry Ga_2O_3 in the previous section, we now propose the possible way to calculate the defect parameters in the crystal. Following are the related formulations.

5.4.1 Relaxation and polarization of ions

With the MPPI model, the first step towards calculation of defect parameters is to set the displacements and dipole moments of individual ions. With ML scheme we are going to treat Region1 and Region2 ions at different levels. Each ion in Region1 experiences the field due to the defect as well as the rest of the ions in the crystal. The ions are in a sense at full liberty to get relaxed in any direction as a response to this composite field. On contrary, the scheme assumes that, it is only the defect field which has significant effect on Region2 ions and is solely responsible for their displacement and polarization.

Since the effect of Region2 will be taken care of while calculating the parameters for Region1, we first formulate the problem for Region2 ions.

Formulations for Region2 Ions

With reference to §2.1.2, the displacement of an ion in the presence of the field **F** is given by

$$\xi^{\alpha} = \left(\left[\mathbf{W}^{-1} \right]^{\alpha\beta} \left\{ \mathrm{q} + \sum_{\gamma} \left(\delta\mu_{\gamma} \right)^{\beta} \right\} \right) \mathrm{F}^{\beta} \tag{5.14}$$

where **W** is the hessian matrix and q are the charges. The field **F** can be written in terms of electric displacement vector **D** and dielectric constant matrix **K** as

$$\mathbf{F} = \mathbf{K}^{-1}\mathbf{D} \tag{5.15}$$

So

$$\xi^{\alpha} = \left(\left[\mathbf{W}^{-1} \right]^{\alpha\beta} \left\{ \mathrm{q} + \sum_{\gamma} \left(\delta\mu_{\gamma} \right)^{\beta} \right\} \right) \left[\mathbf{K}^{-1} \right]^{\beta\gamma} \mathrm{D}^{\gamma} \tag{5.16}$$

The electric displacement vector **D** can be written as

$$\mathbf{D} = -\frac{\mathrm{Q}\mathbf{R}}{|\mathbf{R}|^{3}} \tag{5.17}$$

with Q as the effective defect charge.

As for the polarization, with the inclusion of the defect, the new electronic dipole moment is

$$\mu_{\mathrm{d}}^{\beta} = \alpha \left(\mathrm{F}_{\mathrm{perf}}^{\beta} + \frac{\mathrm{Q}\mathrm{r}^{\beta}}{|\mathbf{r}|^{3}} \right) \tag{5.18}$$

Here $\mathbf{r} = \mathbf{R} + \boldsymbol{\xi}$ with $\boldsymbol{\xi}$ the displacement and **R** the undisplaced positions. $\mathbf{F}_{\mathrm{perf}}$ is the net field at the concerned site in the perfect crystal environment.

Formulations for Region1 Ions

The relaxations of Region1 ions are the free parameters with respect to which the crystal is stabilized. To find the dipole moments of Region1 ions we solve a set of linear equations as in the case of the perfect crystal. However, the field at each ion site is now different with the defect coming into the picture.

If $\boldsymbol{\mu}$ represent the dipole moment of Region1 ions, we recall the set of equations for $\boldsymbol{\mu}$ as

$$\begin{aligned} \boldsymbol{\mu} &= \alpha \mathbf{F}_{\text{loc}} \\ &= \alpha \left(\mathbf{F}^m + \mathbf{F}^d \right) \end{aligned} \tag{5.19}$$

Where $\mathbf{F}_{loc}$ is the local field, $\mathbf{F}^m$ and $\mathbf{F}^d$ are the total monopole and dipole fields.

Monopole Field

The field at each of Region1 ion site due to the other Region1 ions and the defect can be evaluated exactly and without much computational effort. The difficulty comes when we deal with the infinite Region2. The monopole field calculations converges very slowly and hence a direct sum over Region2 ions is not recommended.

Let us write the monopole Field at the *i*th ion of Region1 as

$$\begin{aligned} \mathbf{F}_{\text{i}}^{\text{m}} &= \sum_{\text{j}\in \text{L}\prime} \frac{\text{q}_\text{j} \left(\mathbf{r}_\text{i} - \mathbf{r}_\text{j} \right)}{\left| \mathbf{r}_\text{i} - \mathbf{r}_\text{j} \right|^3} \\ &= \sum_{\text{j}\in\{\text{d}\}} \frac{\text{q}_\text{j} \left(\mathbf{r}_\text{i} - \mathbf{r}_\text{j} \right)}{\left| \mathbf{r}_\text{i} - \mathbf{r}_\text{j} \right|^3} + \sum_{\text{j}\in \text{L}} \frac{\text{q}_\text{j} \left(\mathbf{r}_\text{i} - \mathbf{r}_\text{j} \right)}{\left| \mathbf{r}_\text{i} - \mathbf{r}_\text{j} \right|^3} \end{aligned} \tag{5.20}$$

The first term is the field due to the defect, assuming that we have defined the co-ordinate system with the defect at the origin. Here, $\mathbf{r}_i = \mathbf{R}_i + \boldsymbol{\xi}_i$ and $\mathbf{r}_j = \mathbf{R}_j + \boldsymbol{\xi}_j$. $L\prime$ and L are the

sets of entire ion sites with and without the defect whereas d is the set of defects. In the first term q_j will be negative for a vacancy and positive for an interstitial.

Let us expand the second term

$$\begin{aligned}\sum_{j\in L}\frac{q_j\left(\mathbf{r}_i-\mathbf{r}_j\right)}{\left|\mathbf{r}_i-\mathbf{r}_j\right|^3} &= \sum_{j\in L}\frac{q_j\left(\mathbf{r}_i-\mathbf{R}_j-\boldsymbol{\xi}_j\right)}{\left|\mathbf{r}_i-\mathbf{r}_j\right|^3}\\ &= \sum_{j\in L}\frac{q_j\left(\mathbf{r}_i-\mathbf{R}_j\right)}{\left|\mathbf{r}_i-\mathbf{R}_j-\boldsymbol{\xi}_j\right|^3}-\sum_{j\in L}\frac{q_j\boldsymbol{\xi}_j}{\left|\mathbf{r}_i-\mathbf{r}_j\right|^3}\\ &= \sum_{j\in L}\frac{q_j\left(\mathbf{r}_i-\mathbf{R}_j\right)}{\left|\mathbf{r}_i-\mathbf{R}_j\right|^3}+3\sum_{j\in L}\frac{\left(\mathbf{r}_i-\mathbf{R}_j\right)\left\{q_j\boldsymbol{\xi}_j\cdot\left(\mathbf{r}_i-\mathbf{R}_j\right)\right\}}{\left|\mathbf{r}_i-\mathbf{R}_j\right|^5}\\ &\quad-\sum_{j\in L}\frac{q_j\boldsymbol{\xi}_j}{\left|\mathbf{r}_i-\mathbf{R}_j\right|^3}+O\left(\xi^2\right)\end{aligned} \tag{5.21}$$

Neglecting the higher order terms and putting this in eq. 5.20 we get

$$\begin{aligned}\mathbf{F}_i^m &= \sum_{j\in\{d\}}\frac{q_j\left(\mathbf{r}_i-\mathbf{r}_j\right)}{\left|\mathbf{r}_i-\mathbf{r}_j\right|^3}+\sum_{j\in L}\frac{q_j\left(\mathbf{r}_i-\mathbf{R}_j\right)}{\left|\mathbf{r}_i-\mathbf{R}_j\right|^3}\\ &\quad+\sum_{j\in L}\left[\frac{3\left(\mathbf{r}_i-\mathbf{R}_j\right)\left\{\mathbf{p}_{dj}\cdot\left(\mathbf{r}_i-\mathbf{R}_j\right)\right\}}{\left|\mathbf{r}_i-\mathbf{R}_j\right|^5}-\frac{\mathbf{p}_{dj}}{\left|\mathbf{r}_i-\mathbf{R}_j\right|^3}\right]\end{aligned} \tag{5.22}$$

where $\mathbf{p}_{dj}$ is the displacement dipole of j^{th} ion.

Now, the first term is a finite sum over the defects, the second sum can be evaluated using Ewald's method. The last term is the field at the reference point due to the displacement dipoles of all other points in the lattice and converges much faster than the monopole term.

Dipole Field

The dipole field at the *i*th site of Region1 is

$$\mathbf{F}_{\mathrm{i}}^{\mathrm{d}}=\sum_{\mathrm{j}\neq\mathrm{i},\mathrm{j}\in\mathrm{I}}\left(\frac{3\boldsymbol{\mu}_{\mathrm{j,d}}\cdot\left(\mathbf{r}_{\mathrm{i}}-\mathbf{r}_{\mathrm{j}}\right)}{\left|\mathbf{r}_{\mathrm{i}}-\mathbf{r}_{\mathrm{j}}\right|^{5}}\left(\mathbf{r}_{\mathrm{i}}-\mathbf{r}_{\mathrm{j}}\right)-\frac{\boldsymbol{\mu}_{\mathrm{j,d}}}{\left|\mathbf{r}_{\mathrm{i}}-\mathbf{r}_{\mathrm{j}}\right|^{3}}\right)+\mathbf{F}_{\mathrm{i,II}}^{\mathrm{d}} \tag{5.23}$$

where

$$\mathbf{F}_{i,II}^{d}=\sum_{j\in II}\left(\frac{3\boldsymbol{\mu}_{j,d}\cdot\left(\mathbf{r}_{i}-\mathbf{r}_{j}\right)}{\left|\mathbf{r}_{i}-\mathbf{r}_{j}\right|^{5}}\left(\mathbf{r}_{i}-\mathbf{r}_{j}\right)-\frac{\boldsymbol{\mu}_{j,d}}{\left|\mathbf{r}_{i}-\mathbf{r}_{j}\right|^{3}}\right), \tag{5.24}$$

is the contribution from Region2. $\boldsymbol{\mu}_{j,d}$ is the electronic dipole moment of j^{th} ion in the defect crystal. *I* and *II* are sets of Region1 and Region2 ion sites. Here *I* includes the defect also.

In component form eq. 5.19 can be written as

$$\mu_{\mathrm{i,d}}^{\alpha}=\alpha_{\mathrm{i}}\left(\mathrm{F}_{\mathrm{i}}^{\mathrm{m},\alpha}+\sum_{\mathrm{j}\neq\mathrm{i},\mathrm{j}\in\mathrm{I}}\left[3\frac{\sum_{\beta}\mu_{\mathrm{j,d}}^{\beta}\left(\mathrm{r}_{\mathrm{i}}^{\beta}-\mathrm{r}_{\mathrm{j}}^{\beta}\right)}{\left|\mathbf{r}_{\mathrm{i}}-\mathbf{r}_{\mathrm{j}}\right|^{5}}\left(\mathrm{r}_{\mathrm{i}}^{\alpha}-\mathrm{r}_{\mathrm{j}}^{\alpha}\right)-\frac{\boldsymbol{\mu}_{\mathrm{j,d}}^{\alpha}}{\left|\mathbf{r}_{\mathrm{i}}-\mathbf{r}_{\mathrm{j}}\right|^{3}}\right]+\mathrm{F}_{\mathrm{i,II}}^{\mathrm{d},\alpha}\right) \tag{5.25}$$

We further rearrange eq. 5.25 and write it in matrix form as

$$\sum_{\mathrm{i}\in\mathrm{I}}\sum_{\alpha}\mathrm{G}_{\mathrm{ij}}^{\alpha\beta}\mu_{\mathrm{i,d}}^{\alpha}=\mathrm{F}_{\mathrm{i}}^{\mathrm{m},\beta}+\mathrm{F}_{\mathrm{i,II}}^{\mathrm{d},\beta} \tag{5.26}$$

where

$$\mathrm{G}_{\mathrm{ij}}^{\alpha\beta}=\begin{cases}\delta_{\alpha\beta} & i=j\\ -3\alpha_{\mathrm{i}}\dfrac{\left(\mathrm{r}_{\mathrm{i}}^{\alpha}-\mathrm{r}_{\mathrm{j}}^{\alpha}\right)\left(\mathrm{r}_{\mathrm{i}}^{\beta}-\mathrm{r}_{\mathrm{j}}^{\beta}\right)}{\left|\mathbf{r}_{\mathrm{i}}-\mathbf{r}_{\mathrm{j}}\right|^{5}}+\alpha_{\mathrm{i}}\dfrac{\delta_{\alpha\beta}}{\left|\mathbf{r}_{\mathrm{i}}-\mathbf{r}_{\mathrm{j}}\right|^{3}} & i\neq j\end{cases}$$

5.4.2 Energy Terms

The potential energy can be straightaway divided into two parts - the long range electrostatic part and the short range overlap repulsion as well as van der Waal part.i.e.

$$\Phi_{ij} = \Phi_{ij}^{LR} + \Phi_{ij}^{SR} \tag{5.27}$$

There is one point to be addressed here. Though we get rid of the infinite Region2-Region2 interaction term through harmonic approximations, as discussed in §2.5.2, there is still the electrostatic sum, specially the monopole monopole part, for Region1-Region2 interaction which converges very slowly. Hence to simplify the computations, we further divide Region2 into Region2a and Region2b [73] such that Region2a consists of the long range electrostatic as well as short range terms, while Region2b will have only electrostatic part. Now we can do direct summations for Region1 and Region2a, but make some approximations for Region2b which is far enough from the defect and can be supposed to suffer very small displacements due to the defect purturbation.

In the next two subsections we are going to discuss the long range and short range energies separately and build explicit expressions for them.

Electrostatic Energy

As discussed in §2.3 the dipole dipole interaction term gets cancelled with the self energy of formation of the induced dipoles and the expression for electrostatic energy consists of only two terms.

$$\begin{aligned} E^{ES} &= \sum_{i,j\in L, j>i} \frac{q_i q_j}{|\mathbf{r}_i - \mathbf{r}_j|} - \frac{1}{2}\sum_{i\in L} \boldsymbol{\mu}_i \cdot \mathbf{F}_j^m \\ &= E^{mm} - \frac{1}{2}E^{md} \end{aligned} \tag{5.28}$$

Monopole-Monopole Term

With ML scheme, the total monopole energy can be written as

$$\begin{aligned} E^{mm} &= \sum_{i\in I,j\in I}\frac{1}{2}q_i q_j\left(\frac{1}{|\mathbf{r}_i-\mathbf{r}_j|}-\frac{1}{|\mathbf{R}_i-\mathbf{R}_j|}\right)+\sum_{i\in I,j\in II}q_i q_j\left(\frac{1}{|\mathbf{r}_i-\mathbf{r}_j|}-\frac{1}{|\mathbf{R}_i-\mathbf{R}_j|}\right) \\ &\quad -\frac{1}{2}\sum_{i\in I,j\in II}q_i q_j\frac{\partial}{\partial\xi_j}\left(\frac{1}{|\mathbf{r}_i-\mathbf{r}_j|}-\frac{1}{|\mathbf{R}_i-\mathbf{R}_j|}\right)\Bigg|_{\xi_{jo}}\cdot\boldsymbol{\xi}_{jo} \end{aligned} \tag{5.29}$$

$\boldsymbol{\xi}_{jo}$ is the equilibrium displacement of Region2 ions for arbitrary displacement of ions in Region1.

Let us consider the following two terms T_{1m} and T_{2m} which can be calculated by Ewald's method.

$$\begin{aligned} T_{1m} &= \sum_{i\in I,j\in L}\frac{q_i q_j}{|\mathbf{r}_i-\mathbf{R}_j|} \\ &= \sum_{i\in I,j\in I}\frac{q_i q_j}{|\mathbf{r}_i-\mathbf{R}_j|}+\sum_{i\in I,j\in II}\frac{q_i q_j}{|\mathbf{r}_i-\mathbf{R}_j|} \end{aligned} \tag{5.30}$$

$$\begin{aligned} T_{2m} &= -\sum_{i\in I,j\in L}\frac{q_i q_j}{|\mathbf{R}_i-\mathbf{R}_j|} \\ &= -\left[\sum_{i\in I,j\in I}\frac{q_i q_j}{|\mathbf{R}_i-\mathbf{R}_j|}+\sum_{i\in I,j\in II}\frac{q_i q_j}{|\mathbf{R}_i-\mathbf{R}_j|}\right] \end{aligned} \tag{5.31}$$

We calculate these terms separately and hence subtract them from eq. 5.29, so that the

equation becomes

$$
\begin{aligned}
E^{mm} &= \sum_{i\in I,j\in I} q_i q_j \left(\frac{1}{2\left|\mathbf{r}_i-\mathbf{r}_j\right|} + \frac{1}{2\left|\mathbf{R}_i-\mathbf{R}_j\right|} - \frac{1}{\left|\mathbf{r}_i-\mathbf{R}_j\right|} \right) \\
&\quad + \sum_{i\in I,j\in IIa,IIb} q_i q_j \left(\frac{1}{\left|\mathbf{r}_i-\mathbf{r}_j\right|} - \frac{1}{\left|\mathbf{R}_i-\mathbf{r}_j\right|} - \frac{1}{\left|\mathbf{r}_i-\mathbf{R}_j\right|} + \frac{1}{\left|\mathbf{R}_i-\mathbf{R}_j\right|} \right) \\
&\quad - \frac{1}{2} \sum_{i\in I,j\in IIa,IIb} q_i q_j \frac{\partial}{\partial \xi_j} \left(\frac{1}{\left|\mathbf{r}_i-\mathbf{r}_j\right|} - \frac{1}{\left|\mathbf{R}_i-\mathbf{r}_j\right|} - \frac{1}{\left|\mathbf{r}_i-\mathbf{R}_j\right|} + \frac{1}{\left|\mathbf{R}_i-\mathbf{R}_j\right|} \right)\Bigg|_{\xi_{jo}} \cdot \boldsymbol{\xi}_{jo} \\
&= \sum_{i\in I,j\in I} q_i q_j \left(\frac{1}{\left|\mathbf{r}_i-\mathbf{r}_j\right|} - \frac{1}{\left|\mathbf{r}_i-\mathbf{R}_j\right|} \right) \\
&\quad + \sum_{i\in I,j\in IIa,IIb} q_i q_j \left(\frac{1}{\left|\mathbf{r}_i-\mathbf{r}_j\right|} - \frac{1}{\left|\mathbf{R}_i-\mathbf{r}_j\right|} - \frac{1}{\left|\mathbf{r}_i-\mathbf{R}_j\right|} + \frac{1}{\left|\mathbf{R}_i-\mathbf{R}_j\right|} \right) \\
&\quad - \frac{1}{2} \sum_{i\in I,j\in IIa,IIb} q_i \left(\frac{\mathbf{p}_{dj}\cdot\left(\mathbf{r}_i-\mathbf{r}_j\right)}{\left|\mathbf{r}_i-\mathbf{r}_j\right|^3} - \frac{\mathbf{p}_{dj}\cdot\left(\mathbf{R}_i-\mathbf{r}_j\right)}{\left|\mathbf{R}_i-\mathbf{r}_j\right|^3} \right)
\end{aligned}
\tag{5.32}
$$

Here *IIa* and *IIb* are sets of ion sites in Region2a and Region2b.

We simplify the contribution from Region2b as

$$
\begin{aligned}
E^{mm}_{I,IIb} &= \sum_{i\in I,j\in II} q_i q_j \left(\frac{1}{\left|\mathbf{r}_i-\mathbf{r}_j\right|} - \frac{1}{\left|\mathbf{R}_i-\mathbf{r}_j\right|} - \frac{1}{\left|\mathbf{r}_i-\mathbf{R}_j\right|} + \frac{1}{\left|\mathbf{R}_i-\mathbf{R}_j\right|} \right) \\
&= \sum_{i\in I',j\in IIb} q_i q_j \left(\frac{1}{\left|\mathbf{r}_i-\mathbf{r}_j\right|} - \frac{1}{\left|\mathbf{R}_i-\mathbf{r}_j\right|} - \frac{1}{\left|\mathbf{r}_i-\mathbf{R}_j\right|} + \frac{1}{\left|\mathbf{R}_i-\mathbf{R}_j\right|} \right) + Q \sum_{j\in IIb} q_j \left(\frac{1}{\left|\mathbf{R}_j\right|} - \frac{1}{\left|\mathbf{r}_j\right|} \right) \\
&= \sum_{i\in I',j\in IIb} \left(\frac{\mathbf{p}_{di}\cdot\mathbf{p}_{dj}}{\left|\mathbf{R}_i-\mathbf{R}_j\right|^3} - 3\frac{\left[\mathbf{p}_{di}\cdot\left(\mathbf{R}_i-\mathbf{R}_j\right)\right]\left[\mathbf{p}_{dj}\cdot\left(\mathbf{R}_i-\mathbf{R}_j\right)\right]}{\left|\mathbf{R}_i-\mathbf{R}_j\right|^5} + \ldots \right) \\
&\quad - Q \sum_{j\in IIb} q_j \left(\frac{\boldsymbol{\xi}_j\cdot\mathbf{R}_j}{\left|\mathbf{R}_j\right|^3} + \frac{1}{2}\frac{\left|\boldsymbol{\xi}_j\right|^2}{\left|\mathbf{R}_j\right|^3} + \ldots \right)
\end{aligned}
\tag{5.33}
$$

Here Q is the effective charge of the defect which is assumed to be the center of the co-ordinate system and I' is the set of ion sites without the defect. The first term of eq. 5.33 which is the interaction of RegionI displacement dipoles with Region2b displacement

dipoles is going to be sufficiently small and can be neglected. When higher order terms are neglected, $E^{mm}_{I,IIb}$ has contribution from the defect only.

$$\mathrm{E}^{\mathrm{mm}}_{\mathrm{I,IIb}} = -\mathrm{Q}\sum_{\mathrm{j}\in\mathrm{IIb}} \frac{\mathrm{q_j}\left(\boldsymbol{\xi}_\mathrm{j}\cdot\mathbf{R}_\mathrm{j}\right)}{\left|\mathbf{R}_\mathrm{j}\right|^3} \tag{5.34}$$

The total contribution from Region2b is

$$\begin{aligned}\mathrm{E}^{\mathrm{mm}}_{\mathrm{IIb}} - \frac{1}{2}\frac{\partial}{\partial\xi_\mathrm{j}}\left(\mathrm{E}^{\mathrm{mm}}_{\mathrm{I,IIb}}\right)\Big|_{\xi_{\mathrm{jo}}}\cdot\boldsymbol{\xi}_{\mathrm{jo}} &= -\mathrm{Q}\sum_{\mathrm{j}\in\mathrm{IIb}}\frac{\mathrm{q_j}\left(\boldsymbol{\xi}_\mathrm{j}\cdot\mathbf{R}_\mathrm{j}\right)}{\left|\mathbf{R}_\mathrm{j}\right|^3} + \frac{1}{2}\mathrm{Q}\sum_{\mathrm{j}\in\mathrm{IIb}}\frac{\mathrm{q_j}\left(\boldsymbol{\xi}_\mathrm{j}\cdot\mathbf{R}_\mathrm{j}\right)}{\left|\mathbf{R}_\mathrm{j}\right|^3} \\ &= -\frac{1}{2}\mathrm{Q}\sum_{\mathrm{j}\in\mathrm{IIb}}\frac{\mathrm{q_j}\left(\boldsymbol{\xi}_\mathrm{j}\cdot\mathbf{R}_\mathrm{j}\right)}{\left|\mathbf{R}_\mathrm{j}\right|^3}\end{aligned} \tag{5.35}$$

With this, the total monopole-monopole energy in the defect environment can be written as

$$\begin{aligned}\mathrm{E}^{\mathrm{mm}}_{\mathrm{total}} &= \sum_{\mathrm{i}\in\mathrm{I},\mathrm{j}\in\mathrm{I}}\mathrm{q_i q_j}\left(\frac{1}{2\left|\mathbf{r}_\mathrm{i}-\mathbf{r}_\mathrm{j}\right|}+\frac{1}{2\left|\mathbf{R}_\mathrm{i}-\mathbf{R}_\mathrm{j}\right|}-\frac{1}{\left|\mathbf{r}_\mathrm{i}-\mathbf{R}_\mathrm{j}\right|}\right) \\ &+\sum_{\mathrm{i}\in\mathrm{I},\mathrm{j}\in\mathrm{IIa}}\mathrm{q_i q_j}\left(\frac{1}{\left|\mathbf{r}_\mathrm{i}-\mathbf{r}_\mathrm{j}\right|}-\frac{1}{\left|\mathbf{R}_\mathrm{i}-\mathbf{r}_\mathrm{j}\right|}-\frac{1}{\left|\mathbf{r}_\mathrm{i}-\mathbf{R}_\mathrm{j}\right|}+\frac{1}{\left|\mathbf{R}_\mathrm{i}-\mathbf{R}_\mathrm{j}\right|}\right) \\ &-\frac{1}{2}\sum_{\mathrm{i}\in\mathrm{I},\mathrm{j}\in\mathrm{IIa}}\mathrm{q_i}\left(\frac{\mathbf{p}_{\mathrm{dj}}\cdot\left(\mathbf{r}_\mathrm{i}-\mathbf{r}_\mathrm{j}\right)}{\left|\mathbf{r}_\mathrm{i}-\mathbf{r}_\mathrm{j}\right|^3}-\frac{\mathbf{p}_{\mathrm{dj}}\cdot\left(\mathbf{R}_\mathrm{i}-\mathbf{r}_\mathrm{j}\right)}{\left|\mathbf{R}_\mathrm{i}-\mathbf{r}_\mathrm{j}\right|^3}\right) \\ &-\frac{1}{2}\mathrm{Q}\sum_{\mathrm{j}\in\mathrm{IIb}}\frac{\mathbf{p}_{\mathrm{dj}}\cdot\mathbf{R}_\mathrm{j}}{\left|\mathbf{R}_\mathrm{j}\right|^3}+\mathrm{T}_{1\mathrm{m}}+\mathrm{T}_{2\mathrm{m}}\end{aligned} \tag{5.36}$$

Monopole-Dipole Term

With ML scheme, the monopole-dipole energy term is written as

$$
\begin{aligned}
\mathrm{E}^{\mathrm{md}} = & \sum_{\mathrm{i}\in\mathrm{I},\mathrm{j}\in\mathrm{I},\mathrm{j}\neq\mathrm{i}} \left(\frac{\boldsymbol{\mu}_{\mathrm{i,d}} \cdot \left\{ \mathrm{q_j} \left(\mathbf{r_i} - \mathbf{r_j} \right) \right\}}{\left| \mathbf{r_i} - \mathbf{r_j} \right|^3} - \frac{\boldsymbol{\mu}_{\mathrm{i,p}} \cdot \left\{ \mathrm{q_j} \left(\mathbf{R_i} - \mathbf{R_j} \right) \right\}}{\left| \mathbf{R_i} - \mathbf{R_j} \right|^3} \right) \\
& + \underbrace{\sum_{i\in I, j\in II} \left(\frac{q_i \left\{ \boldsymbol{\mu}_{j,d} \cdot \left(\mathbf{r}_i - \mathbf{r}_j \right) \right\}}{\left| \mathbf{r}_i - \mathbf{r}_j \right|^3} - \frac{q_i \left\{ \boldsymbol{\mu}_{j,d} \cdot \left(\mathbf{R}_i - \mathbf{r}_j \right) \right\}}{\left| \mathbf{R}_i - \mathbf{r}_j \right|^3} \right)}_{\mathrm{T}_1} \\
& + \underbrace{\sum_{i\in I, j\in II} \left(\frac{\boldsymbol{\mu}_{i,d} \cdot \left\{ q_j \left(\mathbf{r}_i - \mathbf{r}_j \right) \right\}}{\left| \mathbf{r}_i - \mathbf{r}_j \right|^3} - \frac{\boldsymbol{\mu}_{i,p} \cdot \left\{ q_j \left(\mathbf{R}_i - \mathbf{r}_j \right) \right\}}{\left| \mathbf{R}_i - \mathbf{r}_j \right|^3} \right)}_{\mathrm{T}_2} \\
& - \frac{1}{2} \frac{\partial}{\partial \xi_{\mathrm{j}}} \mathrm{T}_1 \Big|_{\boldsymbol{\xi}_{\mathrm{j_o}}} \cdot \boldsymbol{\xi}_{\mathrm{j_o}} - \frac{1}{2} \frac{\partial}{\partial \xi_{\mathrm{j}}} \mathrm{T}_2 \Big|_{\boldsymbol{\xi}_{\mathrm{j_o}}} \cdot \boldsymbol{\xi}_{\mathrm{j_o}}
\end{aligned}
\tag{5.37}
$$

Here, $\boldsymbol{\mu}_{i,p}$ and $\boldsymbol{\mu}_{i,d}$ are the dipole moments of i^{th} ion in perfect and defect crystal respectively. As in the previous section, to ensure a better convergence, we introduce the following two energy terms which can be caculated by Ewald's method.

$$
\begin{aligned}
\mathrm{T}^1_{\mathrm{md}} &= \sum_{\mathrm{i}\in\mathrm{I},\mathrm{j}\in\mathrm{L}} \frac{\boldsymbol{\mu}_{\mathrm{i,d}} \cdot \left\{ \mathrm{q_j} \left(\mathbf{r_i} - \mathbf{R_j} \right) \right\}}{\left| \mathbf{r_i} - \mathbf{R_j} \right|^3} \\
&= \sum_{\mathrm{i}\in\mathrm{I},\mathrm{j}\in\mathrm{I}} \frac{\boldsymbol{\mu}_{\mathrm{i,d}} \cdot \left\{ \mathrm{q_j} \left(\mathbf{r_i} - \mathbf{R_j} \right) \right\}}{\left| \mathbf{r_i} - \mathbf{R_j} \right|} + \sum_{\mathrm{i}\in\mathrm{I},\mathrm{j}\in\mathrm{II}} \frac{\boldsymbol{\mu}_{\mathrm{i,d}} \cdot \left\{ \mathrm{q_j} \left(\mathbf{r_i} - \mathbf{R_j} \right) \right\}}{\left| \mathbf{r_i} - \mathbf{R_j} \right|^3}
\end{aligned}
\tag{5.38}
$$

$$
\begin{aligned}
\mathrm{T}^2_{\mathrm{md}} &= - \sum_{\mathrm{i}\in\mathrm{I},\mathrm{j}\in\mathrm{L}} \frac{\boldsymbol{\mu}_{\mathrm{i,p}} \cdot \left\{ \mathrm{q_j} \left(\mathbf{R_i} - \mathbf{R_j} \right) \right\}}{\left| \mathbf{R_i} - \mathbf{R_j} \right|^3} \\
&= - \left[\sum_{\mathrm{i}\in\mathrm{I},\mathrm{j}\in\mathrm{I}} \frac{\boldsymbol{\mu}_{\mathrm{i,p}} \cdot \left\{ \mathrm{q_j} \left(\mathbf{R_i} - \mathbf{R_j} \right) \right\}}{\left| \mathbf{R_i} - \mathbf{R_j} \right|^3} + \sum_{\mathrm{i}\in\mathrm{I},\mathrm{j}\in\mathrm{II}} \frac{\boldsymbol{\mu}_{\mathrm{i,p}} \cdot \left\{ \mathrm{q_j} \left(\mathbf{R_i} - \mathbf{R_j} \right) \right\}}{\left| \mathbf{R_i} - \mathbf{R_j} \right|^3} \right]
\end{aligned}
\tag{5.39}
$$

We calculate these terms separately and hence subtract them from eq. 5.37. So

$$
\begin{aligned}
\mathrm{E}^{\mathrm{md}} = & \sum_{\mathrm{i}\in\mathrm{I},\mathrm{j}\in\mathrm{I},\mathrm{j}\neq\mathrm{i}}\left(\frac{\boldsymbol{\mu}_{\mathrm{i,d}}\cdot\left\{\mathrm{q_j}\left(\mathbf{r}_\mathrm{i}-\mathbf{r}_\mathrm{j}\right)\right\}}{\left|\mathbf{r}_\mathrm{i}-\mathbf{r}_\mathrm{j}\right|^3}-\frac{\boldsymbol{\mu}_{\mathrm{i,p}}\cdot\left\{\mathrm{q_j}\left(\mathbf{r}_\mathrm{i}-\mathbf{R}_\mathrm{j}\right)\right\}}{\left|\mathbf{r}_\mathrm{i}-\mathbf{R}_\mathrm{j}\right|^3}\right) \\
& \underbrace{+\sum_{i\in I,j\in II}\left(\frac{q_i\left\{\boldsymbol{\mu}_{j,d}\cdot\left(\mathbf{r}_i-\mathbf{r}_j\right)\right\}}{\left|\mathbf{r}_i-\mathbf{r}_j\right|^3}-\frac{q_i\left\{\boldsymbol{\mu}_{j,d}\cdot\left(\mathbf{R}_i-\mathbf{r}_j\right)\right\}}{\left|\mathbf{R}_i-\mathbf{r}_j\right|^3}\right)}_{\mathrm{T_1}} \\
& +\sum_{\mathrm{i}\in\mathrm{I},\mathrm{j}\in\mathrm{II}}\left(\frac{\boldsymbol{\mu}_{\mathrm{i,d}}\cdot\left\{\mathrm{q_j}\left(\mathbf{r}_\mathrm{i}-\mathbf{r}_\mathrm{j}\right)\right\}}{\left|\mathbf{r}_\mathrm{i}-\mathbf{r}_\mathrm{j}\right|^3}-\frac{\boldsymbol{\mu}_{\mathrm{i,d}}\cdot\left\{\mathrm{q_j}\left(\mathbf{r}_\mathrm{i}-\mathbf{R}_\mathrm{j}\right)\right\}}{\left|\mathbf{r}_\mathrm{i}-\mathbf{R}_\mathrm{j}\right|^3}\right. \\
& \underbrace{\left.-\frac{\boldsymbol{\mu}_{\mathrm{i,p}}\cdot\left\{\mathrm{q_j}\left(\mathbf{R}_\mathrm{i}-\mathbf{r}_\mathrm{j}\right)\right\}}{\left|\mathbf{R}_\mathrm{i}-\mathbf{r}_\mathrm{j}\right|^3}+\frac{\boldsymbol{\mu}_{\mathrm{i,p}}\cdot\left\{\mathrm{q_j}\left(\mathbf{R}_\mathrm{i}-\mathbf{R}_\mathrm{j}\right)\right\}}{\left|\mathbf{R}_\mathrm{i}-\mathbf{R}_\mathrm{j}\right|^3}\right)}_{T_2'} \\
& \underbrace{-\frac{1}{2}\frac{\partial}{\partial\xi_j}T_1\Big|_{\boldsymbol{\xi}_{j_o}}\cdot\boldsymbol{\xi}_{j_o}}_{\mathrm{T_3}}\underbrace{-\frac{1}{2}\frac{\partial}{\partial\xi_j}T_2\Big|_{\boldsymbol{\xi}_{j_o}}\cdot\boldsymbol{\xi}_{j_o}}_{\mathrm{T_4}}
\end{aligned}
\tag{5.40}
$$

As for Region2a, a direct sum is performed without any approximation.The derivative terms are

$$
\begin{aligned}
\mathrm{T}_{\mathrm{3,IIa}} = & \sum_{\mathrm{i}\in\mathrm{I},\mathrm{j}\in\mathrm{IIa}}\left(\left[\frac{3\mathrm{q_i}\left\{\boldsymbol{\mu}_{\mathrm{j,d}}\cdot\left(\mathbf{r}_\mathrm{i}-\mathbf{r}_\mathrm{j}\right)\right\}\left\{\boldsymbol{\xi}_\mathrm{j}\cdot\left(\mathbf{r}_\mathrm{i}-\mathbf{r}_\mathrm{j}\right)\right\}}{\left|\mathbf{r}_\mathrm{i}-\mathbf{r}_\mathrm{j}\right|^5}-\frac{\mathrm{q_i}\left(\boldsymbol{\mu}_{\mathrm{j,d}}\cdot\boldsymbol{\xi}_\mathrm{j}\right)}{\left|\mathbf{r}_\mathrm{i}-\mathbf{r}_\mathrm{j}\right|^3}\right]\right. \\
& \left.-\left[\frac{3\mathrm{q_i}\left\{\boldsymbol{\mu}_{\mathrm{j,d}}\cdot\left(\mathbf{R}_\mathrm{i}-\mathbf{r}_\mathrm{j}\right)\right\}\left\{\boldsymbol{\xi}_\mathrm{j}\cdot\left(\mathbf{R}_\mathrm{i}-\mathbf{r}_\mathrm{j}\right)\right\}}{\left|\mathbf{R}_\mathrm{i}-\mathbf{r}_\mathrm{j}\right|^5}-\frac{\mathrm{q_i}\left(\boldsymbol{\mu}_{\mathrm{j,d}}\cdot\boldsymbol{\xi}_\mathrm{j}\right)}{\left|\mathbf{R}_\mathrm{i}-\mathbf{r}_\mathrm{j}\right|^3}\right]\right)
\end{aligned}
\tag{5.41}
$$

$$
\begin{aligned}
\mathrm{T}_{\mathrm{4,IIa}} = & \sum_{\mathrm{i}\in\mathrm{I},\mathrm{j}\in\mathrm{IIa}}\left(\left[\frac{3\left\{\boldsymbol{\mu}_{\mathrm{i,d}}\cdot\left(\mathbf{r}_\mathrm{i}-\mathbf{r}_\mathrm{j}\right)\right\}\left\{\mathbf{p}_{\mathrm{dj}}\cdot\left(\mathbf{r}_\mathrm{i}-\mathbf{r}_\mathrm{j}\right)\right\}}{\left|\mathbf{r}_\mathrm{i}-\mathbf{r}_\mathrm{j}\right|^5}-\frac{\left(\boldsymbol{\mu}_{\mathrm{i,d}}\cdot\mathbf{p}_{\mathrm{dj}}\right)}{\left|\mathbf{r}_\mathrm{i}-\mathbf{r}_\mathrm{j}\right|^3}\right]\right. \\
& \left.-\left[\frac{3\left\{\boldsymbol{\mu}_{\mathrm{i,p}}\cdot\left(\mathbf{R}_\mathrm{i}-\mathbf{r}_\mathrm{j}\right)\right\}\left\{\mathbf{p}_{\mathrm{dj}}\cdot\left(\mathbf{R}_\mathrm{i}-\mathbf{r}_\mathrm{j}\right)\right\}}{\left|\mathbf{R}_\mathrm{i}-\mathbf{r}_\mathrm{j}\right|^5}-\frac{\left(\boldsymbol{\mu}_{\mathrm{i,p}}\cdot\mathbf{p}_{\mathrm{dj}}\right)}{\left|\mathbf{R}_\mathrm{i}-\mathbf{r}_\mathrm{j}\right|^3}\right]\right)
\end{aligned}
\tag{5.42}
$$

However, for Region2b which is far away from the defect, we simplify and approximate the different terms as follows.

$$\begin{aligned} T_{1,IIb} &= \sum_{i\in I, j\in IIb}\left[\frac{q_i\left\{\boldsymbol{\mu}_{j,d}\cdot\left(\mathbf{r}_i-\mathbf{r}_j\right)\right\}}{\left|\mathbf{r}_i-\mathbf{r}_j\right|^3}-\frac{q_i\left\{\boldsymbol{\mu}_{j,p}\cdot\left(\mathbf{R}_i-\mathbf{r}_j\right)\right\}}{\left|\mathbf{R}_i-\mathbf{r}_j\right|^3}\right] \\ &= \sum_{i\in I, j\in II}\left[\frac{q_i\left\{\boldsymbol{\mu}_{j,d}\cdot\left(\mathbf{R}_i-\mathbf{r}_j\right)\right\}}{\left|\mathbf{R}_i-\mathbf{r}_j+\boldsymbol{\xi}_i\right|^3}+\frac{\mathbf{p}_{di}\cdot\boldsymbol{\mu}_{j,d}}{\left|\mathbf{R}_i-\mathbf{r}_j+\boldsymbol{\xi}_i\right|^3}\right. \\ &\qquad \left.-\frac{q_i\left\{\boldsymbol{\mu}_{j,d}\cdot\left(\mathbf{R}_i-\mathbf{r}_j\right)\right\}}{\left|\mathbf{R}_i-\mathbf{r}_j\right|^3}\right] \\ &= \sum_{i\in I, j\in IIb}\left[\mathbf{p}_{di}\cdot\left\{\frac{\boldsymbol{\mu}_{j,d}}{\left|\mathbf{R}_i-\mathbf{r}_j\right|^3}-\frac{\left(\mathbf{R}_i-\mathbf{r}_j\right)\left\{\boldsymbol{\mu}_{j,d}\cdot\left(\mathbf{R}_i-\mathbf{r}_j\right)\right\}}{\left|\mathbf{R}_i-\mathbf{r}_j\right|^5}\right\}\right] \end{aligned} \tag{5.43}$$

Neglecting the higher order terms in displacement, the Region1-Region2b monopole-dipole term thus reduces to the interaction between the Region1 displacement dipoles with the Region2b induced dipoles which is expected to converge faster. Similarly

$$\begin{aligned} T'_{2,IIb} &= \sum_{i\in I, j\in II}\left(\frac{\boldsymbol{\mu}_{i,d}\cdot\left\{q_j\left(\mathbf{r}_i-\mathbf{r}_j\right)\right\}}{\left|\mathbf{r}_i-\mathbf{r}_j\right|^3}-\frac{\boldsymbol{\mu}_{i,p}\cdot\left\{q_j\left(\mathbf{r}_i-\mathbf{R}_j\right)\right\}}{\left|\mathbf{r}_i-\mathbf{R}_j\right|^3}\right. \\ &\qquad \left.-\frac{\boldsymbol{\mu}_{i,p}\cdot\left\{q_j\left(\mathbf{R}_i-\mathbf{r}_j\right)\right\}}{\left|\mathbf{R}_i-\mathbf{r}_j\right|^3}+\frac{\boldsymbol{\mu}_{i,p}\cdot\left\{q_j\left(\mathbf{R}_i-\mathbf{R}_j\right)\right\}}{\left|\mathbf{R}_i-\mathbf{R}_j\right|^3}\right) \\ &= \sum_{i\in I, j\in II}\left(\left[\frac{3\left\{\boldsymbol{\mu}_{i,d}\cdot\left(\mathbf{r}_i-\mathbf{R}_j\right)\right\}\left\{\mathbf{p}_{dj}\cdot\left(\mathbf{r}_i-\mathbf{R}_j\right)\right\}}{\left|\mathbf{r}_i-\mathbf{R}_j\right|^5}-\frac{\boldsymbol{\mu}_{i,d}\cdot\mathbf{p}_{dj}}{\left|\mathbf{r}_i-\mathbf{R}_j\right|^3}\right]\right. \\ &\qquad \left.-\left[\frac{3\left\{\boldsymbol{\mu}_{i,p}\cdot\left(\mathbf{R}_i-\mathbf{R}_j\right)\right\}\left\{\mathbf{p}_{dj}\cdot\left(\mathbf{R}_i-\mathbf{R}_j\right)\right\}}{\left|\mathbf{R}_i-\mathbf{R}_j\right|^5}-\frac{\boldsymbol{\mu}_{i,p}\cdot q_j\mathbf{p}_{dj}}{\left|\mathbf{R}_i-\mathbf{R}_j\right|^3}\right]\right) \end{aligned} \tag{5.44}$$

The contribution of RegionIIb to the derivative terms will be very small.

Short Range Energy

The short range energy term in the defect crystal is

$$\begin{aligned} E^{SR} &= \sum_{i\in I, j\in I}\left[\Phi_{ij}^{SR}\left(|\mathbf{r}_i-\mathbf{r}_j|\right)-\Phi_{ij}^{SR}\left(|\mathbf{r}_i-\mathbf{r}_j|\right)\right]+\sum_{i\in I, j\in IIa}\left[\Phi_{ij}^{SR}\left(|\mathbf{r}_i-\mathbf{r}_j|\right)-\Phi_{ij}^{SR}\left(|\mathbf{R}_i-\mathbf{r}_j|\right)\right] \\ &\quad -\frac{1}{2}\sum_{i\in I, j\in IIa}\frac{\partial}{\partial\xi_j}\left[\Phi_{ij}^{SR}\left(|\mathbf{r}_i-\mathbf{r}_j|\right)-\Phi_{ij}^{SR}\left(|\mathbf{R}_i-\mathbf{r}_j|\right)\right]\Big|_{\xi_{jo}}\cdot\boldsymbol{\xi_{jo}} \end{aligned} \tag{5.45}$$

Here, $\Phi_{ij}^{SR}(r_{ij})$ is the two body short range interaction potential between ions i and j separated by a distance r_{ij} .

$$\Phi_{ij}^{SR}(r_{ij}) = A_{ij}\exp\left(-\frac{r_{ij}}{\rho_{ij}}-\frac{C_{ij}}{r_{ij}^6}\right) \tag{5.46}$$

5.4.3 Results and Future Plan

Unlike the case of a perfect crystal where the translational symmetry reduces the lattice energy calculations to a single cell calculation, the void or extra entity created by the point defect breaks the symmetry and the entire lattice now needs to be treated accordingly as far as ions closer to or far from the defect are concerned. The calculations become very difficult in case of a low symmetry crystal as the different energy terms show slow rate of convergence and large accumulated numerical errors.

We extended our perfect crystal codes to calculate the point defect energies in $\beta-Ga_2O_3$ with the formulations deduced in the previous sections. These codes were written for MS Windows operating system with user interface to provide the structure, the potentials and other bulk and ionic properties. A Ga_I vacancy was simulated in the crystal with the structural and short range parameters deduced in §5.2. Owing to the complex form of the energy terms, specially the dipole terms, we didnot calculate the gradients analytically. We use va04 hsl package for optimization which does not require energy gradients as inputs. How-

ever our attempt to locate the minimum in energy surface of the crystal failed. The total energy of the system assumes lower and lower values showing divergence in the energy surface. There are several reasons for this.

We believe that the numerical errors from the computations of the energy terms and gradients are too large to initiate the necessary convergence of the surface. Second reason is that, we have used va04 routine from Harwell library for optimization. It is necessary to write separate code for optimization which tightly integrates with the energy calcuations so that numerical errors can be reduced by appropriate energy and gradient optimizations.

The defect calculations in ML like scheme, depends on Region1. The dependence on the size of Region1 has been explored earlier. In these calculations, we have found that, in case of low symmetry crystals the defect calculations not only depend on the size but also on the shape of the Region1. Usually, in case of cubic crystals, spherical inner regions are taken owing to the symmetry of the medium[73]. On the other hand, in case of low symmetry crystals, nonspherical inner regions, increasing clusters of unit cells is more useful since the net charge of Region1 is same as the defect charge and is expected to give a better convergence and reduce numerical errors.

In spite of the failure in our first attempt, the firm physical background of the PPI model based on straightforward electrostatics insist us to pursue the defect optimization problem. In our immediate future task, we will vary and adjust the different parameters in the optimization codes to ensure that the algorithm does not skip the minimum in the energy surface.

Chapter 6

Summary and Outlook

In this thesis, we have presented a new technique of estimating point defect parameters based on the Polarizable Point Ion model and studied a high symmetry crystal with the technique. Then we simulated crystals of low as well as high symmetry with the same model and the existing Mott-Littleton approach with the aim to add a new measure to the model.

There have been adequate efforts for theoretical simulation of point defects in ionic crystals starting from the first half of the last century. As a result, a number of models and techniques have been developed with their own merits and demerits. We have first discussed these techniques and models in brief with a special attention to the Polarizable Point Ion model which has a unique identity for its simple and straightforward way of measurements. The modified and extended forms of the model assumed importance in the discussion as they were of direct relevance to the present work. An account of some of the relevant works done in last few decades from the viewpoint of different structures and different parameters were also presented in the thesis as an introduction. All these helped in formulating the background of our work.

We started our work with an attempt to devise a new technique where finite size calcu-

lations were done to estimate the infinite size defect parameters. A detail of the calculations were presented along with associated formulations. The modified form of the dipolar PPI model i.e. the MPPI model described the interactions for the host ions. The crystal was divided into two regions and only the first region was relaxed while optimizing the crystal to reduce the computational time. Dipole moments were estimated explicitly by solving a large set of electrostatic equations for the entire crystal. The calculations were repeated twice, once for the perfect crystal and then for the crystal with the defect incorporated into it. With this technique, we studied the vacancy defect in cubic *NaCl* crystal. We observed that the size of the Region2 should be sufficiently large than that of Region1 so that the dipoles on the surface of the crystal do not interact with those of the inner regions in the presence of the defect. The defect energies for both the sublattices for a fixed Region1 size showed good asymptotic behaviour with the increase of the crystal size. Interestingly, with this technique, the Schottky energy was not found to be a constant of Region1 size as predicted by the MPPI model. Rather, the energy converged to a much lower value in the infinite limit than that for the smallest inner region. The Schottky energy thus obtained matched fairly well with the experimental results. Further study in this line can be expected with an attempt to apply the technique to a comparatively low symmetry crystal.

We then turned our attention to the EPPI model. The simulation of Schottky and Frenkel defect energies in *AgCl* and *AgBr* with this model predicted good prospects for other highly polarizable ionic crystals. The best candidates were the alkaline earth oxides, an important set of materials in the field of material science and engineering. With the quadrupole moments included into the picture, the EPPI model gives a better understanding of the defect environment. However, the formulations with this model needs more care as new terms are introduced both in field and energy calculations. We observed that inclusion of the quadrupolar terms had substantial effects in the defect formation energies of all the four

members of the oxide class, i.e. MgO, CaO, SrO and BaO. The experimental value of MgO was then reinterpreted with an account of the impurity-vacancy association effect and was found to be in excellent agreement with the EPPI value. The whole calculations were done with Mott Littleton scheme and quadrupoles of the second region were neglected. We however did not study the energy as a function of Region1 and restricted this region to only first shell ions around the defect according to the MPPI predictions. The oxides being highly polarizable, there may be some deviations from this prediction and needs to be studied.

From the very beginning, it had been our effort to upgrade the existing codes based on polarizable models to be applicable to lower symmetry crystals. We attempted to simulate the very low symmetry monoclinic $\beta - Ga_2O_3$ crystal with these codes. It soon turned out that the computations are not easy with the ions of the crystal being in a non-zero electric field even in the perfect environment. The whole problem split into two parts, first simulating the perfect crystal to find a suitable set of potential parameters, and then using them in simulating the defect. With the lower symmetry, the otherwise simple PPI formulation becomes complicated. We however presented an approach to find an optimized set of short range potentials with this formulation starting from a rigid model definition. These parameters could reproduce the dielectric property of the crystal to a good accuracy. The defect calculations came out to be rather more complicated with a large number of terms in the energy expression. It turned out to be difficult to find the energy gradient in this case unlike the perfect crystal where the energy gradient helped in finding a quick and assured path to the equilibrium state. This, however, is a pioneering attempt and a lot of promising works are left to be done. Firstly, the defect calculations can be completed with more careful use of the step size and probably a better optimization code. Secondly, codes can be constructed to fit the short range parameters to crystal properties right with

the PPI definitions, instead of starting with a rigid model which ends up in somewhat low estimate of the electronic polarizabilities. Thirdly, the whole work can be extended to EPPI formulations which is expected to give considerable effect on the defect energetics with very high field gradient around the defect owing to the low symmetry.

Exploring all the points in above discussion, there seems to be a possibility of taking up a project to work out a full fledged user friendly computational package generalized to any structure based on EPPI model with both Mott-Littleton and Finite size techniques incorporated into it.

Appendix A

Ewald's Method for Lattice Sums

A.1 Coulomb Energy

Ewald method involves splitting of the lattice sum into two separate parts, one in real space and one in reciprocal space[133].

The inverse of the distance $\frac{1}{r}$ between two lattice points can be expressed as

$$\frac{1}{\mathrm{r}} = \frac{2}{\sqrt{\pi}} \int_0^\infty \exp\left(-\mathrm{r}^2\rho^2\right) \mathrm{d}\rho \qquad \text{(A.1)}$$

So, the Coulomb contribution to the lattice energy of the crystal, W_c, becomes

$$\mathrm{W_c} = \frac{1}{2} \sum_{\mathrm{l}=0}^{\infty} \sum_{\mathrm{i,j}} \frac{\mathrm{Q_i Q_j}}{4\pi\varepsilon_\mathrm{o} \mathrm{r_{ij}(l)}} = \frac{1}{2} \sum_{\mathrm{l}=0}^{\infty} \sum_{\mathrm{i,j}} \frac{\mathrm{Q_i Q_j}}{2\pi^{3/2}\varepsilon_\mathrm{o}} \int_0^\infty \exp\left(-\mathrm{r_{ij}^2(l)}\rho^2\right) \mathrm{d}\rho \qquad \text{(A.2)}$$

where $r_{ij}(l)$ is the distance between the i-th atom in the reference unit cell and the j-th atom in the l-th unit cell. Q_i and Q_j's are the charges on the atoms.

The integral can be split into two parts

$$\begin{aligned}\int_0^\infty \exp\left(-r^2\rho^2\right) d\rho &= \int_0^g \exp\left(-r^2\rho^2\right) d\rho + \int_g^\infty \exp\left(-r^2\rho^2\right) d\rho \\ &= \int_0^g \exp\left(-r^2\rho^2\right) d\rho + \frac{\sqrt{\pi}}{2}\frac{\mathrm{erfc}(gr)}{r} \end{aligned} \quad (A.3)$$

where g is a free parameter and $erfc(x)$ is the complementary error function given as

$$\mathrm{erfc}(x) = 1 - \mathrm{erf}(x) = \frac{2}{\sqrt{\pi}}\int_x^\infty \exp\left(-y^2\right) dy \quad (A.4)$$

The second term of Eq. A.3 consisting of the complementary error function is a rapidly converging function of r while the first term is a slowly converging function.

Transforming the first expression from real space to reciprocal space as

$$\frac{2}{\sqrt{\pi}}\sum_l \exp\left(-r_{ij}^2(l)\rho^2\right) = \frac{2\pi}{V_c}\sum_G \rho^{-3}\exp\left(-\frac{G^2}{4\rho^2}\right)\exp\left(i\mathbf{G}.(\mathbf{r}_j - \mathbf{r}_i)\right) d\rho \quad (A.5)$$

where V_c is the volume of the unit cell, **G** is a reciprocal lattice vector and both the atomic positions $\mathbf{r}_i$ and $\mathbf{r}_j$ lying within the reference unit cell, W_c can be written as

$$\begin{aligned} W_c &= \frac{1}{2}\sum_{l=0}^{\infty}\sum_{i,j}\frac{Q_iQ_j}{4\pi\varepsilon_o}\frac{\mathrm{erfc}\left(gr_{ij}(l)\right)}{r_{ij}(l)} \\ &\quad + \frac{1}{2}\sum_{i,j}\frac{Q_iQ_j}{4\pi\varepsilon_o}\frac{2\pi}{V_c}\int_0^g\sum_G \rho^{-3}\exp\left(-\frac{G^2}{4\rho^2}\right)\exp\left(i\mathbf{G}.\left(\mathbf{r}_j - \mathbf{r}_i\right)\right) d\rho \\ &= \frac{1}{2}\sum_{l=0}^{\infty}\sum_{i,j}\frac{Q_iQ_j}{4\pi\varepsilon_o}\frac{\mathrm{erfc}\left(gr_{ij}(l)\right)}{r_{ij}(l)} \\ &\quad + \frac{1}{2}\sum_{i,j}\frac{Q_iQ_j}{4\pi\varepsilon_o}\frac{4\pi}{V_c}\sum_G \frac{\exp\left(-\frac{G^2}{4g^2}\right)}{G^2}\exp\left(i\mathbf{G}.\left(\mathbf{r}_j - \mathbf{r}_i\right)\right) \end{aligned} \quad (A.6)$$

There are two points to be addressed here.

- The interactions for $i = j$ when $l = 0$ is to be subtracted from Eq. A.6 which was included for the reciprocal space summation to work. This term, known as the self term W_{self} can be written as,

$$W_{self} = \lim(r \to 0)\frac{1}{2}\frac{1}{4\pi\varepsilon_o}\sum_i \frac{Q_i^2\,[\mathrm{erfc}(gr) - 1]}{r} \tag{A.7}$$

Using the small argument expansion

$$1 - \mathrm{erfc}(x) = \mathrm{erf}(x) \quad \text{and} \quad \lim(x \to 0)\mathrm{erf}(x) = \frac{2x}{\sqrt{\pi}}$$

the self term is given by

$$W_{self} = -\frac{1}{4\pi\varepsilon_o}\sum_i \frac{gQ_i^2}{\sqrt{\pi}} \tag{A.8}$$

- The contribution from $\mathbf{G} = 0$ is to be excluded. Dropping the constant terms the contribution for $\mathbf{G} = 0$ can be written as

$$\lim\left(\tilde{G} \to 0\right)\frac{\exp\left(-\frac{G^2}{4g^2}\right)}{G^2}\left|F_Q\left(\tilde{G}\right)\right|^2$$

where

$$F_Q(\mathbf{G}) = \sum_j Q_j \exp\left(i\mathbf{G}.\mathbf{r}_j\right)$$

In the limit $\mathbf{G} \to 0$,

$$\lim(\mathbf{G} \to 0)\, F_Q(\mathbf{G}) \approx \sum_j Q_j \left(1 + i\mathbf{G}.\mathbf{r}_j\right) \qquad \left|\sum_j Q_j = 0 \text{(for a unit cell)}\right.$$
$$= i\mathbf{G}.\sum_j Q_j \mathbf{r}_j = i\mathbf{G}.\boldsymbol{\mu} \tag{A.9}$$

Here $\boldsymbol{\mu}$ is the dipole moment of the unit cell. For a centrosymmetric crystal, $\boldsymbol{\mu} = 0$. So, the term for $\mathbf{G} = 0$ vanishes.

Hence the Coulomb sum can be written in final form as

$$W_c = \frac{1}{2}\sum_{l=0}^{\infty}\sum_{i,j}\frac{Q_i Q_j}{4\pi\varepsilon_o}\frac{\operatorname{erfc}\left(g r_{ij}(l)\right)}{r_{ij}(l)}$$
$$+\frac{1}{2}\sum_{i,j}\frac{Q_i Q_j}{4\pi\varepsilon_o}\frac{4\pi}{V_c}\sum_{G}\frac{\exp\left(-\frac{G^2}{4g^2}\right)}{G^2}\exp\left(i\mathbf{G}.\left(\mathbf{r}_j - \mathbf{r}_i\right)\right) + W_{self} \tag{A.10}$$

A.2 Coulomb Field

Using Ewald sum as described in §A.1 the Coulomb Potential at ion *i* can be written as,

$$\Phi_i = \sum_l \sum_{j\neq i} Q_j \frac{\operatorname{erfc}(gr)}{r} \qquad \left|\mathbf{r} = \mathbf{R}_i - \mathbf{R}_j, \quad r = |\mathbf{r}|\right.$$
$$+\sum_{j\neq i}\frac{4\pi Q_j}{V_c}\sum_{G\neq 0}\frac{\exp\left(-\frac{G^2}{4g^2}\right)}{G^2}\cos(\mathbf{G}.\mathbf{r}) \tag{A.11}$$

The direct term is

$$\Phi_i^1 = \sum_l \sum_{j\neq i} Q_j \frac{\text{erfc}(gr)}{r} \tag{A.12}$$

Taking derivative

$$\begin{aligned}
\frac{\partial \Phi_i^1}{\partial r^\alpha} &= \sum_l \sum_{j\neq i} Q_j \frac{\partial}{\partial r}\left(\frac{\text{erfc}(gr)}{r}\right).\frac{\partial r}{\partial r^\alpha} \\
&= \sum_l \sum_{j\neq i} Q_j \left[\frac{1}{r}\frac{\partial}{\partial r}(\text{erfc}(gr)) - \frac{1}{r^2}\text{erfc}(gr)\right].\frac{r^\alpha}{r} \\
&= -\sum_l \sum_{j\neq i} Q_j \left[\frac{1}{r}\left(\frac{2g}{\sqrt{\pi}}e^{-g^2r^2}\right) + \frac{1}{r^2}\text{erfc}(gr)\right].\frac{r^\alpha}{r}
\end{aligned} \tag{A.13}$$

The reciprocal term is

$$\Phi_i^2 = \sum_{j\neq i} \frac{4\pi Q_j}{V_c} \sum_{G\neq 0} \frac{\exp\left(-\frac{G^2}{4g^2}\right)}{G^2} \cos(\mathbf{G}.\mathbf{r}) \tag{A.14}$$

Taking derivative

$$\frac{\partial \Phi_i^2}{\partial r^\alpha} = -\sum_{j\neq i} \frac{4\pi Q_j}{V_c} \sum_{G\neq 0} \frac{\exp\left(-\frac{G^2}{4g^2}\right)}{G^2} G_\alpha \sin(\mathbf{G}.\mathbf{r}) \tag{A.15}$$

So the expression for F_i^α , the component of the monopole field at ion i along α is

$$F_i^\alpha = -\left(\frac{\partial \Phi_i^1}{\partial r^\alpha} + \frac{\partial \Phi_i^2}{\partial r^\alpha}\right) \tag{A.16}$$

A.3 Coulomb Force Constant

Force constant or hessian is the second derivative of the lattice energy which has the Coulomb as well as short range terms. While finding second derivative of short range term

is quite straightforward, that of Coulomb term needs to be evaluated with Ewald's method for a better convergence. We give here only the Coulomb part of the force constant.

As derived in §A.1, the Coulomb energy is

$$W_c = \frac{1}{2}\sum_l\sum_i\sum_j Q_i Qj \frac{\text{erfc}(g r_{ij}(l))}{r_{ij}(l)} + \frac{1}{2}\sum_i\sum_j Q_i Q_j \frac{4\pi}{v_c}\sum_{G\neq 0}\frac{\exp(\frac{-G^2}{4g^2})}{G^2}\exp\{i\mathbf{G}.(\mathbf{r}_i - \mathbf{r}_j)\}$$

Let $\mathbf{r}' = \mathbf{r}_{ij}(l) = \mathbf{R_l} + \mathbf{R}_i - \mathbf{R}_j + \mathbf{r}_i - \mathbf{r}_j$ and $r' = r_{ij}(l) = \left|\mathbf{R_l} + \mathbf{R}_i - \mathbf{R}_j + \mathbf{r}_i - \mathbf{r}_j\right|$

Here, R_l is the lattice vector of the l^{th} cell, $\mathbf{R}_i$ and $\mathbf{R}_j$ are the position vectors of ion i and j with small displacements $\mathbf{r}_i$ and $\mathbf{r}_j$.

We now define a function $f(r')$ as

$$f(r') = \frac{\text{erfc}(gr')}{r'}$$

So, the direct term can be written as

$$W_c^1 = \frac{1}{2}\sum_l\sum_i\sum_{j\neq i} Q_i Q_j f(r') \qquad \text{(A.17)}$$

which gives

$$\begin{aligned}
\frac{\partial W_c^1}{\partial r_k^\alpha} &= \frac{1}{2}\sum_l\sum_i\sum_{j\neq i} Q_i Q_j \frac{\partial f(r')}{\partial r_k^\alpha} \\
&= \frac{1}{2}\sum_l\sum_i\sum_{j\neq i} Q_i Q_j \frac{\partial f(r')}{\partial r'^\alpha}(\delta_{ik}-\delta_{jk}) \\
&= \sum_l\sum_{j\neq i} Q_k Q_j \frac{\partial f(r')}{\partial r'^\alpha} + (\text{term ind. of } r_i,\, r_j) \\
\frac{\partial^2 W_c^1}{\partial r_k^\alpha \partial r_m^\beta} &= \sum_l\sum_{j\neq k} Q_k Q_j \frac{\partial^2 f(r')}{\partial r'^\alpha \partial r'^\beta}(\delta_{km}-\delta_{jm}) \\
&= \delta_{km}\sum_l\sum_{j\neq k} Q_k Q_j \frac{\partial^2 f(r')}{\partial r'^\alpha \partial r'^\beta} - \sum_l Q_k Q_m \frac{\partial^2 f(r')}{\partial r'^\alpha \partial r'^\beta}
\end{aligned}$$

$$\left.\frac{\partial^2 W_c^1}{\partial r_k^\alpha \partial r_m^\beta}\right|_0 = \delta_{km}\sum_l\sum_{j\neq k} Q_k Q_j \frac{\partial^2 f(r)}{\partial r^\alpha \partial r^\beta} - \sum_l Q_k Q_m \frac{\partial^2 f(r)}{\partial r^\alpha \partial r^\beta} \tag{A.18}$$

with $\mathbf{r} = \mathbf{R}_l + \mathbf{R}_k - \mathbf{R}_m$.

Now,

$$\frac{\partial^2 f(r)}{\partial r^\alpha \partial r^\beta} = J_{\alpha\beta}\frac{\partial^2 f(r)}{\partial r^2} + M_{\alpha\beta}\frac{\partial f(r)}{\partial r} \tag{A.19}$$

where $J_{\alpha\beta} = \dfrac{r^\alpha r^\beta}{r^2}$ and $M_{\alpha\beta} = \frac{1}{r}\left(\delta_{\alpha\beta} - \dfrac{r^\alpha r^\beta}{r^2}\right)$. Substituting the value of $f(r)$

$$\begin{aligned}
\frac{\partial f(r)}{\partial r} &= \frac{\partial}{\partial r}\left(\frac{\operatorname{erfc}(gr)}{r}\right) \\
&= \frac{1}{r}\frac{\partial}{\partial r}(\operatorname{erfc}(gr)) - \frac{\operatorname{erfc}(gr)}{r^2} \qquad \text{(A.20)} \\
\frac{\partial^2 f(r)}{\partial r^2} &= \frac{1}{r}\frac{\partial^2}{\partial r^2}(\operatorname{erfc}(gr)) - \frac{1}{r^2}\frac{\partial}{\partial r}(\operatorname{erfc}(gr)) \\
&\quad \frac{1}{r^2}\frac{\partial}{\partial r}(\operatorname{erfc}(gr)) + \frac{2}{r^3}\operatorname{erfc}(gr) \\
&= \frac{1}{r}\frac{\partial^2}{\partial r^2}(\operatorname{erfc}(gr)) - \frac{2}{r^2}\frac{\partial}{\partial r}(\operatorname{erfc}(gr)) \\
&\quad + \frac{2}{r^3}\operatorname{erfc}(gr) \qquad \text{(A.21)}
\end{aligned}$$

Now, using $\frac{d^{n+1}}{dz^{n+1}}\text{erf}(z) = (-1)^n \frac{2}{\sqrt{\pi}} H_n(z)e^{-z^2}$, we get

$$\frac{d}{dz}\text{erf}(z) = -\frac{d}{dz}\text{erf}(z) = -\frac{2}{\sqrt{\pi}} H_o(z)e^{-z^2}$$

and

$$\frac{d^2}{dz^2}\text{erfc}(z) = -\frac{d^2}{dz^2}\text{erf}(z) = \frac{2}{\sqrt{\pi}} H_1(z)e^{-z^2}$$

with

$$H_o(z) = 1 \qquad \text{and} \qquad H_1(z) = 2z$$

Eq. A.20 and Eq. A.21 become

$$\frac{\partial f(r)}{\partial r} = \frac{1}{r}\left\{-\frac{2g}{\sqrt{\pi}}e^{-g^2r^2}\right\} - \frac{1}{r^2}\text{erfc}(gr) \tag{A.22}$$

$$\frac{\partial^2 f(r)}{\partial r^2} = \left(2g^3 + \frac{2g}{r^2}\right)\frac{2}{\sqrt{\pi}}e^{-g^2r^2} + \frac{2}{r^3}\text{erfc}(gr) \tag{A.23}$$

Putting these expressions back in Eq. A.19 and then back in Eq. A.18 we get the second derivative of the direct term. As for the reciprocal term

$$W_c^2 = \frac{1}{2}\sum_i\sum_j Q_iQ_j\frac{4\pi}{v_c}\sum_{G\neq 0}\frac{\exp\left(-\frac{G^2}{4g^2}\right)}{G^2}\exp\left\{i\mathbf{G}.\left(\mathbf{r}_i - \mathbf{r}_j\right)\right\} \tag{A.24}$$

The second derivative is

$$\frac{\partial^2 W_c^2}{\partial r_k^\alpha r_m^\beta} = -\frac{1}{2}\sum_i\sum_j Q_iQ_j\frac{4\pi}{v_c}\sum_{G\neq 0}\frac{\exp\left(-\frac{G^2}{4g^2}\right)}{G^2}G_\alpha G_\beta \exp\left\{i\mathbf{G}.\left(\mathbf{r}_i - \mathbf{r}_j\right)\right\} \tag{A.25}$$

A.4 Ewald sum of $\frac{1}{R^2}$ Term

In general, $\frac{1}{R^{2n}}$ can be written as

$$\frac{1}{R^{2n}} = \frac{2}{(n-1)!}\int_0^\infty \rho^{2n-1}\exp\left(-r^2\rho^2\right)d\rho \tag{A.26}$$

So,

$$\begin{aligned}\sum_{l=0}^{\infty}\frac{1}{R^2} &= \sum_{l=0}^{\infty} 2\int_0^\infty \rho\exp\left(-R^2\rho^2\right)d\rho \\ &= \sum_{l=0}^{\infty}\int_0^g \rho\exp\left(-R^2\rho^2\right)d\rho + 2\sum_{l=0}^{\infty}\rho\exp\left(-R^2\rho^2\right)d\rho \\ &= I_1 + I_2 \end{aligned} \tag{A.27}$$

The direct term is

$$\begin{aligned} I_2 &= 2\sum_{l=0}^{\infty}\int_g^\infty \rho\exp\left(-R^2\rho^2\right)d\rho \\ &= 2\sum_{l=0}^{\infty}\frac{\exp\left(-g^2R^2\right)}{2R^2}\end{aligned} \tag{A.28}$$

and the reciprocal term is

$$\begin{aligned} I_1 &= 2\sum_{l=0}^{\infty}\int_0^g \rho\exp\left(-R^2\rho^2\right)d\rho \\ &= 2\int_0^g \rho d\rho\left[\sum_{l=0}^{\infty}\exp\left(-R^2\rho^2\right)\right] \\ &= 2\int_0^g \rho d\rho\left[\frac{\pi^{\frac{3}{2}}}{V_c}\sum_G \rho^{-3}\exp\left(-\frac{G^2}{4\rho^2}\right)\exp\left(i\mathbf{G}.\mathbf{R}\right)\right] \\ &= \frac{2\pi^{\frac{3}{2}}}{V_c}\sum_G \exp\left(i\mathbf{G}.\mathbf{R}\right) I_3\end{aligned} \tag{A.29}$$

where

$$\begin{aligned} I_3 &= \int_0^g \rho^{-2} \exp\left(-\frac{G^2}{4\rho^2}\right) d\rho \\ &= -\int_a^\infty \left(-\frac{2}{G}\right) \exp\left(-t^2\right) dt, \qquad t = \frac{G}{2\rho} \& a = \frac{G}{2g} \\ &= \frac{\sqrt{\pi}}{G} \text{erfc}\left(\frac{G}{2g}\right) \end{aligned} \tag{A.30}$$

So,

$$I_1 = \frac{2\pi^2}{V_c} \sum_G \frac{1}{G} \text{erfc}\left(\frac{G}{2g}\right) \exp\left(i\mathbf{G}.\mathbf{R}\right) \tag{A.31}$$

Thus eq A.27 becomes

$$\sum_{l=0}^{\infty} \frac{1}{R^2} = \sum_{l=0}^{\infty} \frac{\exp\left(-g^2R^2\right)}{R^2} + \frac{4\pi^2}{V_c} \sum_G \frac{1}{G} \text{erfc}\left(\frac{G}{2g}\right) \exp\left(i\mathbf{G}.\mathbf{R}\right) \tag{A.32}$$

A.4.1 Second Derivative of $\frac{1}{R^2}$ Ewald Sum

Taking the derivative of the direct term of eq. A.32

$$\begin{aligned} \frac{\partial}{\partial R_\alpha} \sum_{l=0}^{\infty} \left(\frac{\exp\left(-g^2R^2\right)}{R^2}\right) &= \sum_{l=0}^{\infty} \frac{\partial}{\partial R_\alpha} \left(\frac{\exp\left(-g^2R^2\right)}{R^2}\right) \\ &= -\frac{2R_\alpha}{R^4} \exp\left(g^2R^2\right) - \frac{2g^2R_\alpha}{R^2} \exp\left(-g^2R^2\right) \end{aligned} \tag{A.33}$$

The second derivative gives

$$\begin{aligned} \sum_{l=0}^{\infty} \frac{\partial^2}{\partial R_\beta \partial R_\alpha} \left(\frac{\exp\left(-g^2R^2\right)}{R^2}\right) &= \sum_{l=0}^{\infty} \left(\frac{4R_\alpha R_\beta}{R^6} \exp\left(-g^2R^2\right)\left(2 + 2g^2R^2 + g^4R^4\right)\right. \\ &\left. -\delta_{\alpha\beta} \frac{2}{R^4} \exp\left(-g^2R^2\right)\left(1 + g^2R^2\right)\right) \end{aligned} \tag{A.34}$$

For the reciprocal term

$$\begin{aligned}\frac{\partial^2}{\partial R_\beta \partial R_\alpha}\left(\frac{4\pi^2}{V_c}\sum_G \frac{1}{G}\text{erfc}\left(\frac{G}{2g}\right)\exp\left(i\mathbf{G}.\mathbf{R}\right)\right) &= \frac{4\pi^2}{V_c}\sum_G \frac{1}{G}\text{erfc}\left(\frac{G}{2g}\right)\frac{\partial^2}{\partial R_\beta \partial R_\alpha}\left(\exp\left(i\mathbf{G}.\mathbf{R}\right)\right) \\ &= \frac{4\pi^2}{V_c}\sum_G \frac{G_\alpha G_\beta}{G}\text{erfc}\left(\frac{G}{2g}\right)\exp\left(i\mathbf{G}.\mathbf{R}\right) \quad \text{(A.35)}\end{aligned}$$

So

$$\begin{aligned}\frac{\partial^2}{\partial R_\beta \partial R_\alpha}\left(\sum_{l=0}^{\infty}\frac{1}{R^2}\right) &= \sum_{l=0}^{\infty}\left[\frac{4R_\alpha R_\beta}{R^6}\exp\left(-g^2R^2\right)\left(2+2g^2R^2+g^4R^4\right)\right. \\ &\quad \left.-\delta_{\alpha\beta}\frac{2}{R^4}\exp\left(-g^2R^2\right)\left(1+g^2R^2\right)\right] \\ &\quad +\frac{4\pi^2}{V_c}\sum_G \frac{G_\alpha G_\beta}{G}\text{erfc}\left(\frac{G}{2g}\right)\exp\left(i\mathbf{G}.\mathbf{R}\right) \quad \text{(A.36)}\end{aligned}$$

A.5 Ewald's Sum of $\frac{1}{R^4}$ Term

Using eq.A.26 we write $\frac{1}{R^4}$ as

$$\begin{aligned}\sum_{l=0}^{\infty}\frac{1}{R^4} &= \sum_{l=0}^{\infty} 2\int_0^{\infty}\rho^3\exp\left(-R^2\rho^2\right)d\rho \\ &= \sum_{l=0}^{\infty}\int_0^{g}\rho^3\exp\left(-R^2\rho^2\right)d\rho + 2\sum_{l=0}^{\infty}\int_g^{\infty}\int_0^{g}\rho^3\exp\left(-R^2\rho^2\right)d\rho \\ &= I_1 + I_2 \quad \text{(A.37)}\end{aligned}$$

The direct term is

$$\begin{aligned}I_2 &= 2\sum_{l=0}^{\infty}\int_g^{\infty}\rho^3\exp\left(-R^2\rho^2\right)d\rho \\ &= \sum_{l=0}^{\infty}\frac{\exp\left(-g^2R^2\right)}{R^2}\left(g^2+\frac{1}{R^2}\right) \quad \text{(A.38)}\end{aligned}$$

and the reciprocal term is

$$\begin{aligned} I_1 &= 2\sum_{l=0}^{\infty}\int_0^g \rho^3 \exp\left(-R^2\rho^2\right) d\rho \\ &= 2\int_0^g \rho^3 d\rho \left[\sum_{l=0}^{\infty} \exp\left(-R^2\rho^2\right)\right] \\ &= 2\int_0^g \rho^3 d\rho \left[\frac{\pi^{\frac{3}{2}}}{V_c}\sum_G \rho^{-3} \exp\left(-\frac{G^2}{4\rho^2}\right)\exp\left(i\mathbf{G}.\mathbf{R}\right)\right] \\ &= \frac{2\pi^{\frac{3}{2}}}{V_c}\sum_G \exp\left(i\mathbf{G}.\mathbf{R}\right) I_3 \end{aligned} \tag{A.39}$$

where

$$\begin{aligned} I_3 &= \int_0^g \exp\left(-\frac{G^2}{4\rho^2}\right) d\rho \\ &= g\exp\left(-\frac{G^2}{4g^2}\right) - \frac{2G}{\sqrt{\pi}}\text{erfc}\left(\frac{G}{2g}\right) \end{aligned} \tag{A.40}$$

So,

$$I_1 = \frac{2\pi^2}{V_c}\sum_G \frac{1}{G}\text{erfc}\left(\frac{G}{2g}\right)\exp\left(i\mathbf{G}.\mathbf{R}\right) \tag{A.41}$$

Thus eq A.37 becomes

$$\sum_{l=0}^{\infty}\frac{1}{R^4} = \sum_{l=0}^{\infty}\frac{\exp\left(-g^2R^2\right)}{R^2}\left(g^2+\frac{1}{R^2}\right) + \frac{2\pi^{\frac{3}{2}}}{V_c}\sum_G\left(\left[g\exp\left(-\frac{G^2}{4g^2}\right) - \frac{G\sqrt{\pi}}{2}\text{erfc}\left(\frac{G}{2g}\right)\right]\exp\left(i\mathbf{G}.\mathbf{R}\right)\right) \tag{A.42}$$

Appendix B

The Dielectric Constant and Polarizability

In a dielectric medium, the dipole moment $\boldsymbol{\mu}$ of each atom is proportional to the field **E** causing polarization in the medium[132].

$$\boldsymbol{\mu} = \alpha \mathbf{E} \tag{B.1}$$

where α is called the polarizability of the atom. This relation is true if the electric field is not very high. Otherwise, there will be nonlinear terms in the relationship. The field **E** is the external field $\mathbf{E}_o$ reduced by polarization and is given by

$$\mathbf{E} = \mathbf{E}_o - \frac{1}{\varepsilon_o}\mathbf{P} \tag{B.2}$$

P is the polarization of the medium.

For a system having N number of similar atoms in volume v, the total polarization **P**

can be written as

$$\mathbf{P} = \frac{N\alpha\mathbf{E}}{v} \tag{B.3}$$

In a polarized medium, the displacement vector **D** is given by

$$\mathbf{D} = \varepsilon_o\mathbf{E} + \mathbf{P} \tag{B.4}$$

Putting eq. B.3 in eq. B.4

$$\mathbf{D} = \varepsilon_o\left(1 + \frac{N\alpha}{v\varepsilon_o}\right)\mathbf{E} \tag{B.5}$$

Again

$$\begin{aligned}\mathbf{D} &= \varepsilon\mathbf{E} \\ &= \varepsilon_o\varepsilon_r\mathbf{E}\end{aligned} \tag{B.6}$$

where $\varepsilon_r = \frac{\varepsilon}{\varepsilon_o}$ is the relative dielectric constant.

Comparing eq. B.5 and B.6

$$\varepsilon_r = 1 + \left(\frac{N\alpha}{v\varepsilon_o}\right) \tag{B.7}$$

It has been found from experiments that eq. B.7 which relates the macroscopic dielectric constant with the microscopic polarizability is valid only for dilute medium like gases and do not hold for liquid and solids.

For liquids and solids, it is the field **E** which is to be replaced by the local field $\mathbf{E}_{loc}$. In case of a crystal, for example, while considering the field acting on a dipole, we cannot neglect the field of its neighbouring dipoles. Let the system be a unit cell and *i* goes over

the number of ions in the cell. Then **P** is to be redefined as

$$\mathbf{P} = \frac{1}{\mathrm{v_m}} \sum_{\mathrm{i}} \alpha_{\mathrm{i}} \mathbf{E}^{\mathrm{i}}_{\mathrm{loc}} \tag{B.8}$$

$\mathrm{v_m}$ is the volume of the unit cell. The local field acting on the i^{th} dipole within the unit cell is given by

$$\mathbf{E}^i_{loc} = \mathbf{E}^i_o + \mathbf{E}^i_1 + \mathbf{E}^i_2 + \mathbf{E}^i_3 \tag{B.9}$$

Here, $\mathbf{E}^i_o$ is the external field, $\mathbf{E}^i_1$ the field due to the polarization charges lying on the surface of the crystal, $\mathbf{E}^i_2$ the field due to the polarization charges lying on the surface of the unit cell and $\mathbf{E}^i_3$ is the field due to other dipoles lying within the cell.

The field $\mathbf{E}^i_1$, due to the polarization charges on the external surface, known as the depolarization field opposes the external field and can be written as

$$\mathbf{E}^{\mathrm{i}}_1 = -\frac{1}{\varepsilon_{\mathrm{o}}}\mathbf{P} \tag{B.10}$$

On the other hand, the polarization charges on the surface of the unit cell can be written as

$$\mathbf{E}^{\mathrm{i}}_2 = \frac{1}{3\varepsilon_{\mathrm{o}}}\mathbf{P} \tag{B.11}$$

which is in the same direction as $\mathbf{E}_o$.

The fourth field i.e. $\mathbf{E}^i_3$ is

$$\mathbf{E}^{\mathrm{i}}_3 = \sum_{\mathrm{j}\neq\mathrm{i}} \frac{3\left(\boldsymbol{\mu}_{\mathrm{j}}.\mathbf{r}\right)\mathbf{r} - |\mathbf{r}|^2 \boldsymbol{\mu}_{\mathrm{j}}}{|\mathbf{r}|^5} \tag{B.12}$$

j goes over the unit cell ions. Substituting the various terms in eq. B.9 and using $\mathbf{E}^i_{loc}$ in

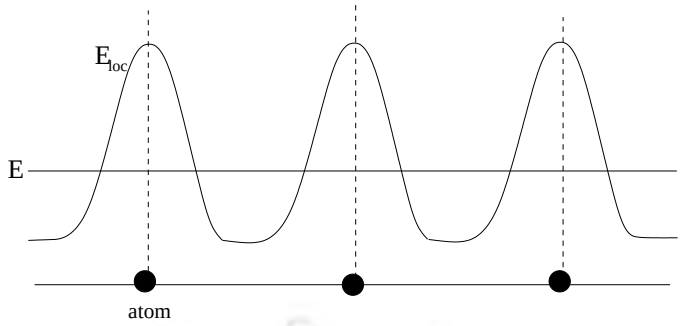

Figure B.1: The Maxwell field E and the local field E_{loc}

eq. B.8 we get

$$\mathbf{P} = \frac{1}{v_m}\left[\left(\mathbf{E} + \frac{1}{3\varepsilon_o}\mathbf{P}\right)\sum_i \alpha_i + \sum_i \alpha_i \sum_{j\neq i} \frac{3\left(\boldsymbol{\mu}_j.\mathbf{r}\right)\mathbf{r} - |\mathbf{r}|^2\boldsymbol{\mu}_j}{|\mathbf{r}|^5}\right] \tag{B.13}$$

For a centrosymmetric unit cell, the second term vanishes. So

$$\begin{aligned}\mathbf{P} &= \frac{1}{v_m}\left(\mathbf{E} + \frac{1}{3\varepsilon_o}\mathbf{P}\right)\sum_i \alpha_i \\ &= \frac{1}{v_m}\left(\mathbf{E} + \frac{1}{3\varepsilon_o}\mathbf{P}\right)\alpha_{tot}\end{aligned} \tag{B.14}$$

where α_{tot} is the total polarizability of the unit cell.

Thus $\mathbf{E}_{loc}$ and $\mathbf{E}$ are indeed different . $\mathbf{E}$ is somewhat an average field taken over large number of atoms in the system, while $\mathbf{E}_{loc}$ is a microscopic field which fluctuates spatially within the medium as shown in fig. B.1. Rearranging the terms in eq. B.14, we get

$$\mathbf{P} = \frac{1}{v_m}\left(\frac{\alpha_{tot}}{1 - \frac{\alpha_{tot}}{3v_m\varepsilon_o}}\right)\mathbf{E} \tag{B.15}$$

This shows that the polarization is enhanced with the theory of local field.

Using this new polarization in eq. B.4 and comparing with eq. B.6 the expression for ε_r

becomes

$$\varepsilon_r = \frac{1 + \frac{2}{3\nu_m \varepsilon_o}\alpha_{tot}}{1 - \frac{\alpha_{tot}}{3\nu_m \varepsilon_o}} \tag{B.16}$$

which can also be written as

$$\frac{\varepsilon_r - 1}{\varepsilon_r + 2} = \frac{\alpha_{tot}}{3\nu_m \varepsilon_o} \tag{B.17}$$

This equation is the Claussius-Mossotti (CM) equation. In SI system the CM equation becomes

$$\frac{\varepsilon_r - 1}{\varepsilon_r + 2} = \frac{4\pi}{3\nu_m}\alpha_{tot} \tag{B.18}$$

Appendix C

Co-ordinate Transformation

Transformation of fractional to cartesian coordinates and cartesian to fractional coordinates is an essential feature in crystallography as far as geometrical calculations are involved. We give here the transformation matrix for the most general case i.e. a triclinic structure[134]. Transformation matrix for other structures can easily be derived from this general one. Let

$$\mathbf{A} = \begin{pmatrix} \mathbf{a} \\ \mathbf{b} \\ \mathbf{c} \end{pmatrix} \quad \text{and} \quad \mathbf{X} = \begin{pmatrix} \mathbf{x} \\ \mathbf{y} \\ \mathbf{z} \end{pmatrix}$$

be the fractional (crystallographic) and cartesian (orthonormal) bases respectively. We can then write the transformation equations in the matrix form as $\mathbf{X} = \mathbf{T_{fc}A}$ and $\mathbf{A} = \mathbf{T_{cf}X}$, where $\mathbf{T_{fc}}$ and $\mathbf{T_{cf}}$ are the transformation matrices for fractional to cartesian and cartesian to fractional respectively.

We choose, as shown in fig. C.1, **x** along **a**, **y** normal to **a** in the (**a, b**) plane, and **z** normal to **x** and **y**. So the unit vectors **a**/a, **b**/b, **c**/c can be expressed in terms of **x, y, z** by

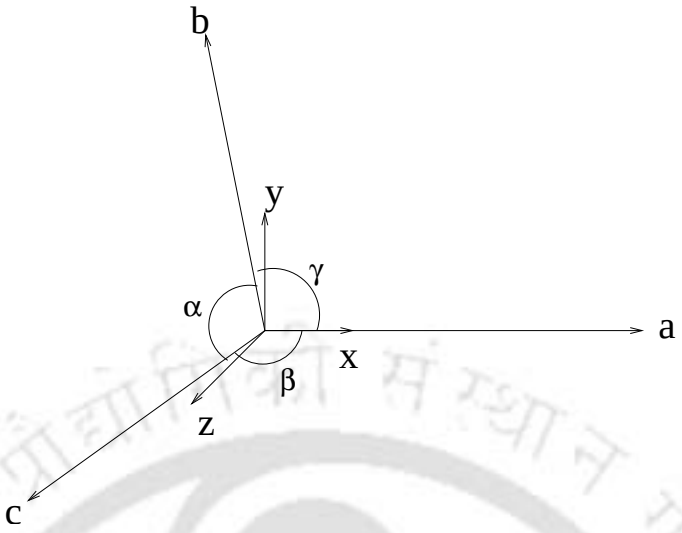

Figure C.1: Fractional and cartesian bases

the following matrix equation.

$$\begin{pmatrix} \mathbf{a}/a \\ \mathbf{b}/b \\ \mathbf{c}/c \end{pmatrix} = \begin{pmatrix} l_1 & l_2 & l_3 \\ m_1 & m_2 & m_3 \\ n_1 & n_2 & n_3 \end{pmatrix} \begin{pmatrix} \mathbf{x} \\ \mathbf{y} \\ \mathbf{z} \end{pmatrix} \tag{C.1}$$

where (l_1, l_2, l_3), (m_1, m_2, m_3) and (n_1, n_2, n_3) are the direction cosines of the unit vectors **a**/a, **b**/b, **c**/c in **E** satisfying the following conditions

$$\sum_i l_i^2 = \sum_i m_i^2 = \sum_i n_i^2 = 1$$

and

$$\cos\alpha = \sum_i m_i n_i, \quad \cos\beta = \sum_i l_i n_i, \quad \cos\gamma = \sum_i l_i m_i$$

From fig. C.1 we can deduce that

$$l_1 = 0, \quad l_2 = 0, \quad l_3 = 0, \quad m_1 = \cos\alpha, \quad m_2 = \sin\gamma, \quad m_3 = 0 \quad \text{and} \quad n_1 = \cos\beta$$

Now, using

$$\cos\alpha = \sum_i m_i n_i = \cos\gamma\cos\beta + \sin\gamma\sin n_2$$

we obtain

$$\begin{aligned} n_2 &= \frac{(\cos\alpha - \cos\beta\cos\gamma)}{\sin\gamma} \\ &= -\sin\beta\cos\alpha^* \end{aligned}$$

Here a^*, b^*, c^* are the reciprocal vectors and α^*, β^*, γ^* are the corresponding reciprocal angles.

The only direction cosine left is n_3 which can be determined from the relation $\sum_i n_i^2 = 1$ and comes out to be

$$n_3 = \sin\beta\sin\alpha^* = \frac{1}{(cc^*)}$$

Finally the relation C.1 becomes

$$\begin{pmatrix} \mathbf{a}/a \\ \mathbf{b}/b \\ \mathbf{c}/c \end{pmatrix} = \begin{pmatrix} 1 & 0 & 0 \\ \cos\gamma & \sin\gamma & 0 \\ \cos\beta & -\sin\beta\cos\alpha^* & \frac{1}{c^*c} \end{pmatrix} \begin{pmatrix} \mathbf{x} \\ \mathbf{y} \\ \mathbf{z} \end{pmatrix} \qquad \text{(C.2)}$$

So the transformation matrix $\mathbf{T_{fc}}$ is

$$\mathbf{T_{fc}} = \begin{pmatrix} a & 0 & 0 \\ b\cos\gamma & b\sin\gamma & 0 \\ c\cos\beta & -c\sin\beta\cos\alpha^* & \frac{1}{c^*} \end{pmatrix} \qquad \text{(C.3)}$$

The inverse of $\mathbf{T_{fc}}$ gives us $\mathbf{T_{cf}}$.

$$\mathbf{T_{cf}} = \begin{pmatrix} \frac{1}{a} & 0 & 0 \\ -\frac{\cos\gamma}{a\sin\gamma} & \frac{1}{b\sin\gamma} & 0 \\ a^*\cos\beta^* & b^*\cos\alpha^* & c^* \end{pmatrix} \qquad \text{(C.4)}$$

Bibliography

[1] Walker A M. PhD thesis, Faraday Research Laboratory, The Royal Institution of Great Britain, 2004.

[2] Ashcroft Neil W. and Mermin N. David. *Solid State Physics*. Harcourt Brace College Publishers, 1976.

[3] Harrison E A et al. *J. Phys. E: Sci. Instrum.*, 5:174–177, 1972.

[4] Dryzek E. *Phys. Status Solidi(a)*, 128:337, 1991.

[5] Dryzek J. *J. Phys. Condensed Matter*, 7:L383, 1995.

[6] Dryzek J. *Mater. Science Forum*, 255-257:533, 1997.

[7] Kauppinen H, Corbel C., Nissila J, Saarinen K, and Hautojarvi P. *Physical Review B*, 57:12911–12922, 1998.

[8] Saarinen K., Nissila J., Kauppinen H., Hakala M., Puska M.J., Hautojarvi P., and Corbel C. *Physical Review Letters*, 82:1883–1886, 1999.

[9] Franklin A D. In Crawford J H and Silfkin L M, editors, *Point Defects in Solids*. Plenum Press, 1972.

[10] Laskar A L and Chandra S, editors. *Superionic Solids and Solid Electrolytes*. Academic Press, London, 1989.

[11] Hohenberg P and Kohn W. *Phys. Rev.*, 136:B864, 1964.

[12] Lunqvist S and March N H. *The Theory of Inhomogeneous Electron Gas*. Plenum, New York, 1983.

[13] Kohn W and Sham L J. *Phys. Rev.*, 140:A1133, 1965.

[14] Becke A D. *Phys. Rev. A*, 38:3098, 1988.

[15] Perdew J P, Burke K, and Ernzernhof M. *Phys. Rev. Lett.*, 77:3865, 1996.

[16] Vita A De and Gillan M J. *J. Phys.:Condensed Matter*, 3:6225–6237, 1991.

[17] Lichanot A, Baranek Ph., Merawa M, Orlando R, and Dovesi R. *Physical Review B*, 62:12812, 2000.

[18] He Jun and Sinnott Susan B. *Journal of American Ceramic Society*, 88:737, 2005.

[19] Jackson K, Pederson Mark R, and Klein Barry M. *Phys. Rev. B*, 43:2364, 1991.

[20] Aguado A, Lopez Jose M, and Alonso Julio A. *Phys. Rev. B*, 62:3086, 2000.

[21] Ogut Serder and Chelikowsky James R. *Phys. Rev. B*, 64:245206, 2001.

[22] Born M and huang K. *Dynamic Theory of Crystal Lattice*. Oxford University Press, London, 1954.

[23] Tosi M P. *Solid State Phys.*, 16, 1964.

[24] Cowley R A. *Phys. Rev.*, 134:A981–97, 1964.

[25] Cran G C and Sangster M J L. *J. Phys. C : Solid State Physics*, 7:1937–48, 1974.

[26] Sangster M J L. *Solid State Commun.*, 15:471–4, 1974.

[27] Catlow C R A and Hayns M R. *J. Phys. C : Solid State Phys.*, 5:L237–40, 1972.

[28] Catlow C R A, Dillar K M, and Norgett M J. *J. Phys. C : Solid State Phys.*, 10:1395–412, 1977.

[29] James R. *AERE Report*, page TP666, 1976.

[30] Catlow C R A and James R. *J. phys. C : Solid State Phys.*, 10:L237–40, 1977.

[31] Calais J L. *Int. J. Quantum Chem. Symp.*, 9:497, 1975.

[32] Fuchs K. *Proc. R. Soc. A*, 151:585–602, 1935.

[33] Jensen K. *Z. Phys.*, 101:141–85, 1936.

[34] Wedepohl P T. *Proc. Phys. Soc.*, 92:79–93, 1967.

[35] Wedepohl P T. *J. Phys. B:Atom. Molec. Phys.*, 1:307–14, 1968.

[36] Gordon R G and Kim Y S. *J. Chem. Phys.*, 56:3122, 1972.

[37] Kim Y S and Gordon R G. *Phys. Rev. B*, 9:3548, 1974.

[38] Waldman M and Gordon R G. *J. Chem. Phys.*, 71:1325, 1979.

[39] Mackrodt W C and Stewart R F. *J. Phys. C*, 12:431, 1979.

[40] Muhlhausen Carl and Gordon Roy G. *Phys. Rev. B*, 23:900, 1981.

[41] Francisco E, Reico J M, Blanco M A, Pedas A M, and Pueyo L. *Phys. Rev. B*, 51:2703–2714, 1995.

[42] Blanco M A, Recio J M, Francisco E, Costales A, luana V, and Pendas A M. *Radiation Effects and Defects in Solids*, 151:223–228, 1999.

[43] Tessman J R et al. *Phys. Rev.*, 92:890, 1953.

[44] Murti Y V G S and Usha V. *Physica*, 83B:275, 1976.

[45] Maradudin A A, Montroll E W, Weiss G H, and Ipatova I P. *Theory of Lattice Dynamics in the Harmonic Approximation*. Academic Press, New York, 2nd edition, 1971.

[46] Rickman J M and LeSar R. *Annu. Rev. Mater. Res.*, 32:195, 2002.

[47] Jost W. *J Chem. Phys.*, 1:255, 1933.

[48] Banhatti Radha D and Murti Y V G S. *Phys. Rev. B*, 48:6839–6853, 1993.

[49] Eshelby J D. *Journal of Applied Physics*, 25:255, 1954.

[50] Mott N F and Littleton M J. *Trans. Faraday Society*, 34:485, 1938.

[51] Kanzaki H. *J Phys Chem Solids*, 15:39, 1960.

[52] Hardy J R. *J Phys Chem Solids*, 23:113–116, 1962.

[53] Tewary V K. *Advances in Physics*, 22:757, 1973.

[54] Kurosawa T. *J Phys Soc Japan*, 13:153, 1958.

[55] Norgett M J. *AERE Report*, page R7650, 1974.

[56] Dick B G and Overhauser A W. *Phys. Rev.*, 112:90, 1958.

[57] Hardy J R and Karo A M. The lattice dynamics and statics of alkali halide crystals. *Plenum Press, NY*, 1979.

[58] Kunc K and Balkanski M. *Physical Review B*, 12:4346, 1975.

[59] Murti Y V G S and Banhatti Radha D. *Indian Journal of Pure and Applied Physics*, 37:285–293, 1999.

[60] Banhatti Radha D. PhD thesis, IIT Madras, 1993.

[61] Banhatti Radha D and Murti Y V G S. *Radiation Effects and Defects in Solids*, 134:157, 1995.

[62] Murti Y V G S and Banhatti Radha D. *Bull Mat Sci*, 20:435–440, 1997.

[63] Boswarva I.M. and Lidiard A.B. *Phil. Mag.*, 16:805, 1967.

[64] Boswarva I.M. *Phil. Mag.*, 16:827, 1967.

[65] Tharmalingam K. *J Phys. C:Solid State Physics*, 3:1856–1860, 1970.

[66] Norgett M J Catlow C R A, Dillar K M. *J Phys. C:Solid State Physics*, 8:L34–L36, 1975.

[67] Murti Y V G S and Usha V. *Crystal Lattice Defects*, 7:31–37, 1977.

[68] Catlow C R A and Norgett M J. *J Phys. C:Solid State Physics*, 6:1325–1339, 1973.

[69] Norgett M J Catlow C R A and Ross T A. *J Phys. C:Solid State Physics*, 10:1627–1640, 1977.

[70] Mackrodt W C and Stewart R F. *J Phys. C:Solid State Physics*, 12:5015, 1979.

[71] Welch D O Danemar A and Royce B S H. *Phys. Stat. Sol.(b)*, 55:201, 1973.

[72] Mackrodt W C and Stewart R F. *Journal De Physique*, 41:C6–64, 1980.

[73] Catlow C R A, James R, Mackrodt W C, and Stewart R F. *Phys. Rev. B*, 25:1006, 1982.

[74] Kurnick S W. *J. Phys. C*, 20:218, 1952.

[75] Abey A E and Tomizuka C T. *J. Phys. Chem. Solids*, 27:1149, 1966.

[76] Faux I D and Lidiard A B. *Z. Nature.(a)*, 26:61, 1971.

[77] Yoon D N and Lazarus D. *Phys. Rev. B*, 5:4935, 1972.

[78] Lidiard A B. *Philosophical Magazine A*, 43:291–300, 1981.

[79] Gillan M J. *Philosophical Magazine A*, 43:301–312, 1981.

[80] Sarma G A. *Phys. Rev. Lett.*, 44:670, 1980.

[81] Lallemand M. *C.R. Acad. Sci. Paris*, B267:715, 1968.

[82] Oberschmidt J and Lazarus D. *Phys. Rev. B*, B267:715, 1980.

[83] Cleaver B. *Z. Phys. Chem.*, 45:360, 1965.

[84] Spalt H, Lohstoter H, and Peisl H. *Phys. Stat. Sol.(b)*, 56:469, 1973.

[85] Catlow C R A, Faux I D, and Norgett M J. *J. Phys. C*, 9:419, 1976.

[86] Bauer R and Leutz R K. *J. Phys., Paris*, 41:516, 1980.

[87] Theimer O. *Phys. Rev.*, 112:1857, 1958.

[88] Chandra S, Pandey G K, and Agrawal V K. *Phys. Rev.*, 144:738, 1966.

[89] Roy D and Ghosh A K. *J. Phys. C:Solid State Phys.*, 4:941–943, 1971.

[90] Das P C, Murti Y V G S, and Haridasan T M. *Physica 138B*, pages 107–117, 1986.

[91] Govindarajan J, Jacobs P W M, and Nerenberg M A. *J. Phys. C:Solid State Phys.*, 9:3911–3924, 1976.

[92] Jacobs P W M, Nerenberg M A, Govindarajan J, and Haridasan T M. *J. Phys. C:Solid State Phys.*, 15:4245–4258, 1982.

[93] Norgett M J. A general formulation of the problem of calculating the energies of lattice defects in ionic crystals. page 49. United Kingdom Atomic Energy Authority, 1974.

[94] Gale Julian D. Gulp: A computer program for the symmetry adapted simulation of solids. *J. Chem. Soc., Faraday Trans*, 93(4):629–637, 1997.

[95] Banhatti Radha D and Murti Y V G S. *Radiation Effects and Defects in Solids*, 134:157–159, 1995.

[96] Murti Y V G S and Banhatti Radha D. *Bull. Mat. Sc.*, 20:435–440, 1997.

[97] Hildebrand F. B. *Introduction to Numerical Analysis*. 1987.

[98] Mullen J.G. *Phys. Rev.*, 143:658, 1966.

[99] Boswarva I.M. and Lidiard A.B. Aere harwell report, t.p.232. *Phil. Mag.*, 16:807, 1967.

[100] Norgett M J. *AERE Report*, page R7015, 1972.

[101] Pierre Donald A. *Optimization Theory with Applications*. Dover Publications Inc., New York, 1986.

[102] Gale Julian D. *Manual of General Utility Lattice Program*, version 1.3.

[103] Press W H, Teukolsky S A, Vetterling W T, and Flannery B P. *Numerical Recipes*. Cambridge University Press, Cambridge, 2nd edition, 1992.

[104] Fletcher R. *Practical Methods of Optimisation*. Wiley, New York, 1980.

[105] Zengwill W I. *The Computer Journal*, 10:293–296, 1967.

[106] Beniere F, Beniere M, and Chemla M. *J.Phys.Chem.Solids*, 31:1205, 1970.

[107] Usha V. PhD thesis, IIT Madras, 1976.

[108] Nowick A.S. Defects in ceramic oxides. In *MRS Bulletin*, pages 38–41. Nov. 1991.

[109] Zhu Yimei, Tafto J., and Suenga M. Defects in high tc cuprate superconductors. In *MRS Bulletin*, pages 54–59. Nov. 1991.

[110] Harding B C and Price D M. *Phil. Mag.*, 26:253–260, 1972.

[111] Mackrodt W.C. and Stewart R.F. *Journal of Physics C: Solid State Physics*, 12:431–448, 1979.

[112] Stoneham A. M. *Handbook of Interionic Potentials. I Ionic Crystals*, AERE Report 9598, 1979.

[113] Schmidt P.C., Weiss Alarich, and Das T.P. *Phys. Rev. B*, 19:5525, 1979.

[114] Clarke F P. *Phil. Mag.*, 2:607, 1957.

[115] Edwards David F. Beta-gallium oxide. In *Handbook of Optical Constants of Solids III*, page 753. 1998.

[116] Naoyuki Ueda and Hideo Hosono. *Appl. Phys. Lett.*, 70:3561, 1997.

[117] Palik E.D., Ginsburg N., Holm R.T., and Gibson J.W. *J. Vac. Sci. Technol.*, 15:1488, 1978.

[118] Peter M. and Schawlow A.L. *Bull. Am. Phys. Soc. Ser.II*, 5:158, 1960.

[119] Ueda N., Hosono H., Waseda R, and Kawazoe H. *Appl. Phys. Lett.*, 71:933, 1997.

[120] Klaus Bernhardt, Maximilian Fleischer, and Hans Meixner. *Siemens Components*, 30:35, 1995.

[121] Harwig T., Kellendonk F., and Slappendal F. *J. Phys. Chem. Solids*, 39:675–680, 1978.

[122] Laurent Binet and Didier Gourier. *J. Phys. Chem. Solids*, 59:1241–1249, 1998.

[123] Remeika J.P. *J. Appl. Phys.*, 31:263S, 1960.

[124] Chase A.B. *J. Am. Ceram. Soc.*, 47:470, 1964.

[125] Matsumoto T., Aoki M., Kinoshita A., and Aono T. *Jpn. J. Appl. Phys.*, 13:737 and 1578, 1974.

[126] Juskowiak H. and Pajaczkowska A. *J. Matter. Sci.*, 21:3430, 1986. n.a.

[127] Wolten G.M.and Chase A.B. *Journal of Solid State Chemistry*, 16:377–383, 1976.

[128] Geller S. *The Journal of Chemical Physics*, 33:676, 1960.

[129] Geller S. *Journal of Solid State Chemistry*, 20:209, 1977.

[130] Ahman Johan, Svensson Goran, and Albertsson Jorgen. *Acta Crystallographica C*, 52:1336–1338, 1996.

[131] Doye Jonathan P K and Wales David J. *cond-mat/9801152 v2*, 1998.

[132] Omar M Ali. *Elementary Solid State Physics*. Pearson Education, Inc., 2002.

[133] Dove Martin T. *Introduction to Lattice Dynamics*. Cambridge University Press, 1993.

[134] Giacovazzo C et. al. *Fundamentals of Crystallography*. Oxford Science Publication, 1998.

[135] Kimble R J et. al. *J Phys C : Solid State Phys*, 15:3441–3453, 1982.